TAMPEREEN TEKNILLINEN YLIOPISTO
TAMPERE UNIVERSITY OF TECHNOLOGY

MATIAS BERG

# DYNAMICS OF GRID-FORMING INVERTER

Master of Science thesis

Examiner: Assist. Prof. Tuomas Messo
Examiner and topic approved by the
Faculty Council of the Faculty of
Computing and Electrical Engineering
on 1st February 2017

# ABSTRACT

**MATIAS BERG**: Dynamics of Grid-Forming Inverter
Tampere University of Technology
Master of Science thesis, 60 pages, 6 Appendix pages
July 2017
Master's Degree Programme in Electrical Engineering
Major: Power Electronics
Examiner: Assist. Prof. Tuomas Messo
Keywords: grid-forming, inverter, dynamics, micro-grid, islanding, islanded, standalone

Islanded micro-grids are increasingly becoming a vital factor in improving the reliability of a power system. In the islanded micro-grid power is produced from a local energy source that can be a renewable energy plant or an energy storage system. If for example, the energy produced from solar panels and energy storage systems is fed to the grid an inverter is required to change the direct current produced by the solar panels to the alternating current. In the islanded micro-grid the inverter is used to form the phase voltages.

Dynamic models of power electronic converters have been previously developed in the literature. A useful feature of a dynamic model is that it can be used to tune controllers for the inverter and analyze stability. However, a dynamic model of the grid-forming inverter with respect to its true dynamics has not been reported and analyzed at the same time properly.

This thesis investigates, how to develop a dynamic model of the grid-forming inverter. A circuit diagram of the inverter, where the load is modeled as an ideal current sink is used as a basis for the modeling. Equations from the circuit diagram are written for a state space model. The state space model consists of linearized equations in a synchronous reference frame. The synchronous reference frame is used so that traditional control theory can be employed. Transfer functions that describe the dynamics from the system inputs to the system outputs are solved from the state-space presentation.

Analysis of the solved open-loop transfer functions shows that the dynamics of the grid-feeding and grid-forming inverter differ significantly. In orderer to tune reasonable controller the size of the capacitor in a commonly used LCL-filter has to be increased compared to grid-feeding inverter. The dynamic model could be used to develop a cascaded controller. It is analyzed that capacitor current feedback provides good output current disturbance rejection.

# TIIVISTELMÄ

**MATIAS BERG**: Verkon muodostavan vaihtosuuntaajan dynamiikka
Tampereen teknillinen yliopisto
Diplomityö, 60 sivua, 6 liitesivua
Heinäkuu 2017
Sähkötekniikan koulutusohjelma
Pääaine: Tehoelektroniikka
Tarkastajat: Assist. Prof. Tuomas Messo
Avainsanat: vaihtosuuntaaja, dynaaminen malli, saarekekäyttö, verkon muodostaminen, mikroverkko

Sähköverkkojen saarekekäyttömahdollisuudesta on tulossa entistä tärkeämpää, kun sähkönjakelun luotettavuutta halutaan parantaa. Saarekkeessa tehoa tuotetaan paikallisesta lähteestä, joka voi olla uusiutuva energialähde tai energian varastointijärjestelmä. Jos esimerkiksi aurinkopaneeleilla tuotettua sähköä halutaan syöttää verkkoon, tarvitaan vaihtosuuntaaja, joka muuttaa aurinkokennojen tuottaman tasajännitteen vaihtojännitteeksi. Saarekekäytössä vaihtosuuntaajaa käytetään muodostamaan jännitteet verkkoon.

Vaihtosuuntaajille on kehitetty dynaamisia malleja, joita voidaan käyttää säätöjen suunnitteluun ja stabiiliusanalyysiin. Verkon muodostavalle vaihtosuuntaajalle ei ole vielä kuitenkaan esitetty kunnollisesti mallia, joka mallintaisi aitoa dynamiikka.

Tässä diplomityössä tutkittiin, miten verkon muodostavan vaihtosuuntaajan dynaaminen malli johdetaan. Dynaamisen mallin johtamisen perustana käytetiin verkon muodostavan vaihtosuuntaajan piirikaaviota, josta kirjoitettiin ja muokattiin yhtälöt tilaesitystä varten. Tilamalli koostuu linearisoiduista yhtälöistä, jotka on esitetty synkronisessa koordinaatistossa, jotta perinteistä säätöteoriaa voidaan käyttää. Tilaesityksestä ratkaistiin siirtofunktiot, jotka kuvaavat tulosuureiden ja lähtösuureiden välistä piensignaalikäyttäytymistä.

Johdettujen siirtofunktioiden taajuusvasteista pääteltiin, että verkon muodostavan vaihtosuuntaajan dynamiikka eroaa merkittävästi verkkoa syöttävän vaihtosuuntaajan dynamiikasta. Jotta säätimet saatiin viritettyä järkevästi, yleisesti käytetyn LCL-suotimen kondensaattorin kokoa täytyi kasvattaa. Dynaamista mallia käyttämällä viritettiin toimiva kaskadisäätö. Analyysi vahvisti aiemmat havainnot, että sisempi takaisinkytkentä kondensaattorin virrasta tuottaa paremman vasteen kuormavirrasta aiheutuviin häiriöihin kuin takaisinkytkentä kelavirrasta.

# PREFACE

This master of science thesis was written within the project Finnish Solar Revolution at the Laboratory of Electrical Energy Engineering at Tampere University of Technology during the spring semester 2017 and summer.

First and foremost, I would like to thank my supervisor Assistant Professor Tuomas Messo for providing detailed comments and support during the process of research and writing. I also wish to thank Professor Teuvo Suntio for advising and encouragement. Thanks are also due to M.Sc Aapo Aapro and M.Sc Jyri Kivimäki who gave me valuable advice.

I express my gratitude to my parents for supporting me during my studies and carrying out this thesis.

Tampere, 31.7.2017

Matias Berg

# CONTENTS

# LIST OF FIGURES

# LIST OF TABLES

# LIST OF ABBREVIATIONS AND SYMBOLS

## ABBREVIATIONS

| | |
|---|---|
| AC | Alternating current |
| CF-VSI | Current-fed voltage-source inverter |
| DC | Direct current |
| ESR | Equivalent series resistance |
| GM | Gain margin |
| HIL | Hardware in the loop |
| P | Proportional controller |
| PI | Proportional-integral controller |
| PM | Phase margin |
| PWM | Pulse width modulation |
| SPDT | Single-pole double throw (switch) |
| UPS | Uninterruptible power supply |
| VSI | Voltage-source inverter |

## CHARACTERS

| | |
|---|---|
| $\mathbf{A}$ | Coefficient matrix A of the state-space representation |
| $\mathbf{B}$ | Coefficient matrix B of the state-space representation |
| $C$ | Input capacitor |
| $\mathbf{C}$ | Coefficient matrix C of the state-space representation |
| $C_\mathrm{f}$ | Filter capacitor |
| $\mathbf{D}$ | Coefficient matrix D of the state-space representation |
| $d_\mathrm{a}$ | Duty ratio of the upper switch in phase A |
| $d_\mathrm{b}$ | Duty ratio of the upper switch in phase B |
| $d_\mathrm{c}$ | Duty ratio of the upper switch in phase C |
| $d_\alpha$ | Alpha component of the duty ratio space vector |
| $d_\beta$ | Beta component of the duty ratio space vector |
| $d_\mathrm{d}$ | Direct component of the duty ratio space vector |
| $\hat{d}$ | Small-signal duty ratio |
| $\hat{d}_\mathrm{d}$ | Small-signal d-component of the duty ratio space vector |
| $d_\mathrm{q}$ | Quadrature component of the duty ratio space vector |
| $\hat{d}_\mathrm{q}$ | Small-signal q-component of the duty ratio space vector |
| $\mathbf{d}^\mathrm{dq}$ | Duty ratio space vector in a synchronous reference frame |

| | |
|---|---|
| $\hat{\mathbf{d}}$ | Small signal duty ratio space vector in a synchronous reference frame |
| $D_{\mathrm{d}}$ | Steady-state d-component of the duty ratio |
| $D_{\mathrm{q}}$ | Steady-state q-component of the duty ratio |
| $\mathbf{G}$ | Transfer function matrix |
| $G_{\mathrm{iL}}$ | Input-to-inductor current transfer function |
| $\mathbf{G}_{\mathrm{iL}}$ | Input-to-inductor current transfer function matrix |
| $G_{\mathrm{io}}$ | Input-to-output transfer function |
| $\mathbf{G}_{\mathrm{io}}$ | Input-to-output transfer function matrix |
| $G_{\mathrm{cc}}$ | Current controller |
| $\mathbf{G}_{\mathrm{cc}}$ | Current controller matrix |
| $G_{\mathrm{cC_f}}$ | Control-to-filter capacitor current transfer function |
| $G_{\mathrm{cL}}$ | Control-to-inductor current transfer function |
| $\mathbf{G}_{\mathrm{cL}}$ | Control-to-inductor current transfer function matrix |
| $G_{\mathrm{ci}}$ | Control-to-input transfer function |
| $\mathbf{G}_{\mathrm{ci}}$ | Control-to-input transfer function matrix |
| $G_{\mathrm{co}}$ | Control-to-output transfer function |
| $\mathbf{G}_{\mathrm{co}}$ | Control-to-output transfer function matrix |
| $G_{\mathrm{vc}}$ | Voltage controller |
| $\mathbf{G}_{\mathrm{vc}}$ | Voltage controller transfer function matrix |
| $G_{\mathrm{oC_fd-o}}$ | Output-to-filter capacitor current transfer function |
| $\mathbf{G}_{\mathrm{scC}}$ | Current sensing gain |
| $\mathbf{G}_{\mathrm{seV}}$ | Voltage sensing gain |
| $G_{\mathrm{oL}}$ | Output-to-inductor current transfer function |
| $\mathbf{G}_{\mathrm{oL}}$ | Output-to-input transfer function matrix |
| $i_{\mathrm{C}}$ | Capacitor current |
| $\langle i_{\mathrm{C}} \rangle$ | Average capacitor current |
| $\hat{i}_{\mathrm{C}}$ | Small-signal capacitor current |
| $i_{\mathrm{C_f}}$ | Filter capacitor current |
| $\langle i_{\mathrm{C_f}} \rangle$ | Average filter capacitor current |
| $\hat{i}_{\mathrm{C_f}}$ | Small-signal filter capacitor current |
| $i_{\mathrm{in}}$ | Input current |
| $\langle i_{\mathrm{in}} \rangle$ | Average input current |
| $\hat{i}_{\mathrm{in}}$ | Small signal input current |
| $I_{in}$ | Steady-state input current |
| $\langle i_{\mathrm{L}\alpha} \rangle$ | Inductor current $\alpha$-component |
| $\langle i_{\mathrm{L}\beta} \rangle$ | Inductor current $\beta$-component |
| $\langle i_{\mathrm{Ld}} \rangle$ | Inductor current d-component |
| $\langle i_{\mathrm{Lq}} \rangle$ | Inductor current q-component |
| $\hat{i}_{\mathrm{L}}$ | Small signal inductor current |

| | |
|---|---|
| $\hat{i}_{\mathrm{Ld}}$ | Small signal inductor current d-component |
| $\hat{i}_{\mathrm{Lq}}$ | Small signal inductor current q-component |
| $\hat{\mathbf{i}}_{\mathrm{L}}$ | Small signal inductor current space vector in a synchronous reference frame |
| $I_{\mathrm{Ld}}$ | Steady-state d-component of the inductor current |
| $I_{\mathrm{Lq}}$ | Steady-state q-component of the inductor current |
| $\left\langle \mathbf{i}_{\mathrm{L}}^{\alpha\beta} \right\rangle$ | Inductor current space vector |
| $\left\langle \mathbf{i}_{\mathrm{L}}^{\mathrm{dq}} \right\rangle$ | Inductor current space vector in a synchronous reference frame |
| $\langle i_{\mathrm{o}\alpha} \rangle$ | Output current $\alpha$-component |
| $\langle i_{\mathrm{o}\beta} \rangle$ | Output current $\beta$-component |
| $\left\langle \mathbf{i}_{o}^{\alpha\beta} \right\rangle$ | Output current space vector |
| $\langle i_{\mathrm{od}} \rangle$ | Output current d-component |
| $\langle i_{\mathrm{oq}} \rangle$ | Output current q-component |
| $\hat{i}_{\mathrm{od}}$ | Small signal output current d-component |
| $\hat{i}_{\mathrm{oq}}$ | Small signal output current q-component |
| $\left\langle \mathbf{i}_{\mathrm{o}}^{\mathrm{dq}} \right\rangle$ | Output current space vector in a synchronous reference frame |
| $\hat{\mathbf{i}}_{\mathrm{o}}$ | Small signal output current space vector in a synchronous reference frame |
| $I_{\mathrm{od}}$ | Steady-state d-component of the output current |
| $I_{\mathrm{oq}}$ | Steady-state q-component of the output current |
| $i_{\mathrm{S}}$ | Source current |
| $L$ | Filter inductance |
| $L_{\mathrm{outC}}$ | Current loop gain |
| $L_{\mathrm{outV}}$ | Voltage loop gain |
| N | Negative rail of the DC-link |
| P | Positive rail of the DC-link |
| $r_{\mathrm{C}}$ | Equivalent series resistance of the input capacitor |
| $r_{\mathrm{L}}$ | Equivalent series resistance of the filter inductor |
| $r_{\mathrm{sw}}$ | Parasitic resistance of a switch |
| $R$ | Resistor |
| $R_{\mathrm{d}}$ | Damping resistance that includes the filter capacitor equivalent series resistance |
| $T_{\mathrm{oi}}$ | Output-to-input transfer function |
| $\mathbf{T}_{\mathrm{oi}}$ | Output-to-input transfer function matrix |
| $\mathbf{U}$ | Input-variable vector in Laplace domain |
| $v_{\mathrm{Cf}a}$ | Filter capacitor voltage in phase A |
| $v_{\mathrm{Cf}b}$ | Filter capacitor voltage in phase B |
| $v_{\mathrm{Cf}c}$ | Filter capacitor voltage in phase C |
| $\langle v_{\mathrm{Cf}a} \rangle$ | Average filter capacitor voltage in phase A |

| | |
|---|---|
| $\langle v_{\mathrm{Cf}b} \rangle$ | Average filter capacitor voltage in phase B |
| $\langle v_{\mathrm{Cf}c} \rangle$ | Average filter capacitor voltage in phase C |
| $\langle v_{\mathrm{Cf}\alpha} \rangle$ | Average filter capacitor voltage $\alpha$-component |
| $\langle v_{\mathrm{Cf}\beta} \rangle$ | Average filter capacitor voltage $\beta$-component |
| $\langle v_{\mathrm{Cfd}} \rangle$ | Average filter capacitor voltage d-component |
| $\langle v_{\mathrm{Cfq}} \rangle$ | Average filter capacitor voltage q-component |
| $\hat{v}_{\mathrm{Cfd}}$ | Small-signal filter capacitor voltage d-component |
| $\hat{v}_{\mathrm{Cfq}}$ | Small-signal filter capacitor voltage q-component |
| $\left\langle \mathbf{v}_{\mathrm{C_f}}^{\alpha\beta} \right\rangle$ | Filter capacitor voltage space vector |
| $\left\langle \mathbf{v}_{\mathrm{Cf}}^{\mathrm{dq}} \right\rangle$ | Filter capacitor voltage space vector in a synchronous reference frame |
| $V_{\mathrm{Cfd}}$ | Steady-state d-component of the filter capacitor voltage |
| $V_{\mathrm{Cfq}}$ | Steady-state q-component of the filter capacitor voltage |
| $v_{\mathrm{in}}$ | Input voltage |
| $\langle v_{\mathrm{in}} \rangle$ | Average input voltage |
| $\hat{v}_{\mathrm{in}}$ | Small signal input voltage |
| $V_{\mathrm{in}}$ | Steady state input voltage |
| $v_{\mathrm{oa}}$ | Output voltage in phase A |
| $v_{\mathrm{ob}}$ | Output voltage in phase B |
| $v_{\mathrm{oc}}$ | Output voltage in phase C |
| $v_{\mathrm{o}\alpha}$ | Output voltage $\alpha$-component |
| $v_{\mathrm{o}\beta}$ | Output voltage $\beta$-component |
| $\langle v_{\mathrm{od}} \rangle$ | Output voltage d-component |
| $\langle v_{\mathrm{oq}} \rangle$ | Output voltage q-component |
| $\hat{v}_{\mathrm{od}}$ | Small signal output voltage d-component |
| $\hat{v}_{\mathrm{oq}}$ | Small signal output voltage q-component |
| $\hat{\mathbf{v}}_{\mathrm{o}}$ | Small signal output voltage space vector in a synchronous reference frame |
| $\mathbf{v}_{\mathrm{o}}^{\alpha\beta}$ | Output voltage space vector |
| $\mathbf{v}_{\mathrm{o}}^{\mathrm{dq}}$ | Output voltage space vector in a synchronous reference frame |
| $V_{\mathrm{od}}$ | Steady-state d-component of the output voltage |
| $V_{\mathrm{oq}}$ | Steady-state q-component of the output voltage |
| $v_{\mathrm{S}}$ | Source voltage |
| $\mathbf{X}$ | State-variable vector in Laplace domain |
| $\mathbf{x}^{\alpha\beta}$ | Space vector |
| $\mathbf{x}^{\mathrm{dq}}$ | Space vector in a synchronous reference frame |
| $\mathbf{Y}$ | Output-variable vector in Laplace domain |
| $Y_{\mathrm{in}}$ | Input admittance |
| $\mathbf{Y}_{\mathrm{in}}$ | Input admittance matrix |

| | |
|---|---|
| $Y_{\mathrm{L}}$ | Load admittance |
| $Z_{\mathrm{o}}$ | Output impedance |
| $\mathbf{Z}_{\mathrm{o}}$ | Output impedance matrix |

SUBSCRIPTS

| | |
|---|---|
| $\alpha\beta$ | Stationary reference frame |
| c | Closed-loop transfer function |
| d | Transfer function related to d-components |
| dq | Transfer function from to d to q-component |
| o | Open-loop transfer function |
| on | Current or voltage during on-time |
| off | Current or voltage during off-time |
| q | Transfer function related to q-components |
| qd | Transfer function from to q to d-component |

SUPERSCRIPTS

| | |
|---|---|
| FO | Full-order transfer function |
| sec | Secondary controller feedback closed |
| tot | Primary and secondary feedback loops closed |
| dq | Synchronous reference frame |

# 1. INTRODUCTION

Global warming and contamination of the environment caused by polluting energy production imperil the diversity of the nature [1],[2] and may reduce the living space due to rising sea level [2],[3]. This threat has been observed and responsible political decisions and guidelines on a national and international level usher and support the change in energy production from using polluting coal and oil to renewable resources [4], [5], [6]. In addition nuclear production is run down completely in Germany [7]. Thus, there will be demand in the marker for renewable energy in many Western countries.

The increase in electrical energy produced by renewable energy sources between 2004 and 2014 in European Union provides view on the rapid increase. In 2004 approximately 480 TWh electrical energy was produced from renewable energy sources and in 2014 the amount was increased to 920 TWh [8]. The three most significant rising sources during that time were wind energy, biomass and solar power. From year 2014 to year 2015 electricity produced from solar power has increased from 92 TWh to 100 TWh in European Union [9].

Solar power is especially interesting since the size of a solar power plant is relatively easy to scale. Individual solar cells that generate electrical energy from sunlight are used as a building block for solar modules [10]. Solar panels that consists of solar modules can be connected series and parallel so that desired nominal current and power can be achieved. Solar panels can be used to form large hundreds of megawatts-size centralized solar power plants [11], small scale centralized micro-grid power plants and roof-top home systems [12].

Electricity produced by photovoltaic cells is direct current (DC) [10]. The direct current must be transformed to alternating current (AC) to be delivered in AC power systems [13]. Thus, a photovoltaic inverter is an essential power electronics device that is needed to transform the direct current to alternating current [14], [15]. Depending on the connection topology, DC-DC converters that step-up the voltage and track the maximum power point of the panels might be required for the connection [15].

Fluctuation in irradiance that reaches the panels causes variation in the power produced by the solar plant [16]. Battery energy storage system (BESS) can be used to attenuate the adverse effect of the power fluctuation of photovoltaic generators [17],[18]. Adding energy storage enables forming of micro-grids. According to a European Commission publication [19] micro-grids contain distributed generation, controllable local loads and energy storage devices. During a failure in the distribution network a micro-grid can operate in islanded mode [19]. In islanded operation the dynamics are denoted by the local loads and sources in which case there is only small amount of inertia in the system [20].

An islanded micro-grid should be controlled by a hierarchical control system so that the frequency and voltage deviations remain acceptable [21]. The lowest level in the hierarchy is the inner control loop of an individual inverter. The controller consists of the inner current controller and voltage controller [21]. This thesis focuses on dynamic modeling the inverter in grid-forming mode. In turn, the model can be used to tune the inner control loop.

The structure of the thesis is following. The second chapter begins by giving a brief overview of the main differences between grid-feeding and grid-forming inverter. The second chapter continues with development of the dynamic model of the grid-forming inverter. Control design and step response test of the grid-forming inverter is presented in the third chapter. The fourth chapter examines the effect of the current feedback variable on the output impedance. Summary of the results and conclusions are presented in Chapter 5.

# 2. DYNAMIC MODELING OF GRID-FORMING INVERTER

The motive of this chapter is to introduce the reader to few major differences in topologies and control between grid-forming and grid-feeding inverters. A detailed discussion of control of grid-feeding inverter falls out of scope of this thesis. Once a circuit diagram of a grid-forming inverter is justified, an open-loop dynamic model of the inverter is derived.

## 2.1 Grid-Feeding Inverter

The grid-feeding mode of the inverter is required when the power produced by a PV generator is fed to the grid. Figure 2.1 shows a simplified diagram of a grid-connected PV inverter. The inverter is fed by the PV generator, which is equipped with an input capacitor. The input capacitor is required for the proper operation of the inverter [22]. On the AC-side a LCL-filter is connected to the inverter to reduce the current ripple. The ideal AC voltage source stands for an ideal grid.

In the grid-feeding mode a current sourced PV inverter is usually controlled by a cascaded controller. If the generator is operated at the constant current region the PV generator can be modeled as a current source. In order to implement a maximum power point tracker the primary control variable is the input voltage of the inverter [22]. The secondary control variable is the output current [23]. When equipped with a shunt capacitor as in the case of the LCL-filter, the feedback current can be the inverter side inductor current or the grid current [24], [25]. Thus, there are multiple options for the feedback variables on the AC-side.

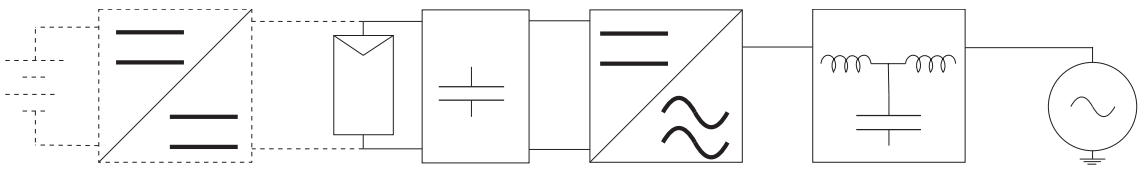

***Figure 2.1*** *Grid-feeding inverter.*

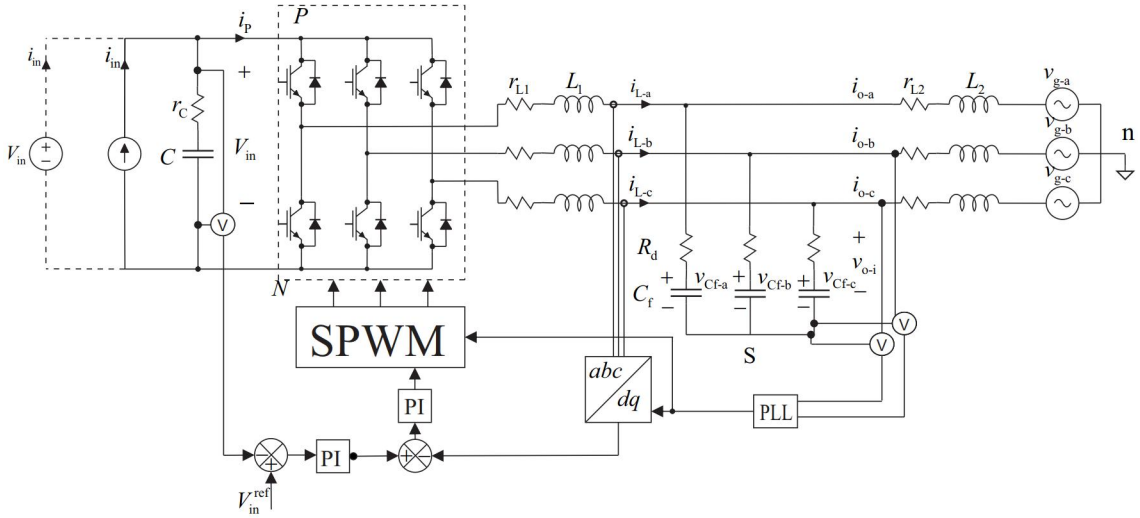


***Figure 2.2*** *Circuit diagram of the grid-feeding inverter including a simplified control block diagram.*

Figure 2.2 shows a more detailed circuit diagram of the grid-feeding inverter. The main points in the figure to be noticed are, how the source and load are modeled and, how the cascaded feedback control is constructed. The ideal uncontrollable current source enables maximum power point tracking by input voltage control [22], [26]. The load is a ideal AC voltage source the same as in Figure 2.1, but all three phases are shown. These simplifications are justified and actually required, because in order to derive a general dynamic model the load and source effects should be excluded [22], [27]. The modeling of nonideality in the sources and loads is helpful for the control design, but they can be included as source and load effects be in the model afterwards [22], [27]. Figures 2.1 and 2.2 show a battery and a constant voltage source drawn by a dashed line as alternative sources, respectively. The alternative sources are needed for purposes of comparison later.

The cascaded controllers are expressed by simplified control block diagrams. It should be noticed from which variables the feedbacks are taken. The secondary control feedback is taken from the inverter side inductor current and the primary feedback is from the input voltage. The voltage reference $V_{\mathrm{in}}^{\mathrm{ref}}$ is created by maximum power point tracker which ensures that maximum available power is produced by the PV generator. The tracker is omitted for clarity from Figure 2.2. The voltage controller creates the current reference that is fed to the current controller. The duty ratio is formed by the error between measured current and its reference from the current error. Sinusoidal pulse-width-modulation (SPWM) is used so that sinusoidal currents are achieved. If the AC side control is realized in the synchronous reference frame the as in the figure the currents and their reference consist of $d$- and $q$- components. Modeling in $dq$-domain is analyzed in more detail in the case

of grid-forming inverter. Both voltage and current controllers can be realized by PI-controllers as the figure shows [28].

## 2.2 Grid-Forming Inverter

According to a European Commission publication, micro-grids contain DG, controllable local loads and energy storage system (ESS) [19]. However, the controllable local loads are not always included in the definition of a micro-grid [29]. If local loads and DG are isolated from the distribution network or the transfer network and the loads are supplied by the local DG the mode is called as standalone operation [30]. This is essentially same as the intentional islanding of a micro-grid [29]. Also the term voltage control mode of the inverter has been used to refer to the stand-alone operation [31].

In the case of the islanded micro-grid the inverter forms the voltages and controls the frequency [32]. Thus, it is reasonable to use the term grid-forming inverter to define the converter during that operation. Throughout this thesis the terms grid-forming inverter and grid-forming mode are used interchangeably.

As mentioned previously an energy storage system is an essential part of a micro-grid system. Batteries are used commonly as the energy storage with PV generators [17], [33], [34]. Figure 2.3 shows a common connection of a battery with DC-DC converter to input capacitor of the inverter [17], [33]. It should be noted that the inverter is voltage-fed and there is no stiff grid in the output of the LCL-filter. The output filter and input filter remain unchanged in comparison to the grid-feeding mode. This is justified by the assumption that no changes are made in the hardware topology of commercial inverters for the purposes of the grid-forming mode. Generally speaking the local load in a micro-grid can vary from industrial loads to house-hold loads. Thus, the load in Fig. 2.3 remains unspecified in the simplified block diagram.

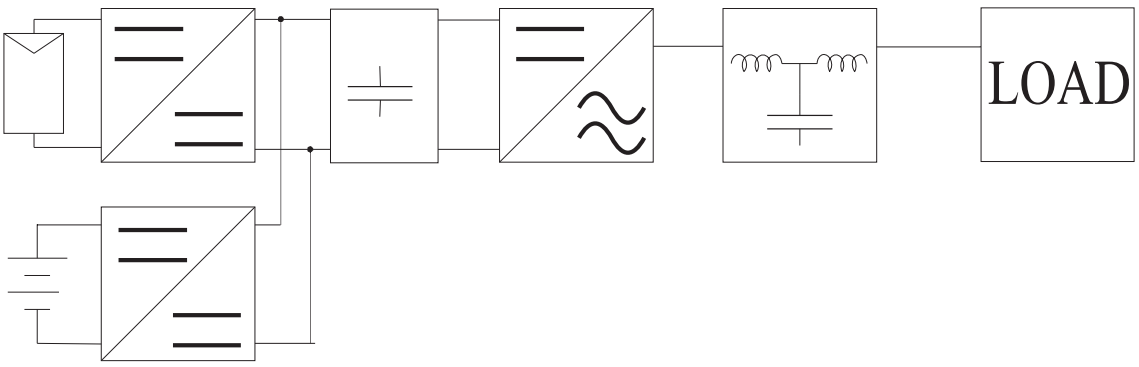


***Figure 2.3*** *Grid-forming inverter.*

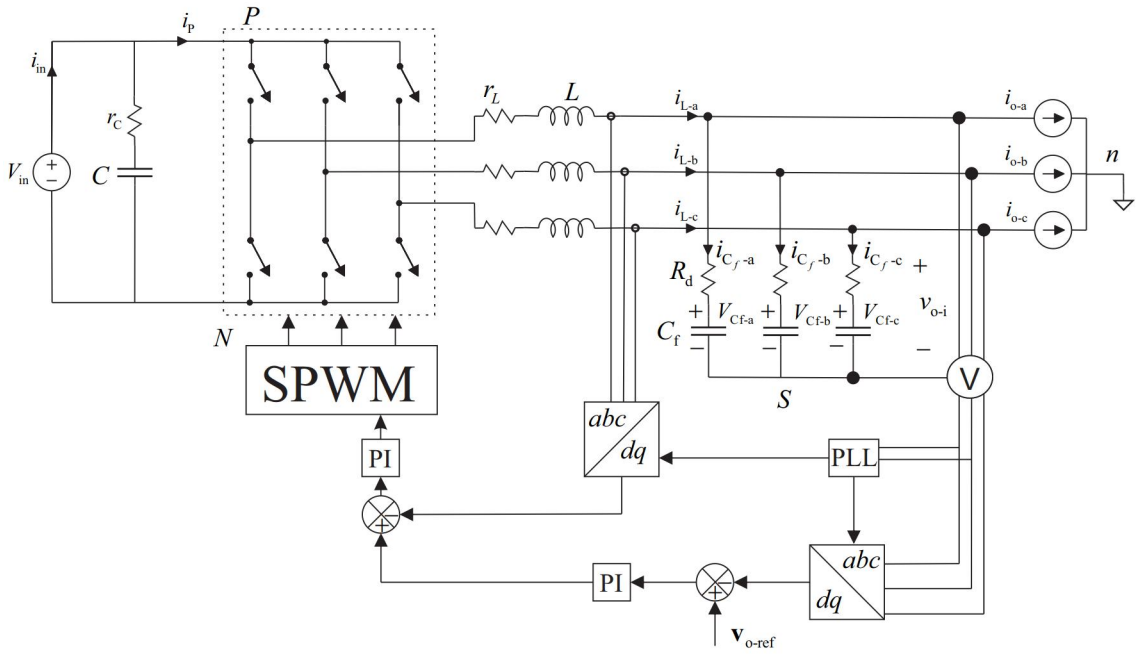


***Figure 2.4*** *Circuit diagram of the grid-forming inverter including a simplified control block diagram.*

This thesis focuses on how to model the true dynamics of the grid-forming inverter. Consequently the grid-forming inverter must be assumed to operate in voltage output mode and the load is assumed to be an ideal current sink. Regarding the source similar assumption must be made. The source is considered as an ideal voltage source. For example if the load would be assumed resistive true dynamics of the inverter would remain hidden. [27]

Figure 2.4 shows a more detailed diagram of the grid-forming inverter. The above mentioned assumptions regarding the sources and loads are applied in the model. The first obvious difference between the simplified model of Figure 2.3 and the more detailed circuit diagram is the AC-side filter. The filter has reduced from a LCL-filter to a LC-filter. The reason for this lies in the circuit theory. It is well known that a series connection of current source and an inductor is inconsistent. Thus, the load side inductor of the LCL-filter must be omitted for analysis.

In the grid-forming mode the most important variables to be controlled are the grid voltage and grid-frequency [21]. Practically when a cascaded controller is implemented, the primary control variable is the output voltage. The secondary control variable is either the inverter side inductor current, capacitor current or output current. It should be noted that the primary feedback and the secondary feedback are taken from the same side of the inverter. In the system of Figure 2.4 the current feedback is realized the same way as in the case of the grid-feeding inverter

in Figure 2.2. This combination of current loop and voltage loop has been widely investigated in the literature in the case of grid-forming inverter a well as in the case of uninterruptible power supply (UPS) solutions [29], [32], [35], [36]. In this thesis, the operating mode of UPS inverters is regarded equivalent to the grid-forming mode. However, an issue of this thesis is to analyze the grid-forming mode as an alternative to the grid-feeding mode in micro-grids.

The circuit in Figure 2.4 resembles the one investigated in the case of UPS systems. The most significant difference between the aforementioned systems is the lack of input capacitor from the input of the inverter in the UPS. A key problem with the much of literature regarding the true dynamics grid-forming inverter is that the load is commonly assumed resistive and inductive [37]. However, in [38] the authors have investigated output impedance of an UPS inverter with respect to true dynamics. The aim is to formulate open loop transfer functions that describe the true dynamics from all input variables to all output variables. The open loop transfer functions are to be used to tune the cascaded controller in the grid-forming mode.

## 2.3 Dynamic Modeling in Synchronous Reference Frame

There is a considerable amount of literature of implementing the cascade controller in the synchronous reference frame [29], [32] and in the stationary reference frame [21], [35]. In the stationary reference frame there are sinusoidally changing variables in the steady state. One of the major drawbacks of the sinusoidally changing steady state is the impossibility to use traditional PI-controllers. Therefore, modeling in a synchronous reference frame is chosen for this thesis because the waveforms have constant steady-sate and controllers from the traditional control theory can be used.

Modeling starts from the open-loop model and the circuit of Figure 2.4 works as basis for analysis. In order to facilitate analysis, switches are modeled as single-pole double-throw (SPDT) switches. Figure 2.5 shows the circuit where the original six switches have been replaced by three SPDT switches. The SPDT switches are always connected either up or down position. In the six switch model this means that constantly either the upper or lower switch is turned on. Hence, the essential dead-time is not taken into account.

The model parameters are chosen in a way that the duty ratios define the on-time of the upper switches. Variables $d_{\mathrm{a}}$, $d_{\mathrm{b}}$ and $d_{\mathrm{c}}$ are used to refer to the duty ratios in upper switch in the phase A, B and C, respectively. The lower switches are turned on when the upper switches are turned off. In the case of SPDT switches the duty ratios denote the ratio of connection time to the positive and negative rail of the

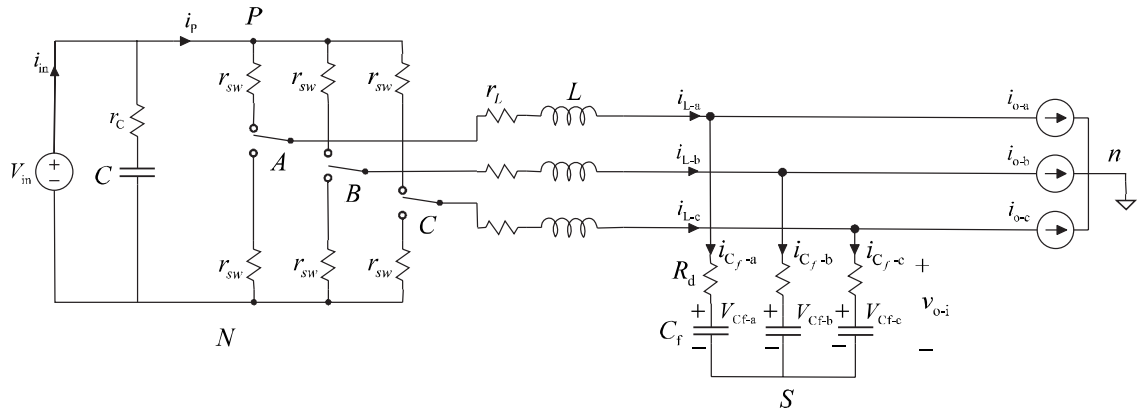


***Figure 2.5*** *Circuit diagram of the grid-forming inverter. The switches are replaced by SPDT switches for the dynamic analysis.*

DC link. The DC rails are denoted by $P$ and $N$, respectively. Parasitic resistance of a switch is referred by $r_{\mathrm{sw}}$. The equivalent series resistance (ESR) of the inductor $L$ is denoted by $r_{\mathrm{L}}$ and the ESR of the filter capacitor $C_{\mathrm{f}}$ is included in the damping resistor $R_{\mathrm{d}}$. The input capacitor and its ESR are denoted by $C$ and $r_{\mathrm{C}}$, respectively.

The input variables of the system are the input voltage, upper switch phase duty ratios and phase load currents. The input voltage and the output phase currents are denoted by $v_{\mathrm{in}}$, $i_{\mathrm{oa}}$, $i_{\mathrm{ob}}$ and $i_{\mathrm{oc}}$, respectively. The outputs of the system are the input current $i_{\mathrm{in}}$, inductor phase currents $i_{\mathrm{La}}$, $i_{\mathrm{Lb}}$ and $i_{\mathrm{Lc}}$ and output voltages $v_{\mathrm{oa}}$, $v_{\mathrm{ob}}$, $v_{\mathrm{oc}}$.

Commonly the currents through the inductors and voltages over the capacitors are chosen as states in the state-space modeling. Thus, the states are the input capacitor voltage $v_{\mathrm{C}}$, filter capacitor voltages $v_{\mathrm{Cfa}}$, $v_{\mathrm{Cfb}}$ and $v_{\mathrm{Cfa}}$ and filter inductor currents.

### 2.3.1 State Space Average Model of Grid-Forming Inverter

An average model means that the system parameters are averaged over one switching cycle [39]. The switch in Figure 2.5 has two possible positions. Thus, two sub circuits can be formed. The on- and off-time equations of derivatives of the state variables are shown in (2.1), (2.2), respectively. The equations are similar for the three phases. Thus, subscript $i$ =a,b,c is used to denote all three phases.

$$\frac{di_{\mathrm{L}i-\mathrm{on}}}{dt} = d_i \frac{1}{L}\left[v_{\mathrm{in}} - (r_{\mathrm{L}} + r_{\mathrm{sw}} + R_{\mathrm{d}})i_{\mathrm{L}i} + R_{\mathrm{d}} i_{\mathrm{o}i} - v_{\mathrm{Cf}i} - v_{nN}\right] \tag{2.1}$$

$$\frac{di_{\mathrm{L}i-\mathrm{off}}}{dt} = (1-d_i)\frac{1}{L}[-(r_{\mathrm{L}}+r_{\mathrm{sw}}+R_{\mathrm{d}})i_{\mathrm{L}i}+R_{\mathrm{d}}i_{oi}-v_{\mathrm{C}fi}-v_{nN}] \tag{2.2}$$

By compiling expression of (2.1) and (2.2) time average equations over one switching period can be achieved. Equations (2.2) and (2.4) show the sum operation and the result, respectively.

$$\frac{d\langle i_{\mathrm{L}i}\rangle}{dt} = \frac{di_{\mathrm{L}i-\mathrm{on}}}{dt} + \frac{di_{\mathrm{L}i-\mathrm{off}}}{dt} \tag{2.3}$$

$$\frac{d\langle i_{\mathrm{L}i}\rangle}{dt} = \frac{1}{L}\left[d_i\langle v_{\mathrm{in}}\rangle - (r_{\mathrm{L}}+r_{\mathrm{sw}}+R_{\mathrm{d}})\langle i_{\mathrm{L}i}\rangle + R_{\mathrm{d}}\langle i_{oi}\rangle - \langle v_{\mathrm{C}fi}\rangle - \langle v_{nN}\rangle\right] \tag{2.4}$$

The remaining state variables are the input capacitor voltage and the output filter voltages. They can be equated with other state variables and input variables. Thus, the equations of these do not contain duty ratio-dependent terms and they directly express the time averaged dependencies. Equations (2.5) and (2.7) show that the capacitor current is expressed in the both cases as a function of one input variable and one state variable. Equation (2.6) shows an intermediate formulation to calculate the average input capacitor current $\langle i_{\mathrm{C}}\rangle$.

$$\frac{d\langle v_{\mathrm{C}fi}\rangle}{dt} = \frac{1}{C_{\mathrm{f}}}\left[\langle i_{\mathrm{L}i}\rangle - \langle i_{oi}\rangle\right] \tag{2.5}$$

$$\langle i_{\mathrm{C}}\rangle = C\frac{d\langle v_{\mathrm{C}}\rangle}{dt} = \frac{\langle v_{\mathrm{in}}\rangle}{r_{\mathrm{C}}} - \frac{\langle v_{\mathrm{C}}\rangle}{r_{\mathrm{C}}} \tag{2.6}$$

$$\frac{d\langle v_{\mathrm{C}}\rangle}{dt} = \frac{1}{C}\left[\frac{\langle v_{\mathrm{in}}\rangle}{r_{\mathrm{C}}} - \frac{\langle v_{\mathrm{C}}\rangle}{r_{\mathrm{C}}}\right] \tag{2.7}$$

The inductor currents are state variables, but they will be also used in the current control feedback. Thus, they are also output variables. The remaining output variables are the input current and the output voltages. The average current $i_{\mathrm{P}}$ flowing from the DC link toward the inverter switches must be solved first in order to calculate the input current. Equation (2.8) shows the intermediate relation that expresses the average current.

$$\langle i_{\mathrm{P}}\rangle = (d_a\langle i_{\mathrm{La}}\rangle + d_b\langle i_{\mathrm{Lb}}\rangle + d_c\langle i_{\mathrm{Lc}}\rangle) \tag{2.8}$$

By summing the average capacitor current $\langle i_{\mathrm{C}}\rangle$ and the average current $\langle i_{\mathrm{P}}\rangle$ from the DC link toward the inverter switches the average input current $\langle i_{\mathrm{in}}\rangle$ is achieved.

Equation (2.9) shows the result.

$$\langle i_{\mathrm{in}} \rangle = \frac{\langle v_{\mathrm{in}} \rangle}{r_{\mathrm{C}}} - \frac{\langle v_{\mathrm{C}} \rangle}{r_{\mathrm{C}}} + (d_{\mathrm{a}} \langle i_{\mathrm{La}} \rangle + d_{\mathrm{b}} \langle i_{\mathrm{Lb}} \rangle + d_{\mathrm{c}} \langle i_{\mathrm{Lc}} \rangle) \tag{2.9}$$

The output voltages $v_{oi}$ that are to be controlled in the system can be expressed as equation (2.10) shows.

$$\langle v_{\mathrm{o}i} \rangle = \langle v_{\mathrm{Cf}i} \rangle + R_{\mathrm{d}} \langle i_{\mathrm{L}a} \rangle - R_{\mathrm{d}} \langle i_{oi} \rangle \tag{2.10}$$

Space vectors can be used to present a three phase system [40]. A three phase three component $x_{\mathrm{a}}$, $x_{\mathrm{b}}$, $x_{\mathrm{c}}$ system reduces to a two component system $x_\alpha$, $x_\beta$ and a zero component $x_0$. Equations (2.11) and (2.12) show the relation between phase domain and stationary reference frame in matrix and vector notation, respectively. In the latter case the zero component has to be calculated separately addition to vector $\mathbf{x}$ that contains the $x_\alpha$ as a real and $x_\beta$ as an imaginary component. In practice the transformation to the stationary reference frame must be made by using the operations defined in (2.11), because complex number calculation cannot be implemented easily. $K$ is the scaling factor. Throughout this thesis 2/3 is used as the scaling factor so that the transformation is amplitude invariant.

$$\begin{bmatrix} x_\alpha \\ x_\beta \\ x_0 \end{bmatrix} = K \begin{bmatrix} 1 & -1/2 & -1/2 \\ 0 & \sqrt{3}/2 & -\sqrt{3}/2 \\ 1/2 & 1/2 & 1/2 \end{bmatrix} \begin{bmatrix} x_{\mathrm{a}} \\ x_{\mathrm{b}} \\ x_{\mathrm{c}} \end{bmatrix} \tag{2.11}$$

$$\mathbf{x} = K(x_{\mathrm{a}} + x_{\mathrm{b}} \mathrm{e}^{-\mathrm{j}2\pi/3} + x_c \mathrm{e}^{\mathrm{j}4\pi/3}) \tag{2.12}$$

However, the vector notation is useful for analyzing the transformations and equations. Making use of the complex vector presentation in equation (2.12) reveals that if $x_{\mathrm{a}}$, $x_{\mathrm{b}}$ and $x_{\mathrm{c}}$ are equal, the sum is zero. This is due to the angles in the complex exponents. Thus, the common mode voltage $\langle v_{nN} \rangle$ sums to zero in the transformation. The zero component on the lower most row of (2.11) is zero in symmetric three wire systems.

By using the transformation to the stationary reference frame equation for the derivatives of the inductor currents can be presented by separate $\alpha$ and $\beta$ components. Equations (2.13) and (2.14) show the transformed equations.

$$\frac{d\left\langle i_{\mathrm{L}\alpha}\right\rangle}{dt}=\frac{1}{L}\left[d_{\alpha}\left\langle v_{\mathrm{in}}\right\rangle-\left(r_{\mathrm{L}}+r_{\mathrm{sw}}+R_{\mathrm{d}}\right)\left\langle i_{\mathrm{L}\alpha}\right\rangle+R_{\mathrm{d}}\left\langle i_{\mathrm{o}\alpha}\right\rangle-\left\langle v_{\mathrm{Cf}\alpha}\right\rangle\right] \tag{2.13}$$

$$\frac{d\left\langle i_{\mathrm{L}\beta}\right\rangle}{dt}=\frac{1}{L}\left[d_{\beta}\left\langle v_{\mathrm{in}}\right\rangle-\left(r_{\mathrm{L}}+r_{\mathrm{sw}}+R_{\mathrm{d}}\right)\left\langle i_{\mathrm{L}\beta}\right\rangle+R_{\mathrm{d}}\left\langle i_{\mathrm{o}\beta}\right\rangle-\left\langle v_{\mathrm{Cf}\beta}\right\rangle\right], \tag{2.14}$$

where subscripts $\alpha$ and $\beta$ denote alpha and beta components, respectively. It is to be noticed that there is no cross coupling between alpha and beta components and the equations are similar to the original ones. By combining equations (2.13) and (2.14) to a vector presentation advantage of vector operations can be taken. The significance of vector presentation will be shown to be important in the later analysis. The vector presentation is shown in equation (2.15)

$$\frac{d\left\langle \mathbf{i}_{\mathrm{L}}^{\alpha\beta}\right\rangle}{dt}=\frac{1}{L}\left[\mathbf{d}^{\alpha\beta}\left\langle v_{\mathrm{in}}\right\rangle-\left(r_{\mathrm{L}}+r_{\mathrm{sw}}+R_{\mathrm{d}}\right)\left\langle \mathbf{i}_{\mathrm{L}}^{\alpha\beta}\right\rangle+R_{\mathrm{d}}\left\langle \mathbf{i}_{\mathrm{o}}^{\alpha\beta}\right\rangle-\left\langle \mathbf{v}_{\mathrm{Cf}}^{\alpha\beta}\right\rangle\right] \tag{2.15}$$

where $\mathbf{d}^{\alpha\beta}$, $\left\langle \mathbf{i}_{\mathrm{L}}^{\alpha\beta}\right\rangle$, $\left\langle \mathbf{i}_{\mathrm{o}}^{\alpha\beta}\right\rangle$, $\left\langle \mathbf{v}_{\mathrm{Cf}}^{\alpha\beta}\right\rangle$ are the vectors containing of the duty ratio and averages of the inductor current, output current and capacitor voltage alpha and beta components. The transformation can be done for the equations of average filter capacitor voltages and output voltages and the results are shown in (2.16) and (2.17).

$$\frac{d\left\langle \mathbf{v}_{\mathrm{C_f}}^{\alpha\beta}\right\rangle}{dt}=\frac{1}{C_f}\left[\left\langle \mathbf{i}_{\mathrm{L}}^{\alpha\beta}\right\rangle-\left\langle \mathbf{i}_{\mathrm{o}}^{\alpha\beta}\right\rangle\right] \tag{2.16}$$

$$\left\langle \mathbf{v}_{o}^{\alpha\beta}\right\rangle=\left\langle \mathbf{v}_{\mathrm{C_f}}^{\alpha\beta}\right\rangle+R_{\mathrm{d}}\left\langle \mathbf{i}_{\mathrm{L}}^{\alpha\beta}\right\rangle-R_{\mathrm{d}}\left\langle \mathbf{i}_{\mathrm{o}}^{\alpha\beta}\right\rangle \tag{2.17}$$

Analyzing the system in the synchronous reference frame is chosen as stated previously. The space vectors in the stationary reference frame must be transformed to synchronous reference frame. Equations (2.18) and (2.19) show complex vector presentation of the transformation and its inverse, respectively. The superscript dq denotes the synchronous reference frame. Throughout this thesis terms synchronous reference frame and dq-domain are used interchangeably.

$$\mathbf{x}^{\mathrm{dq}}=\mathbf{x}^{\alpha\beta}\mathrm{e}^{-\mathrm{j}\omega_s t}=x_d+\mathrm{j}x_q \tag{2.18}$$

$$\mathbf{x}^{\alpha\beta}=\mathrm{e}^{\mathrm{j}\omega_s t}\mathbf{x}^{\mathrm{dq}}, \tag{2.19}$$

where $\mathbf{x}^{\mathrm{dq}}$ is a variable in the synchronous reference frame and $\mathbf{x}^{\alpha\beta}$ the variables in the stationary reference frame. Step by step transformation for (2.15) to the synchronous reference is shown in (2.20)–(2.23).

$$\begin{aligned}\frac{d\left\langle \mathbf{i}_{\mathrm{L}}^{\mathrm{dq}}\right\rangle \mathrm{e}^{\mathrm{j}\omega_s t}}{dt} =&\frac{1}{L}\Big[\mathbf{d}^{\mathrm{dq}}\mathrm{e}^{\mathrm{j}\omega_s t}\left\langle v_{\mathrm{in}}\right\rangle - \left(r_{\mathrm{L}}+r_{\mathrm{sw}}+R_{\mathrm{d}}\right)\left\langle \mathbf{i}_{\mathrm{L}}^{\mathrm{dq}}\right\rangle \mathrm{e}^{\mathrm{j}\omega_s t}\\ &+R_{\mathrm{d}}\left\langle \mathbf{i}_{\mathrm{o}}^{\mathrm{dq}}\right\rangle \mathrm{e}^{\mathrm{j}\omega_s t} - \left\langle \mathbf{v}_{\mathrm{Cf}}^{\mathrm{dq}}\right\rangle \mathrm{e}^{\mathrm{j}\omega_s t}\end{aligned} \tag{2.20}$$

$$\begin{aligned}\mathrm{j}\omega_{\mathrm{s}}\mathrm{e}^{\mathrm{j}\omega_{\mathrm{s}}\mathrm{t}}\left\langle \mathbf{i}_{\mathrm{L}}^{\mathrm{dq}}\right\rangle + \mathrm{e}^{\mathrm{j}\omega_{\mathrm{s}}\mathrm{t}}\frac{\mathrm{d}\left\langle \mathbf{i}_{\mathrm{L}}^{\mathrm{dq}}\right\rangle}{\mathrm{dt}} =&\frac{1}{L}\Big[\mathbf{d}^{\mathrm{dq}}\mathrm{e}^{\mathrm{j}\omega_s t}\left\langle v_{\mathrm{in}}\right\rangle\\ &-\left(r_{\mathrm{L}}+r_{\mathrm{sw}}+R_{\mathrm{d}}\right)\left\langle \mathbf{i}_{\mathrm{L}}^{\mathrm{dq}}\right\rangle \mathrm{e}^{\mathrm{j}\omega_s t}\\ &+R_{\mathrm{d}}\left\langle \mathbf{i}_{\mathrm{o}}^{\mathrm{dq}}\right\rangle \mathrm{e}^{\mathrm{j}\omega_s t} - \left\langle \mathbf{v}_{\mathrm{Cf}}^{\mathrm{dq}}\right\rangle \mathrm{e}^{\mathrm{j}\omega_s t}\end{aligned} \tag{2.21}$$

$$\begin{aligned}\mathrm{j}\omega_{\mathrm{s}}\left\langle \mathbf{i}_{\mathrm{L}}^{\mathrm{dq}}\right\rangle + \frac{\mathrm{d}\left\langle \mathbf{i}_{\mathrm{L}}^{\mathrm{dq}}\right\rangle}{\mathrm{dt}} =&\frac{1}{L}\Big[\mathbf{d}^{\mathrm{dq}}\left\langle v_{\mathrm{in}}\right\rangle - \left(r_{\mathrm{L}}+r_{\mathrm{sw}}+R_{\mathrm{d}}\right)\left\langle \mathbf{i}_{\mathrm{L}}^{\mathrm{dq}}\right\rangle\\ &+R_{\mathrm{d}}\left\langle \mathbf{i}_{\mathrm{o}}^{\mathrm{dq}}\right\rangle - \left\langle \mathbf{v}_{\mathrm{Cf}}^{\mathrm{dq}}\right\rangle\end{aligned} \tag{2.22}$$

$$\begin{aligned}\frac{d\left\langle \mathbf{i}_{\mathrm{L}}^{\mathrm{dq}}\right\rangle}{dt} =&\frac{1}{L}\Big[\mathbf{d}^{\mathrm{dq}}\left\langle v_{\mathrm{in}}\right\rangle - \left(r_{\mathrm{L}}+r_{\mathrm{sw}}+R_{\mathrm{d}}\right)\left\langle \mathbf{i}_{\mathrm{L}}^{\mathrm{dq}}\right\rangle - \mathrm{j}\omega_{\mathrm{s}}\left\langle \mathbf{i}_{\mathrm{L}}^{\mathrm{dq}}\right\rangle\\ &+R_{\mathrm{d}}\left\langle \mathbf{i}_{\mathrm{o}}^{\mathrm{dq}}\right\rangle - \left\langle \mathbf{v}_{\mathrm{Cf}}^{\mathrm{dq}}\right\rangle\end{aligned} \tag{2.23}$$

In Equation (2.20) the variables in the stationary reference frame are expressed as a inverse Clark's transformation of the corresponding *dq*-variables to the stationary reference frame. The product rule for derivatives is applied in (2.21). At the next step in (2.22) the both sides of the equation are divided by the inverse transformation operator. Equation (2.23) shows the end result. It should noted that there is a cross coupling between d- and q-components. In order to clarify the effect of cross coupling, the vector notation is divided to d and q components in (2.24) and (2.25).

$$\frac{d\left\langle i_{\mathrm{Ld}}\right\rangle}{dt} = \frac{1}{L}\left[d_{\mathrm{d}}\left\langle v_{\mathrm{in}}\right\rangle - \left(r_{\mathrm{L}}+r_{\mathrm{sw}}+R_{\mathrm{d}}\right)\left\langle i_{\mathrm{Ld}}\right\rangle + \omega_s i_{\mathrm{Lq}} + R_{\mathrm{d}}\left\langle i_{\mathrm{od}}\right\rangle - \left\langle v_{\mathrm{Cfd}}\right\rangle\right] \tag{2.24}$$

$$\frac{d\left\langle i_{\mathrm{Lq}}\right\rangle}{dt} = \frac{1}{L}\left[d_{\mathrm{q}}\left\langle v_{\mathrm{in}}\right\rangle - \left(r_{\mathrm{L}}+r_{\mathrm{sw}}+R_{\mathrm{d}}\right)\left\langle i_{\mathrm{Lq}}\right\rangle - \omega_s i_{\mathrm{Ld}} + R_{\mathrm{d}}\left\langle i_{\mathrm{oq}}\right\rangle - \left\langle v_{\mathrm{Cfq}}\right\rangle\right] \tag{2.25}$$

In the above equations subscripts d and q denote if the corresponding variable is the direct or quadrature component of the vector. The equations for derivatives of the filter capacitor voltage in dq-domain can be derived similarly. The filter capacitor

equations are shown in (2.26) and (2.27).

$$\frac{d\langle v_{\mathrm{Cfd}}\rangle}{dt} = \frac{1}{C_f}\left[\langle i_{\mathrm{Ld}}\rangle + \omega_s v_{\mathrm{Cfq}} - \langle i_{\mathrm{od}}\rangle\right] \tag{2.26}$$

$$\frac{d\langle v_{\mathrm{Cfq}}\rangle}{dt} = \frac{1}{C_{\mathrm{f}}}\left[\langle i_{\mathrm{Lq}}\rangle - \omega_s v_{\mathrm{Cfd}} - \langle i_{\mathrm{oq}}\rangle\right] \tag{2.27}$$

Equation 2.7 for the derivative of the input capacitor voltage remains unchanged, because coordinate transformation are only used on three phase AC variables. The average input current can be calculate from dq-variables as Equation (2.28) shows.

$$\langle i_{in}\rangle = \langle i_C\rangle + \langle i_P\rangle = \frac{\langle v_{in}\rangle}{r_C} - \frac{\langle v_C\rangle}{r_C} + \frac{3}{2}\left(d_{\mathrm{d}}\langle i_{\mathrm{Ld}}\rangle + d_{\mathrm{q}}\langle i_{\mathrm{Lq}}\rangle\right) \tag{2.28}$$

The output voltages are solved in dq-domain in equations (2.29) and (2.30).

$$\langle v_{\mathrm{od}}\rangle = \langle v_{\mathrm{Cfd}}\rangle + R_{\mathrm{d}}\langle i_{\mathrm{Ld}}\rangle - R_{\mathrm{d}}\langle i_{\mathrm{od}}\rangle \tag{2.29}$$

$$\langle v_{\mathrm{oq}}\rangle = \langle v_{\mathrm{Cfq}}\rangle + R_{\mathrm{d}}\langle i_{\mathrm{Lq}}\rangle - R_{\mathrm{d}}\langle i_{\mathrm{oq}}\rangle \tag{2.30}$$

### 2.3.2 Steady-State Operating Point

In order to derive transfer functions and use linear controllers for the systems the system must be linearized in an operation point [41]. The equations in the dq-domain are inspected in steady-state. Capital letters are used to denote steady state. In steady-state the value of all derivatives is zero. Output current q-component $I_{\mathrm{oq}}$ is defined zero and output voltage q-component $V_{\mathrm{oq}}$ is chosen zero so that the synchronous reference frame is aligned with the d-component. Now the filter capacitor voltage q-component can be solved from (2.30) that is presented in (2.31) in the steady-state. Equation (2.32) shows an intermediate solution for $V_{\mathrm{Cfq}}$.

$$V_{\mathrm{oq}} = R_{\mathrm{d}}I_{\mathrm{Lq}} - R_{\mathrm{d}}I_{\mathrm{oq}} + V_{\mathrm{Cfq}} \tag{2.31}$$

$$V_{\mathrm{Cfq}} = -R_{\mathrm{d}}I_{\mathrm{Lq}} \tag{2.32}$$

Inductor current d-component in steady-state can be solved from (2.33) as the capacitor voltage derivative is zero. Solved $V_{\mathrm{Cfq}}$ from (2.32) can be substituted to

(2.34). The solution is shown in (2.35).

$$\frac{1}{C_\mathrm{f}} I_\mathrm{Ld} + \omega_\mathrm{s} V_\mathrm{Cfq} - \frac{1}{C_\mathrm{f}} I_\mathrm{od} = 0 \tag{2.33}$$

$$I_\mathrm{Ld} = I_\mathrm{od} - \omega_\mathrm{s} C_\mathrm{f} V_\mathrm{Cfq} \tag{2.34}$$

$$I_\mathrm{Ld} = I_\mathrm{od} + \omega_\mathrm{s} C_\mathrm{f} (R_\mathrm{d} I_\mathrm{Lq}) \tag{2.35}$$

The solved $I_\mathrm{Ld}$ can be substituted to (2.36). The equation for $V_\mathrm{od}$ reduces then to (2.37).

$$V_\mathrm{od} = R_\mathrm{d} I_\mathrm{Ld} - R_\mathrm{d} I_\mathrm{od} + V_\mathrm{Cfd} \tag{2.36}$$

$$V_\mathrm{od} = V_\mathrm{Cfd} + R_\mathrm{d}^2 \omega_\mathrm{s} C_\mathrm{f} I_\mathrm{Lq} \tag{2.37}$$

Equation (2.38) shows a steady state relation from which the inductor current q-component can be solved. Since $I_\mathrm{oq}$ is zero, the solution reduces to (2.39).

$$\frac{1}{C_\mathrm{f}} I_\mathrm{Lq} - \omega_\mathrm{s} V_\mathrm{Cfd} - \frac{1}{C_\mathrm{f}} I_\mathrm{oq} = 0 \tag{2.38}$$

$$I_\mathrm{Lq} = \omega_\mathrm{s} C_\mathrm{f} V_\mathrm{Cfd} \tag{2.39}$$

Solved $I_\mathrm{Lq}$ from (2.39) can be substituted to (2.37). Capacitor voltage d-component can be expressed as a function of input variable $V_\mathrm{od}$ as shown in (2.40).

$$V_\mathrm{Cfd} = \frac{1}{1 + R_\mathrm{d}^2 \omega_\mathrm{s}^2 C_\mathrm{f}^2} V_\mathrm{od} \tag{2.40}$$

$I_\mathrm{Lq}$ from Equation (2.39) is known now and so is $V_\mathrm{Cfq}$ from (2.32). $I_\mathrm{Ld}$ is shown in (2.34) as a function of known variables. Equations (2.24) and (2.25) contain duty ratio d-and q-components $D_\mathrm{d}$ and $D_\mathrm{q}$ when written in the steady state. All other variables in the operation point are known now. Equations (2.41) and (2.42) show the solved steady-state duty ratios $D_\mathrm{d}$ and $D_\mathrm{q}$.

$$D_\mathrm{d} = \frac{(r_\mathrm{sw} + r_\mathrm{L} + R_\mathrm{d}) I_\mathrm{Ld} - \omega_\mathrm{s} L I_\mathrm{Lq} - R_\mathrm{d} I_\mathrm{od} + V_\mathrm{Cfd}}{V_\mathrm{in}} \tag{2.41}$$

$$D_{\mathrm{q}} = \frac{(r_{\mathrm{sw}} + r_{\mathrm{L}} + R_{\mathrm{d}})I_{\mathrm{Lq}} + \omega_{\mathrm{s}} L I_{\mathrm{Ld}} - R_{\mathrm{d}} I_{\mathrm{oq}} + V_{\mathrm{Cfq}}}{V_{\mathrm{in}}} \tag{2.42}$$

### 2.3.3 Linearization

The model must be linearized in the steady state operation point. Linearization is done by taking derivatives of the equations in respect to all variables separately and multiplied by the small signal variation of the variable [27]. It corresponds to the first degree Taylor series approximation. This means that the system is considered linear around the steady state operating point. The linearized equations for state derivatives and outputs are shown in (2.43–2.50).

$$\frac{d\hat{i}_{\mathrm{Ld}}}{dt} = -\frac{(r_{\mathrm{L}} + r_{\mathrm{sw}} + R_{\mathrm{d}})}{L}\hat{i}_{\mathrm{Ld}} + \omega_{\mathrm{s}}\hat{i}_{\mathrm{Lq}} - \frac{1}{L}\hat{v}_{\mathrm{Cfd}} + \frac{D_d}{L}\hat{v}_{\mathrm{in}} + \frac{R_{\mathrm{d}}}{L}\hat{i}_{\mathrm{od}} + \frac{V_{\mathrm{in}}}{L}\hat{d}_{\mathrm{d}} \tag{2.43}$$

$$\frac{d\hat{i}_{\mathrm{Lq}}}{dt} = -\frac{(r_{\mathrm{L}} + r_{\mathrm{sw}} + R_{\mathrm{d}})}{L}\hat{i}_{\mathrm{Lq}} - \omega_{\mathrm{s}}\hat{i}_{\mathrm{Ld}} - \frac{1}{L}\hat{v}_{\mathrm{Cfq}} + \frac{D_{\mathrm{q}}}{L}\hat{v}_{\mathrm{in}} + \frac{R_{\mathrm{d}}}{L}\hat{i}_{\mathrm{oq}} + \frac{V_{\mathrm{in}}}{L}\hat{d}_{\mathrm{q}} \tag{2.44}$$

$$\frac{d\hat{v}_{\mathrm{Cfd}}}{dt} = \frac{1}{C_{\mathrm{f}}}\hat{i}_{\mathrm{Ld}} + \omega_{\mathrm{s}}\hat{v}_{\mathrm{Cfq}} - \frac{1}{C_{\mathrm{f}}}\hat{i}_{\mathrm{od}} \tag{2.45}$$

$$\frac{d\hat{v}_{\mathrm{Cfq}}}{dt} = \frac{1}{C_{\mathrm{f}}}\hat{i}_{\mathrm{Lq}} - \omega_{\mathrm{s}}\hat{v}_{\mathrm{Cfd}} - \frac{1}{C_{\mathrm{f}}}\hat{i}_{\mathrm{oq}} \tag{2.46}$$

$$\frac{d\hat{v}_C}{dt} = -\frac{1}{r_C C}\hat{v}_C + \frac{1}{r_C C}\hat{v}_{in} \tag{2.47}$$

$$\hat{i}_{in} = -\frac{1}{r_C}\hat{v}_C + \frac{1}{r_C}\hat{v}_{in} + \frac{3}{2}D_d\hat{i}_{Ld} + \frac{3}{2}D_q\hat{i}_{Lq} + \frac{3}{2}I_{Ld}\hat{d}_d + \frac{3}{2}I_{Lq}\hat{d}_q \tag{2.48}$$

$$\hat{v}_{\mathrm{od}} = R_{\mathrm{d}}\hat{i}_{\mathrm{Ld}} - R_{\mathrm{d}}\hat{i}_{\mathrm{od}} + \hat{v}_{\mathrm{Cfd}} \tag{2.49}$$

$$\hat{v}_{\mathrm{oq}} = R_{\mathrm{d}}\hat{i}_{\mathrm{Lq}} - R_{\mathrm{d}}\hat{i}_{\mathrm{oq}} + \hat{v}_{\mathrm{Cfq}} \tag{2.50}$$

Hats over the variables denote small signals. The variables are organized in the equations so that first are the input variables followed by the state variables. Equation (2.51) shows the inputs and the outputs as well the states in the vector notation. The input and output variables are arranged among themselves from the DC side to the AC side.

$$\hat{\mathbf{u}} = \begin{bmatrix} \hat{v}_{\mathrm{in}} \\ \hat{i}_{\mathrm{od}} \\ \hat{i}_{\mathrm{oq}} \\ \hat{d}_{\mathrm{d}} \\ \hat{d}_{\mathrm{q}} \end{bmatrix} \quad \hat{\mathbf{y}} = \begin{bmatrix} \hat{i}_{\mathrm{in}} \\ \hat{i}_{\mathrm{Ld}} \\ \hat{i}_{\mathrm{Lq}} \\ \hat{v}_{\mathrm{od}} \\ \hat{v}_{\mathrm{oq}} \end{bmatrix} \quad \hat{\mathbf{x}} = \begin{bmatrix} \hat{i}_{\mathrm{Ld}} \\ \hat{i}_{\mathrm{Lq}} \\ \hat{v}_{\mathrm{Cfd}} \\ \hat{v}_{\mathrm{Cfq}} \\ \hat{v}_{\mathrm{C}} \end{bmatrix}, \tag{2.51}$$

where $\mathbf{u}$, $\mathbf{y}$ and $\mathbf{x}$ stand for input vector, output vector and state vector, respectively. By using the vectors and collecting the coefficients from (2.43–2.50) the linearized state-space model can expressed in (2.52) similarly as it has been done in [42].

$$\begin{aligned} \frac{\mathrm{d}\hat{\mathbf{x}}}{\mathrm{dt}} &= \mathbf{A}\hat{\mathbf{x}} + \mathbf{B}\hat{\mathbf{u}} \\ \hat{\mathbf{y}} &= \mathbf{C}\hat{\mathbf{x}} + \mathbf{D}\hat{\mathbf{u}} \end{bmatrix} \tag{2.52}$$

where matrices $\mathbf{A}$, $\mathbf{B}$, $\mathbf{C}$ and $\mathbf{D}$ are coefficient matrices. The matrices are shown in (2.53)–(2.55).

$$\mathbf{A} = \begin{bmatrix} -\frac{(r_{\mathrm{L}}+r_{\mathrm{sw}}+R_{\mathrm{d}})}{L} & \omega_{\mathrm{s}} & -\frac{1}{L} & 0 & 0 \\ -\omega_{\mathrm{s}} & -\frac{(r_{\mathrm{L}}+r_{\mathrm{sw}}+R_{\mathrm{d}})}{L} & 0 & -\frac{1}{L} & 0 \\ \frac{1}{C_{\mathrm{f}}} & 0 & 0 & \omega_{\mathrm{s}} & 0 \\ 0 & \frac{1}{C_{\mathrm{f}}} & -\omega_{\mathrm{s}} & 0 & 0 \\ 0 & 0 & 0 & 0 & -\frac{1}{r_{\mathrm{C}}C} \end{bmatrix} \tag{2.53}$$

$$\mathbf{B} = \begin{bmatrix} \frac{D_{\mathrm{d}}}{L} & \frac{R_{\mathrm{d}}}{L} & 0 & \frac{V_{\mathrm{in}}}{L} & 0 \\ \frac{D_{\mathrm{q}}}{L} & 0 & R_{\mathrm{d}} & 0 & \frac{V_{\mathrm{in}}}{L} \\ 0 & -\frac{1}{C_{\mathrm{f}}} & 0 & 0 & 0 \\ 0 & 0 & -\frac{1}{C_{\mathrm{f}}} & 0 & 0 \\ \frac{1}{r_{\mathrm{C}}C} & 0 & 0 & 0 & 0 \end{bmatrix} \quad \mathbf{C} = \begin{bmatrix} \frac{3D_{\mathrm{d}}}{2} & \frac{3D_{\mathrm{q}}}{2} & 0 & 0 & \frac{-1}{r_{\mathrm{C}}} \\ 1 & 0 & 0 & 0 & 0 \\ 0 & 1 & 0 & 0 & 0 \\ R_{\mathrm{d}} & 0 & 1 & 0 & 0 \\ 0 & R_{\mathrm{d}} & 0 & 1 & 0 \end{bmatrix} \tag{2.54}$$

$$\mathbf{D} = \begin{bmatrix} \frac{1}{r_{\mathrm{C}}} & 0 & 0 & \frac{3I_{\mathrm{Ld}}}{2} & \frac{3I_{\mathrm{Lq}}}{2} \\ 0 & 0 & 0 & 0 & 0 \\ 0 & 0 & 0 & 0 & 0 \\ 0 & -R_{\mathrm{d}} & 0 & 0 & 0 \\ 0 & 0 & -R_{\mathrm{d}} & 0 & 0 \end{bmatrix} \tag{2.55}$$

## 2.4 Open-Loop Dynamics

### 2.4.1 Deriving Transfer Functions

In order to solve the transfer functions (2.52) is transferred to frequency domain. Equation (2.56) shows the frequency domain notation.

$$\begin{aligned} s\mathbf{X}(s) &= \mathbf{A}\mathbf{X}(s) + \mathbf{B}\mathbf{U}(s) \\ \mathbf{Y}(s) &= \mathbf{C}\mathbf{X}(s) + \mathbf{D}\mathbf{U}(s) \end{aligned} \tag{2.56}$$

The transfer functions from the inputs to the outputs can be solved as shown in (2.57).

$$\mathbf{Y}(s) = \overbrace{\left(\mathbf{C}(s\mathbf{I} - \mathbf{A})^{-1}\mathbf{B} + \mathbf{D}\right)}^{\mathbf{G}}\mathbf{U}(s), \tag{2.57}$$

where matrix $\mathbf{G}$ contains the transfer functions. Equation (2.58) shows the expanded transfer function matrix.

$$\begin{bmatrix} \hat{i}_{\mathrm{in}} \\ \hat{i}_{\mathrm{Ld}} \\ \hat{i}_{\mathrm{Lq}} \\ \hat{v}_{\mathrm{od}} \\ \hat{v}_{\mathrm{oq}} \end{bmatrix} = \begin{bmatrix} Y_{\mathrm{in-o}} & T_{\mathrm{oid-o}} & T_{\mathrm{oiq-o}} & G_{\mathrm{cid-o}} & G_{\mathrm{ciq-o}} \\ G_{\mathrm{ioLd-o}} & G_{\mathrm{oLd-o}} & G_{\mathrm{oLqd-o}} & G_{\mathrm{cLd-o}} & G_{\mathrm{cLqd-o}} \\ G_{\mathrm{ioLq-o}} & G_{\mathrm{oLdq-o}} & G_{\mathrm{oLq-o}} & G_{\mathrm{cLdq-o}} & G_{\mathrm{cLq-o}} \\ G_{\mathrm{iod-o}} & -Z_{\mathrm{od-o}} & -Z_{\mathrm{oqd-o}} & G_{\mathrm{cod-o}} & G_{\mathrm{coqd-o}} \\ G_{\mathrm{ioq-o}} & -Z_{\mathrm{odq-o}} & -Z_{\mathrm{oq-o}} & G_{\mathrm{codq-o}} & G_{\mathrm{coq-o}} \end{bmatrix} \begin{bmatrix} \hat{v}_{\mathrm{in}} \\ \hat{i}_{\mathrm{od}} \\ \hat{i}_{\mathrm{oq}} \\ \hat{d}_{\mathrm{d}} \\ \hat{d}_{\mathrm{q}} \end{bmatrix}, \tag{2.58}$$

where elements of the matrix are the transfer functions. Because the converter is voltage fed and voltage output the system is defined by G-parameters.

The subscripts of the elements define in order the input variable, output variable, necessary information on the d- and q-components and if there are closed control loops in the system. For example $G_{\mathrm{cLdq-o}}$ is the transfer function from the control d-component (i.e. duty ratio d-component) to the inductor current q-component in the open-loop system. Exceptions are the transfer functions from output terminal to input terminal, input side to input side and output side to output side. Transmittances $T_{\mathrm{oid-o}}$ and $T_{\mathrm{oiq-o}}$ denote transfer functions from the output-side terminal to the input-side terminal. The transfer function from the input voltage to the input current is input admittance $Y_{\mathrm{in-o}}$. The transfer functions from the output currents to the output voltages are denoted by $-Z_{\mathrm{od-o}}$, $-Z_{\mathrm{oqd-o}}$, $-Z_{\mathrm{odq-o}}$ and $-Z_{\mathrm{oq-o}}$. The minus is required in front of the impedances because the output current is defined

to flow away from the inverter. Thus, the sign convention of impedance is fulfilled. In oder to facilitate further analysis the notation of (2.58) is condensed. The d- and q-components of the same variable are replaced by vectors and transfer functions are collected to transfer matrices. Equation (2.59) shows the condensed notation.

$$\begin{bmatrix} \widehat{i}_{\mathrm{in}} \\ \widehat{\mathbf{i}}_{\mathrm{L}} \\ \widehat{\mathbf{v}}_{\mathrm{o}} \end{bmatrix} = \begin{bmatrix} \mathbf{Y}_{\mathrm{in-o}} & \mathbf{T}_{\mathrm{oi-o}} & \mathbf{G}_{\mathrm{ci-o}} \\ \mathbf{G}_{\mathrm{iL-o}} & \mathbf{G}_{\mathrm{oL-o}} & \mathbf{G}_{\mathrm{cL-o}} \\ \mathbf{G}_{\mathrm{io-o}} & -\mathbf{Z}_{\mathrm{o-o}} & \mathbf{G}_{\mathrm{co-o}} \end{bmatrix} \begin{bmatrix} \widehat{v}_{\mathrm{in}} \\ \widehat{\mathbf{i}}_{\mathrm{o}} \\ \widehat{\mathbf{d}} \end{bmatrix} \tag{2.59}$$

This matrix notation is useful when calculating closed loop systems, because the effect of cross coupling is automatically taken into account. Matrices are chosen so that matrix multiplication gives the same result as scalar calculation. Matrices $\mathbf{Y}_{\mathrm{in-o}}$ and $\mathbf{Z}_{\mathrm{o-o}}$ are shown in (2.60) for example.

$$\mathbf{Y}_{\mathrm{in-o}} = \begin{bmatrix} Y_{\mathrm{in-o}} & 0 \\ 0 & 0 \end{bmatrix} \mathbf{Z}_{\mathrm{o-o}} = \begin{bmatrix} Z_{\mathrm{o-d}} & Z_{\mathrm{oqd-o}} \\ Z_{\mathrm{odq-o}} & Z_{\mathrm{od-o}} \end{bmatrix} \tag{2.60}$$

It is to be noted that as the minus sign is in (2.59) in front of $\mathbf{Z}_{\mathrm{o-o}}$ there are no minus signs in front of the elements of $\mathbf{Z}_{\mathrm{o-o}}$. All matrices are shown in detail in Appendix A. Figure 2.6 shows a small signal diagram of the grid-forming inverter.

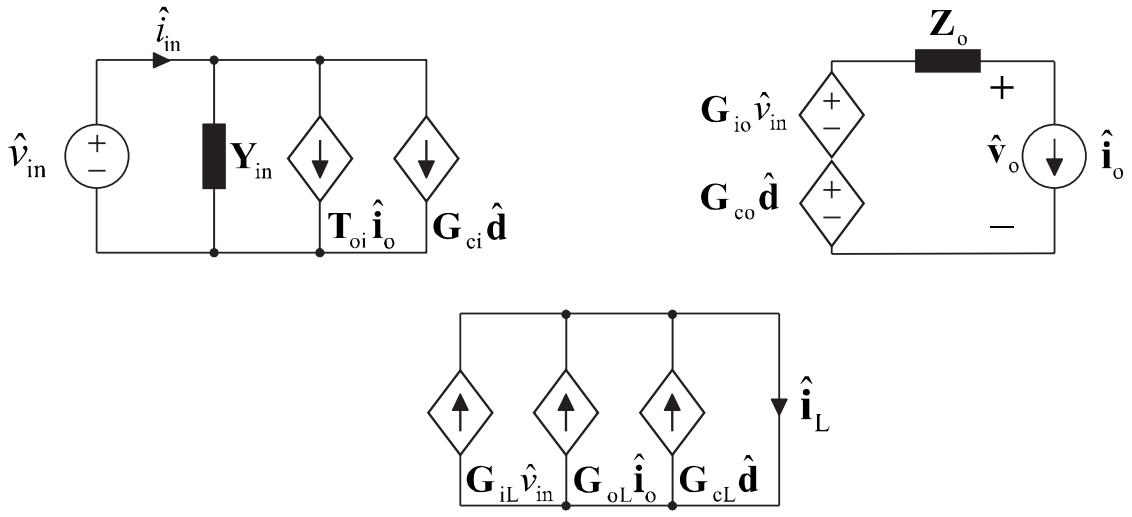


***Figure 2.6*** *Small-signal diagram of the grid-forming inverter.*

The diagrams in Fig. 2.6 visualize the dependencies of the variables. The subscript o that would denote open-loop is omitted from the matrices, because the the same diagrams can be used also in the case of closed-loop transfer functions.

### 2.4.2 Comparison to Open-Loop Dynamics of Grid-Feeding Inverter

The grid-forming inverter is analyzed with parameters that have been used in research of the grid-feeding inverter in [24]. A damping resistor of 2.00 Ω is added to the system that is not present in the grid-feeding inverter. The parameters are shown in Table 2.1. It is to be noted that the formed grid is a three phase 60 Hz 120 V system. As stated earlier the grid side inductor is not taken into account in the dynamical analysis of the grid-forming inverter. Thus, the grid-side inductor $L_2$ is needed only for purposes of comparison between the dynamics of the operation modes. Table 2.2 shows the parameter values in the steady state operating point. The voltage 120 V is the root mean square (rms) phase voltage of the system. Since amplitude invariant transformation is used, the output voltage d-component $V_{\mathrm{od}}$ is the peak value of the sinusoidal voltage. The parameters and solved steady-state values in (2.31)–(2.42) are applied to the derived model equations in (2.43)–(2.50) and the transfer functions are solved.

Figure 2.7 shows the frequency response of $G_{\mathrm{cLd-o}}$. In addition to the frequency response of the derived transfer function a simulated frequency response is shown. The simulated frequency response is measured from a Matlab Simulink model of the system and it is used to verify the derived model. Figure 2.7 shows that the correlation between the simulated frequency response and the derived model is exact. The model derived by the state-space averaging method is valid up to half the switching frequency [42]. Thus, the frequency response is shown up to the frequency of 4 kHz that is sufficient for the purposes of dynamic analysis. Half the switching frequency $f_{\mathrm{s}}$ is 5 kHz.

***Table 2.1*** *Inverter parameter values*

| Parameter | Value | Parameter | Value |
|---|---|---|---|
| $C$ | 1.9 mF | $r_{\mathrm{C}}$ | 100 mΩ |
| $L$ | 2.5 mH | $r_{\mathrm{L}}$ | 25 mΩ |
| $L_2$ | 0.6 mH | $r_{\mathrm{L2}}$ | 22 mΩ |
| $C_{\mathrm{f}}$ | 10 $\mu$F | $R_{\mathrm{d}}$ | 2.1 Ω |
| $f_{\mathrm{s}}$ | 10 kHz | $r_{\mathrm{sw}}$ | 10 mΩ |
| $\omega_{\mathrm{s}}$ | 2$\pi$60 Hz | | |

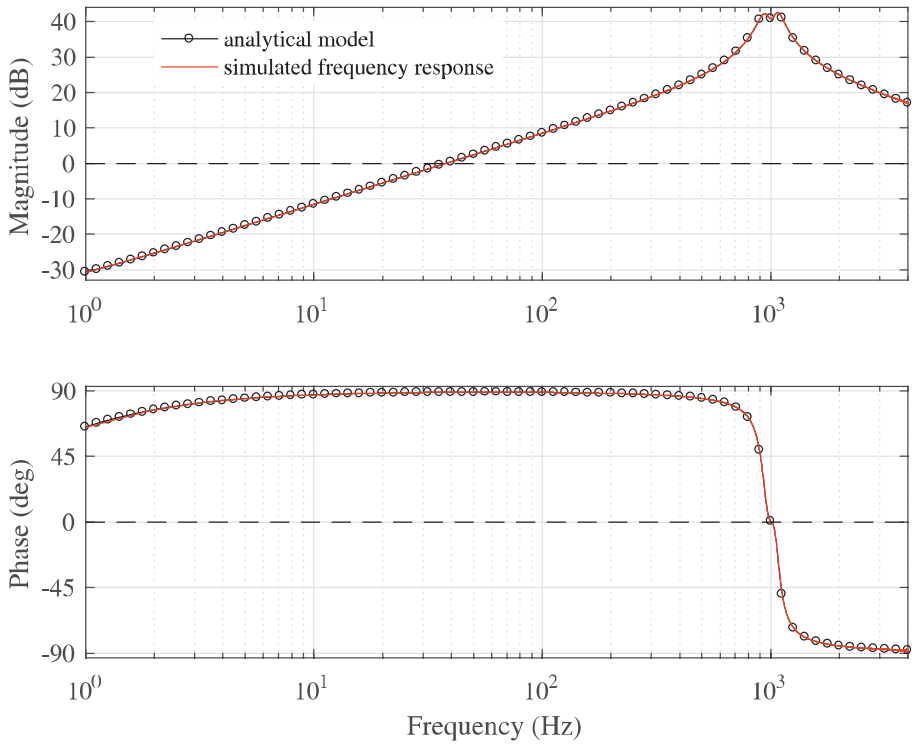


***Figure 2.7*** *Simulated frequency response (solid line) and model based frequency response (dotted line) of* $G_{\mathrm{cLd-o}}$.

As explained earlier the grid-forming inverter is controlled by a cascaded controller. The control-to-inductor d and q-component transfer functions $G_{\mathrm{cLd-o}}$ and $G_{\mathrm{cLq-o}}$ are identical. Thus, similar controllers can be used for both d- and q-components. It would be straightforward if the same tuning of the current controllers could be used both in the grid-feeding and grid-forming modes. Therefore, comparison between the frequency responses of $G_{\mathrm{cLd-o}}$ in the both operation modes needs to be made. Appendix B shows the averaged and linearized equations in dq-domain that have been used to develop the state-space model and transfer functions of the grid-feeding inverter that is used in the comparison. A voltage source is shown as an alternative input source for the grid-feeding inverter in Section 2.1 in Fig. 2.2. The grid-feeding inverter is considered to be voltage fed now.

***Table 2.2*** *Operating point values*

| Parameter | Value | Parameter | Value |
|---|---|---|---|
| $V_{\mathrm{od}}$ | 169.7 V | $V_{\mathrm{oq}}$ | 0.0000 V |
| $I_{\mathrm{od}}$ | 27.49 A | $I_{\mathrm{oq}}$ | 0.0000 A |
| $I_{\mathrm{Ld}}$ | 27.50 A | $I_{\mathrm{Lq}}$ | 0.6397 A |
| $V_{\mathrm{Cfd}}$ | 169.7 V | $V_{\mathrm{Cfq}}$ | -1.286 V |
| $V_{\mathrm{in}}$ | 416.0 V | $I_{\mathrm{in}}$ | 16.93 A |
| $D_{\mathrm{d}}$ | 0.4088 | $D_{\mathrm{q}}$ | 0.0624 |

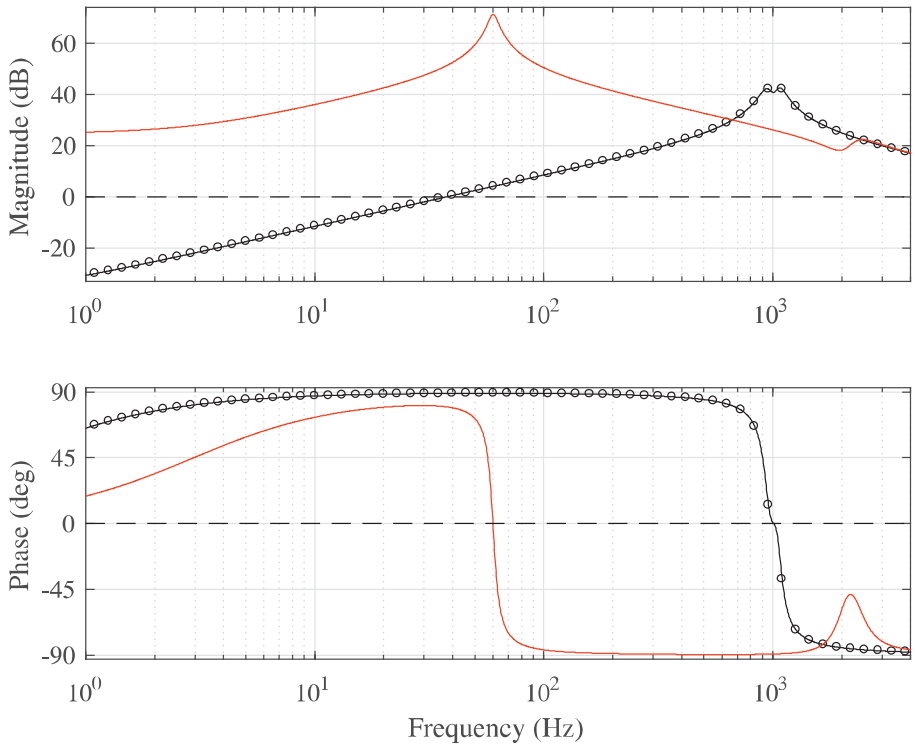


***Figure 2.8*** *Frequency response of $G_{\mathrm{cLd-o}}$ in the grid-forming mode (dotted line) and in the grid-feeding mode (thin line).*

Obviously the inverter component parameters are the same in the grid-feeding operation. Nevertheless, in the grid-feeding mode the grid side inductor $L_2$ of the LCL-filter is taken into account and it affects the dynamics of the grid-feeding inverter. Therefore, an additional resonance can be seen in the frequency response of the grid-feeding inverter. Figure 2.8 shows frequency responses of $G_{\mathrm{cLd-o}}$ in the grid-forming and grid-feeding modes. A significant difference can be seen in the frequency responses. The gain of the grid-forming inverter is low at high frequencies, whereas the gain of the grid-feeding inverter is low. In the case of the grid-feeding operation the frequency response contains a parallel resonance at 60 Hz that comes from the coordinate transformation. The resonances at around 2 kHz stem from the LCL-filter. The parallel resonance is at 1kHz in the case of the grid-forming inverter. Due to the different locations of the resonances the phase drops at different frequencies in different modes. Generally speaking the frequency responses differ considerably from each other apart from the high frequencies above 3 kHz.

The differences in the transfer functions can be understood by analyzing simplified dynamics of both inverters. Figure 2.9(a) shows a single-phase circuit that can be used to analyze dynamics of the grid-feeding inverter. In order to analyze the dynamics from the duty ratio to the inductor current a steady state operation must be assumed. Small signal perturbation is made to the duty-ratio and it is analyzed,

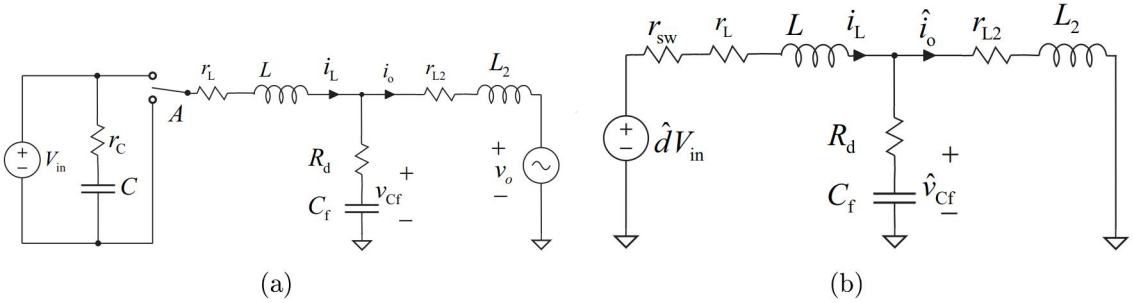


***Figure 2.9*** *a) Single-phase equivalent circuit b) Linearized DC circuit for the dynamic analysis of the grid-feeding inverter.*

how it affects the state and output variables. Other input variables than the duty ratio are kept constant. On the basis of the previous, a DC-model is derived for dynamic analysis and it is shown in Fig. 2.9(b). The DC-model approximates the d or q-channel of the dq-system that has been presented by equations in the previous section. The voltage source presenting grid-voltages is replaced by a short circuit. This stems from dynamic model of the voltage source. The grid voltage is an input variable that is kept constant, because only the dynamics from the duty ratio to the inductor current are inspected. Thus, small signal perturbation in other variables on the system have no effect on the voltage source. However, the current through an ideal voltage source is defined by the circuit that is connected to the terminals of the source. Only the perturbations outside the source are taken into account. Hence, in the small signal sense a constant voltage source is presented by a short circuit.

It is approximated that the short circuit branch draws all the current and the capacitor branch does not need to be taken into account. This is a significant simplification, but it is done in order to highlight the differences between the grid-feeding and grid-forming modes later. The current through the inductors $L$ and $L_2$ is same. Equation (2.61) is formed on basis of this.

$$\frac{d\hat{i}_{\mathrm{L}}}{dt} = \frac{V_{\mathrm{in}}}{L+L_2}\hat{d} - \frac{r_{sw}+r_{\mathrm{L}}+r_{\mathrm{L2}}}{L+L_2}\hat{i}_{\mathrm{L}} \tag{2.61}$$

The derivative is replaced by the Laplace variable s and the relation from $\hat{i}_{\mathrm{L}}$ to $\hat{d}$ is solved in (2.62).

$$G_{\mathrm{cL-o}} = \frac{\hat{i}_{\mathrm{L}}}{\hat{d}} = \frac{V_{\mathrm{in}}}{(L+L_2)\,s + r_{sw} + r_{\mathrm{L}} + r_{\mathrm{L2}}} \tag{2.62}$$

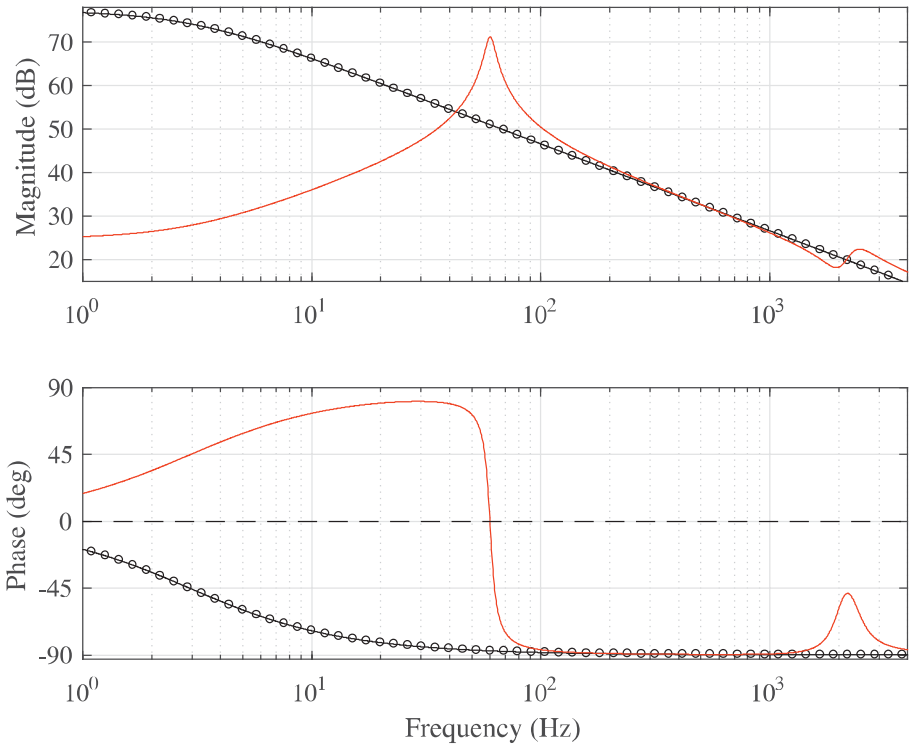


***Figure 2.10*** *Frequency response of the transfer function from the duty ratio to the inductor current by the simple model (dotted line) and the state space average model (thin line) in the grid-feeding mode.*

The accuracy of this less lengthy approach is compared to the $G_{\mathrm{cLd-o}}$ of the LCL-filtered grid-feeding inverter in Fig. 2.10. It can be seen that there is great difference in the simple model and in the complete state space average model. However, with the given parameters the dynamic behavior of the phase of the simple model corresponds to the state-space averaged model at frequencies ranging from 200 Hz to 1 Khz. The accuracy at this frequency range is particularly important because the crossover frequency of the current loop is commonly within it. Comparison between the frequency responses of the simplified transfer of the grid-feeding inverter and the state-space average model of the grid-forming inverter in Fig. 2.10 shows that the simplified model cannot be used to tune the current controller of the inverter in the grid-forming mode.

A simplified single-phase model is derived for the grid-forming inverter. Figure2.11(a) shows a single-phase equivalent circuit that can be used to analyze the dynamics in a more convenient way. As in the case of the grid-feeding inverter only the dynamics from the duty ratio to the inductor current are analyzed. The load current is kept constant. Thus, the load current is not affected by the small signal perturbations in the input and state variables. However, the voltage over the constant current sink is dependent on circuit connected to its terminals. Figure2.11(b) shows a DC circuit

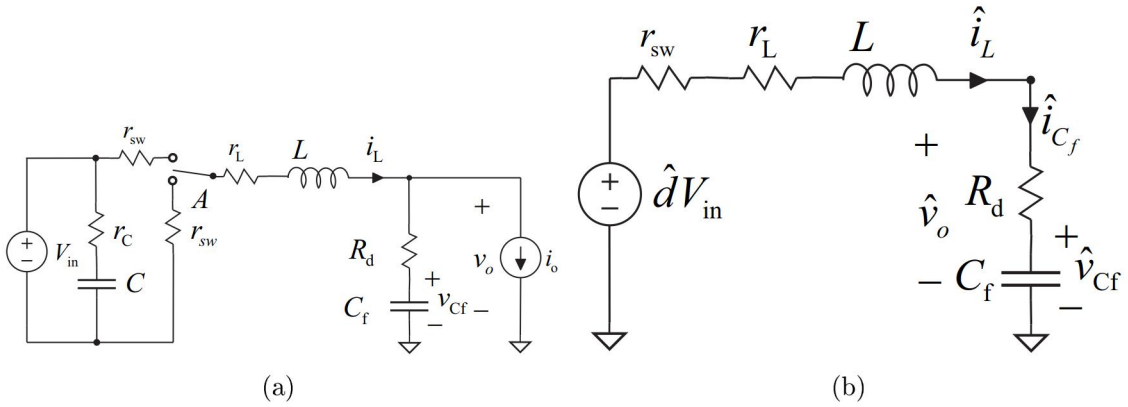


***Figure 2.11*** *a) Single-phase equivalent circuit b) Linearized DC circuit for the dynamic analysis of the grid-forming inverter.*

where the constant current sink is replace by an open branch in order to model the above mentioned small signal behavior.

Equation for the derivative of the inductor current is shown in (2.63). The circuit diagram in Fig. 2.11(b) shows that there is no other path for the inductor current than capacitor. Due to this small signal changes in the filter capacitor voltage has to be taken into account. The small signal derivative of the filter capacitor voltage can expressed as in (2.64). Equation (2.65) shows the filter capacitor small signal dependency on the inductor current. The expression in (2.65) can be substituted to (2.63). The equation after the substitution is shown in (2.66).

$$\frac{d\hat{i}_{\mathrm{L}}}{dt} = \frac{V_{\mathrm{in}}}{L}\hat{d} - \frac{r_{sw} + r_{\mathrm{L}}}{L}\hat{i}_{\mathrm{L}} - \frac{R_{\mathrm{d}}}{L}\hat{i}_{\mathrm{L}} - \frac{1}{L}\hat{v}_{\mathrm{C_f}} \tag{2.63}$$

$$\frac{d\hat{v}_{\mathrm{C_f}}}{dt} = \frac{1}{C_{\mathrm{f}}}\hat{i}_{\mathrm{C_f}} \tag{2.64}$$

$$\hat{v}_{\mathrm{C_f}} = \frac{1}{sC_{\mathrm{f}}}\hat{i}_{\mathrm{L}} \tag{2.65}$$

$$s\hat{i}_{\mathrm{L}} = \frac{V_{\mathrm{in}}}{L}\hat{d} - \frac{r_{sw} + r_{\mathrm{L}} + R_{\mathrm{d}}}{L}\hat{i}_{\mathrm{L}} - \frac{1}{L}\frac{1}{sC_{\mathrm{f}}}\hat{i}_{\mathrm{L}} \tag{2.66}$$

Equation (2.67) shows the solved simplified $G_{\mathrm{cLd-o}}$.

$$G_{\mathrm{cL-o}} = \frac{\hat{i}_{\mathrm{L}}}{\hat{d}} = \frac{\frac{V_{\mathrm{in}}}{L}s}{s^2 + \frac{(r_{sw}+r_{\mathrm{L}}+R_{\mathrm{d}})}{L}s + \frac{1}{LC_{\mathrm{f}}}} \tag{2.67}$$

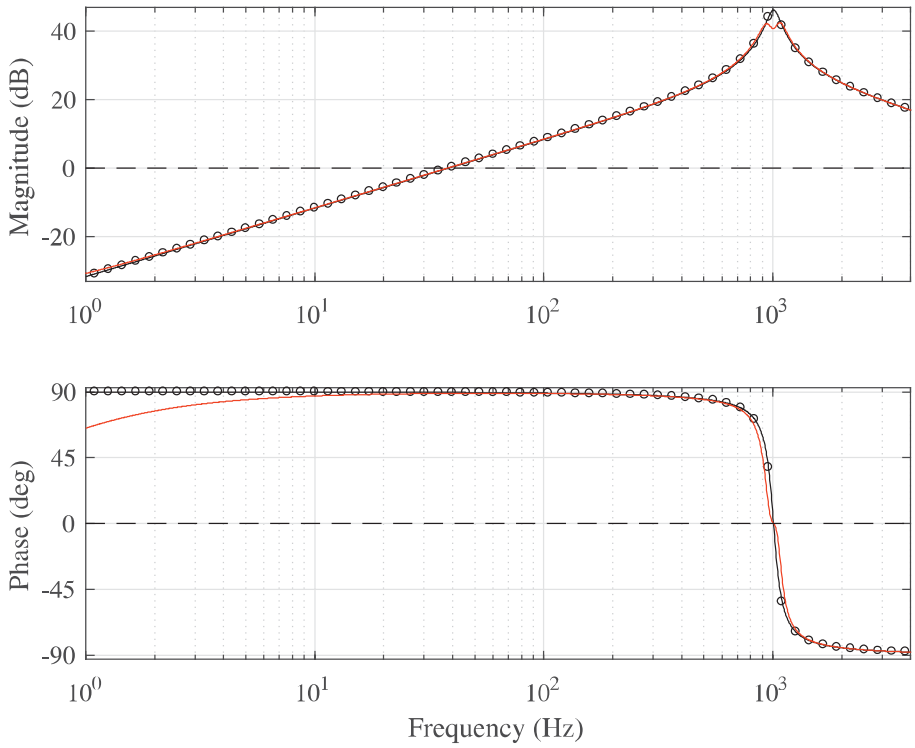


***Figure 2.12*** *Frequency response of the transfer function from the duty ratio to the inductor current by the simple model (dotted line) and the state space average model (thin line) in the grid-forming mode.*

Figure 2.12 shows a comparison between the simplified model and the derived state-space average model. It can be seen from Fig. 2.12 that the simplified DC model corresponds to the dynamics of the state space average model well. The difference in the frequency response at around the parallel resonance originates from the different domains. The parallel resonance has two peaks in the synchronous reference frame. The simplified dynamics are derived from a DC-circuit and the state-space average model is derived in dq-domain that contains the cross coupling.

The simplified DC circuits in Figures 2.9(b) and 2.11(b) and the transfer functions derived from them show, why the dynamics of $G_{\mathrm{cLd-o}}$ in the grid-forming mode and grid-feeding mode differ. Equation (2.68) shows a transfer function that is commonly used to tune the current controller of the grid-feeding inverter. The equation describes the dynamics from the duty ratio to the inductor current.

$$G_{\mathrm{cL-o}} = \frac{V_{\mathrm{in}}}{sL + R}, \tag{2.68}$$

where $L$ and $R$ are an inductor and a resistor connected in series. A reason why the filter capacitor was not taken into account in the simplified transfer function of the grid-feeding inverter is to highlight that equation form of (2.68) cannot be used to

approximate dynamics of the grid-forming inverter. It is important to be conscious of the different dynamics of ideal voltage sources and ideal current sinks.

### 2.4.3 LCL-Filter Parameter Influence on Transfer Functions

The parameters shown in Table 2.1 are suitable for the grid-feeding mode. With the given parameters the parallel resonance of the LC-filter is at around 1 kHz. The location of the resonance is disadvantageous to the current controller tuning. It has been noted in [43] that enabling of the grid-forming mode requires a larger filter capacitor in the LCL-filter. The larger capacitor can cause problems in the grid-feeding operation and might require special attention in the controller design [43]. Thus, it is beneficial to inspect, how the changes in the LCL-filter parameter values affects the transfer functions. Figure 2.13 shows the frequency response of $G_{\mathrm{cLd-o}}$ with different capacitance values of the filter capacitor $C_{\mathrm{f}}$. The inductor $L$ remains unchanged.

Figure 2.13 shows that as the filter capacitor size is increased the resonant frequency moves to lower frequencies. The same can be seen in Fig. 2.14 that shows the frequency response of output impedance $Z_{\mathrm{od-o}}$. Apparently the magnitude of the output impedance decreases when the capacitor is increased. A large capacitor can

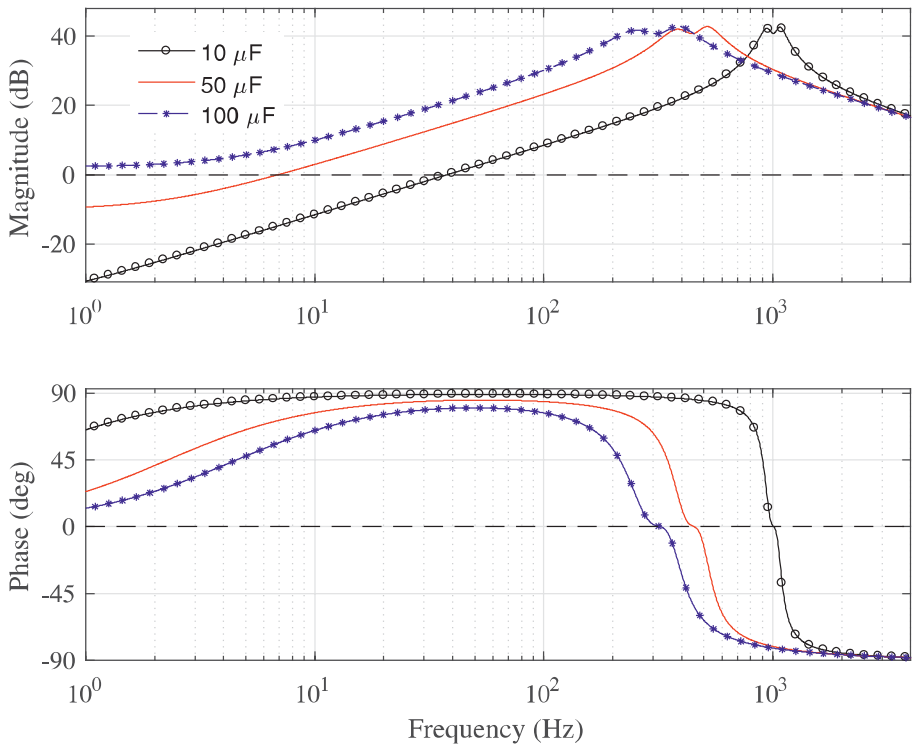


***Figure 2.13*** *Frequency response of the transfer function $G_{\mathrm{cLd-o}}$ with different capacitor $C_{\mathrm{f}}$ sizes.*

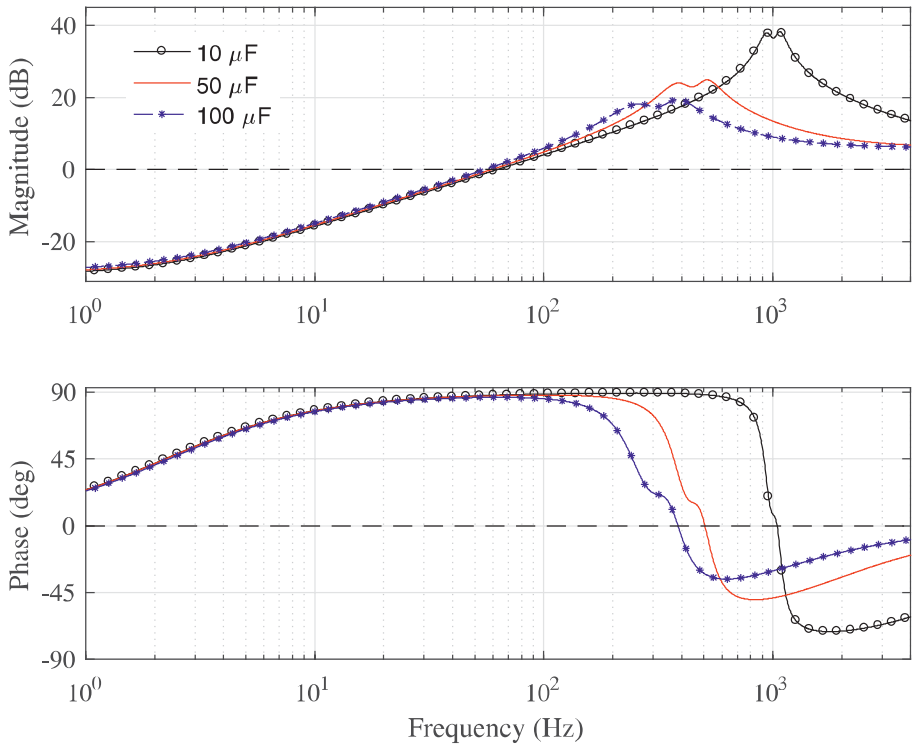


***Figure 2.14*** *Frequency response of the output impedance $Z_{\mathrm{od-o}}$ with different capacitor $C_{\mathrm{f}}$ sizes.*

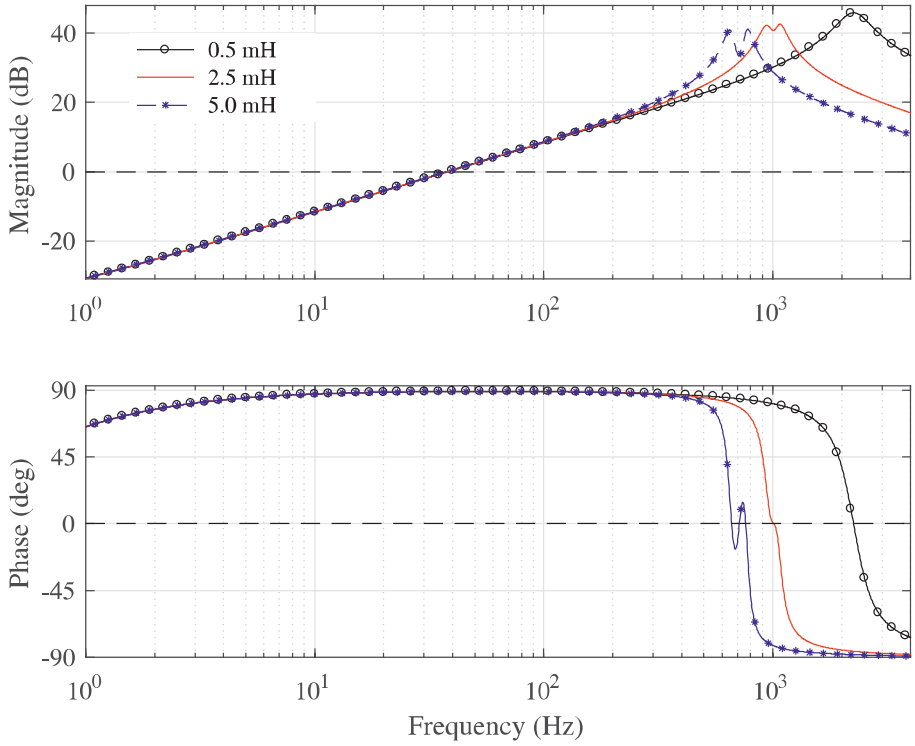


***Figure 2.15*** *Frequency response of the output impedance $G_{\mathrm{cLd-o}}$ with different inductor $L$ sizes.*

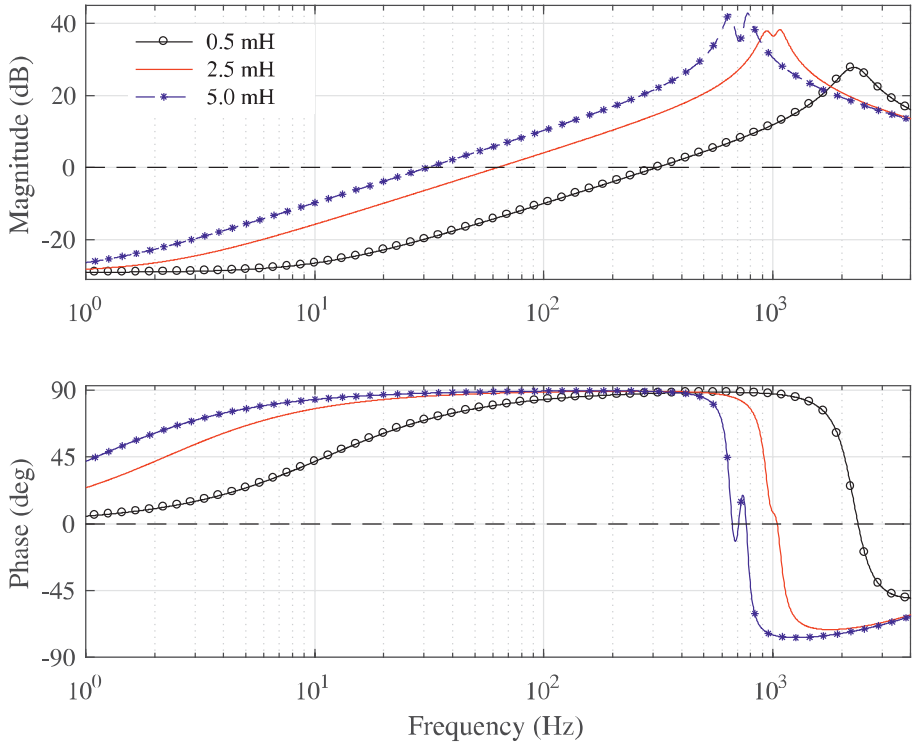


***Figure 2.16*** *Frequency response of the output impedance $Z_{\mathrm{od-o}}$ with different inductor L sizes.*

be charged or discharged longer without a noticeable change in the voltage. This originates from the fact that Farad can be defined as ampere second per volt.

Figure 2.15 shows that as the inductor size is increased the resonant frequency moves to lower frequencies. Naturally the resonant frequency of the output impedance $Z_{\mathrm{od-o}}$ moves also to lower frequencies in Fig. 2.16. However, the output impedance still increases. The advantage of decreasing or increasing the output impedance with respect to operation mode can ne analyzed from an equivalent small-signal circuit.

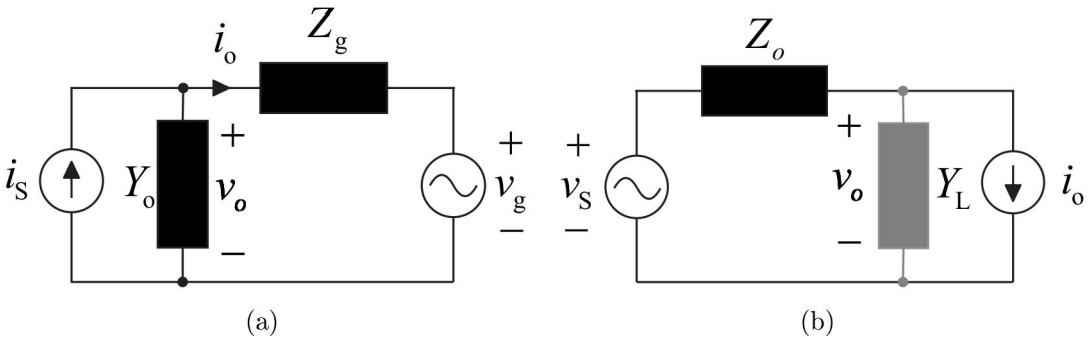


***Figure 2.17*** *Equivalent small-signal circuits of the grid-feeding inverter (a) and grid-forming inverter (b).*

Figure 2.17(a) shows the equivalent small-signal circuit of the grid-feeding inverter, where $i_\mathrm{S}$ is the source current. A small admittance $Y_\mathrm{o}$ (i.e. large impedance $Z_\mathrm{o}$) is favorable for the grid-feeding mode. When the impedance is large deviations in the grid voltage $v_\mathrm{g}$ have small effect on the current that is fed to the grid. Figure 2.17(b) shows the equivalent small-signal circuit of the grid-forming inverter, where $v_\mathrm{S}$ is the source voltage. Regarding the grid-forming mode a small output impedance $Z_\mathrm{o}$ is advantageous. Changes in the load current $i_\mathrm{o}$ have small effect on the output voltage $v_\mathrm{o}$ when the output impedance is small. The load impedance $Y_\mathrm{L}$ is drawn in gray in Fig. 2.17(b), because the load is modeled as an ideal current sink in this thesis. Increasing the capacitor size is beneficial for the grid-forming mode and disadvantageous to the grid-feeding mode. On the other hand the final analysis of the output impedances and admittances has to be made from the closed-loop model.

# 3. CONTROL DESIGN OF GRID-FORMING INVERTER

As was mentioned in Section 2.2 a cascaded control is commonly used to control the grid-forming inverter. The controller consists of the inner current controller and outer voltage controller. This chapter investigates the tuning of the cascaded control and forming of the closed loop transfer functions. The functionality of the controllers is tested by time-domain responses.

## 3.1 Cascaded Control Scheme

### 3.1.1 Inner Loop Current Controller Tuning

Since the load is an ideal constant current sink, the load current is not an option for the current feedback. Thus, the current feedback alternatives are the inductor current and the filter capacitor current. Comparison on the inductor current and filter capacitor current feedbacks has been carried out in [35],[44]. According to them the capacitor current feedback is superior to the inductor current feedback in terms of rejection of disturbances caused by the load current change. However, the controllers were P+Resonant controllers in the comparisons in [35],[44]. Still the inductor current feedback is considered first because it has been implemented in the case of the grid-feeding inverter [24].

Delay has to be taken into account in the tuning of the controllers. Delay is caused by sampling and pulse width modulation (PWM). The time delay of the sapling is one switching period $T_\mathrm{s}$ that is the inverse of the switching frequency of $f_\mathrm{s}$. PWM causes a time delay that is half the switching period. Thus, the total time delay $T_\mathrm{d}$ of the system is $1.5T_\mathrm{s}$. Similar to [24] the whole delay in the system is considered to take place before PWM. Equation (3.1) shows, how the delay $e^{-T_\mathrm{d}s}$ in *Laplace* domain can be approximated by a third-order *Padé* approximation, where $G_\mathrm{del}$ is the delay transfer function.

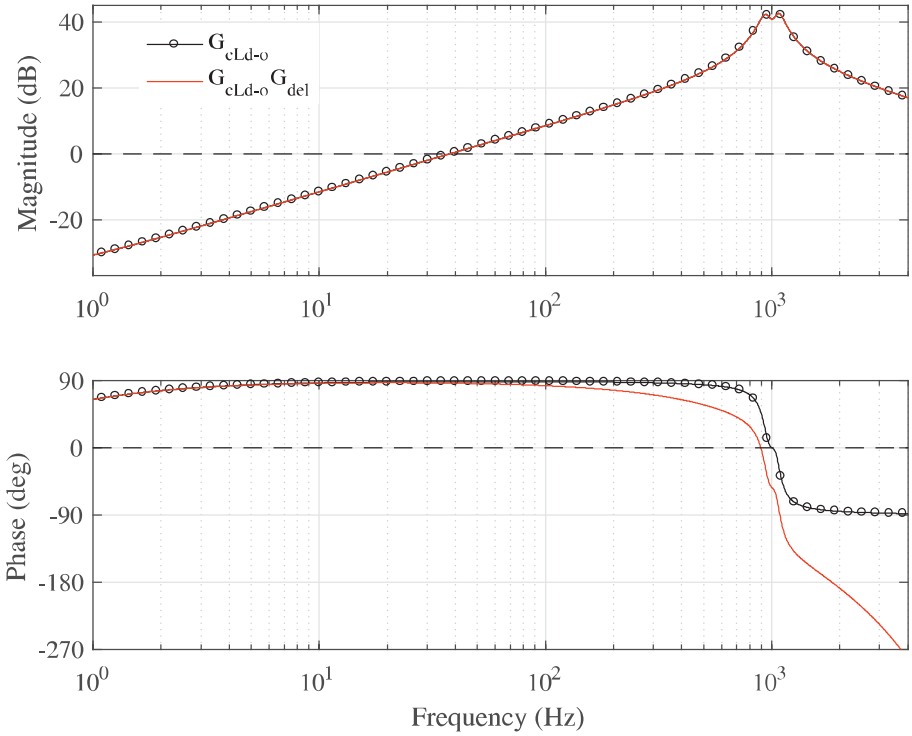


***Figure 3.1*** *Frequency response from the control d-component to the inductor current d-component with and without the delay.*

$$G_{\text{del}} = \frac{1 - s\frac{T_\text{d}}{2} + s^2\frac{T_\text{d}^2}{10} - s^3\frac{T_\text{d}^3}{120}}{1 + s\frac{T_\text{d}}{2} + s^2\frac{T_\text{d}^2}{10} + s^3\frac{T_\text{d}^3}{120}} \tag{3.1}$$

Figure 3.1 shows the frequency response from the control d-component to the inductor current d-component with and without delay. It can be clearly seen that the delay has a significant effect on the phase. The maximum feedback loop crossover frequency is $f_\text{s}/5$ [27]. In this case the maximum current loop crossover frequency would be 2 kHz. Nevertheless, Figure 3.1 shows that phase lag due to the delay is too high to be compensated by loop shaping at higher frequencies than 1 kHz. Thus, the target crossover frequency of the current loop is 1 kHz. This is required for a voltage controller with a bandwidth of 100 Hz since the secondary control loop should be approximately 10 times faster than the primary control loop in a cascaded control. However, the resonance location in the frequency response is a challenge. It is very difficult or even impossible to achieve a reasonable crossover frequency by using P-, PI- and PID-controllers even if low pass filtering is used.

It was shown in Section 2.4.2 that the dynamics from the duty ratio to the inductor current are different in the grid-forming inverter and the grid-feeding inverter. However, it is still useful to verify what happens if similar controller are used. The current controller that could be used for a grid-feeding inverter consists of two poles

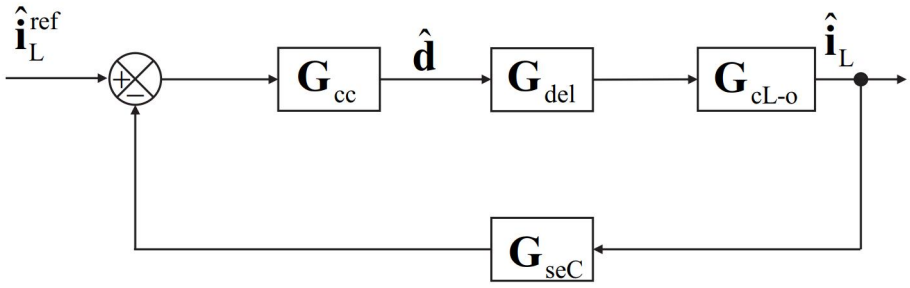


***Figure 3.2*** *Control block diagram of the inductor current loop gain d-component.*

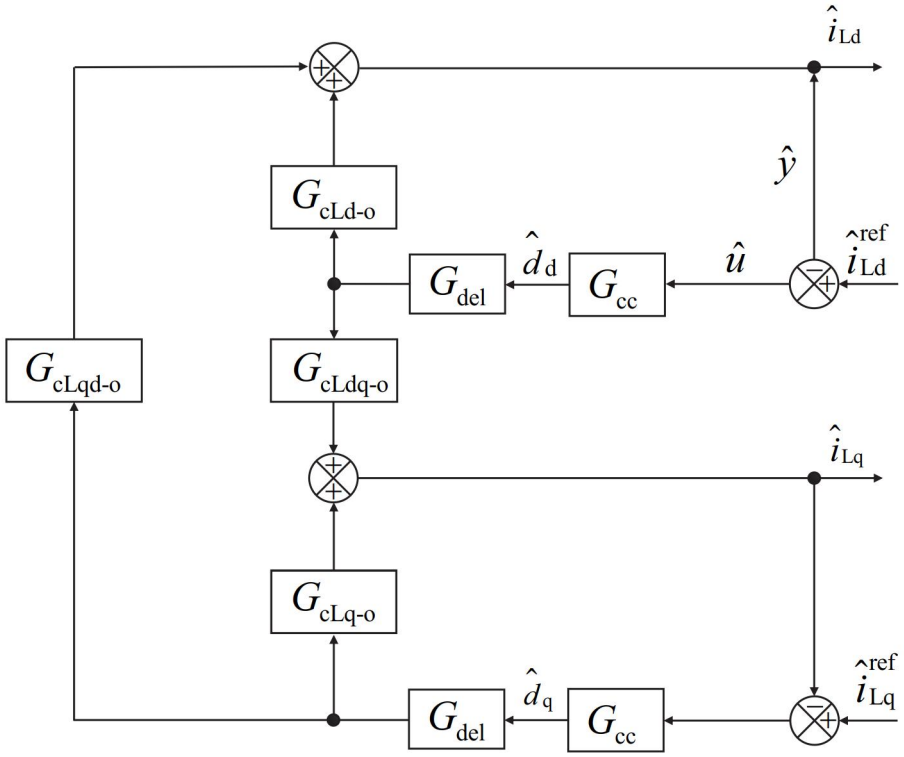


***Figure 3.3*** *Control block diagram of the full-order inductor current loop gain d-component.*

at 1950 Hz, zeros at 60 Hz and 600 Hz, an integrator and a gain of 15.8 dB. Figure 3.2 shows a control a block diagram of the inductor current d-component. Sensing gain $G_{\mathrm{seC}}$ is included in the model. The control block diagram for the q-component is similar and both channels are controlled by identical controllers that are denoted by the transfer function $G_{\mathrm{cc}}$.

Equation (3.2) shows the current loop gain $L_{\mathrm{outC-d}}$ that is written from the block diagram in Fig. 3.2. Figure 3.4 shows the frequency response of $L_{\mathrm{outC-d}}$. The gain margin is only 2.74 dB at 1630 Hz. The phase margin at 1430 Hz is 17.2 °.

$$L_{\mathrm{outC-d}} = G_{\mathrm{cL-d}}\mathrm{G_{del}G_{cc}G_{se}} \tag{3.2}$$

The block diagram in Fig. 3.2 does not include the fact that the duty ratio d-component has an effect on the inductor current q-component due to the cross coupling between the channels. Transfer function $G_{\mathrm{cLdq-o}}$ describes this effect. The deviation in the current q-component is compensated by the q-channel control loop that adjusts the duty ratio q-component. The deviation in the duty-ratio q-component affects the d-channel current according to $G_{\mathrm{cLqd-o}}$. Figure 3.3 shows the d-component current loop where the cross coupling between the control loops is included. The current sensing gain is assumed to be 1. Thus, $G_{\mathrm{seC}}$ is omitted from the control block diagram for simplicity. By using the model, the full-order loop gain $L^{\mathrm{FO}}_{\mathrm{outC-d}}$ that includes the cross coupling can be solved. Input $\hat{u}$ and output $\hat{y}$ are marked in the control block diagram in Fig. 3.3. They are defined on different sides of the sum operator so that the minus does not affect the loop gain. $L^{\mathrm{FO}}_{\mathrm{outC-d}}$ is solved from $\hat{u}$ to $\hat{y}$. The steps to solve the transfer function are shown in (3.3)–(3.9).

Small signal duty ratio d-component $\hat{d}_{\mathrm{d}}$ is expressed as a function of $\hat{u}$ in (3.3). $\hat{d}_{\mathrm{q}}$ is expressed as a function of $\hat{d}_{\mathrm{q}}$ and $\hat{d}_{\mathrm{d}}$ in (3.4). Equation (3.5) shows the relation from $\hat{d}_{\mathrm{d}}$ to $\hat{d}_{\mathrm{q}}$. Inductor current d-component is expressed as a function of the both duty ratios in (3.6). Duty ratio q-component in (3.6) is substituted by (3.5) in (3.7). Inductor current d-component $\hat{i}_{\mathrm{Ld}}$ and duty ratio d-component $\hat{d}_{\mathrm{d}}$ are replaced by $\hat{y}$ and $\hat{u}$ in (3.8). Solved $L^{\mathrm{FO}}_{\mathrm{outC-d}}$ is shown in (3.9).

$$\hat{d}_{\mathrm{d}} = G_{\mathrm{del}}\mathrm{G_{cc}}\hat{u} \tag{3.3}$$

$$\hat{d}_{\mathrm{q}} = -G_{\mathrm{cLdq-o}}G_{\mathrm{del}}\mathrm{G_{cc}}\hat{d}_{\mathrm{d}} - G_{\mathrm{cLq-o}}G_{\mathrm{del}}G_{\mathrm{cc}}\hat{d}_{\mathrm{q}} \tag{3.4}$$

$$\frac{\hat{d}_{\mathrm{q}}}{\hat{d}_{\mathrm{d}}} = \frac{-G_{\mathrm{cLdq-o}}G_{\mathrm{del}}\mathrm{G_{cc}}}{1 + G_{\mathrm{cLq-o}}G_{\mathrm{del}}G_{\mathrm{cc}}} \tag{3.5}$$

$$\hat{i}_{\mathrm{Ld}} = G_{\mathrm{cLqd-o}}\hat{d}_{\mathrm{q}} + G_{\mathrm{cLd-o}}\hat{d}_{\mathrm{d}} \tag{3.6}$$

$$\hat{i}_{\mathrm{Ld}} = G_{\mathrm{cLqd-o}}\frac{-G_{\mathrm{cLdq-o}}G_{\mathrm{del}}\mathrm{G_{cc}}}{1 + G_{\mathrm{cLq-o}}G_{\mathrm{del}}G_{\mathrm{cc}}}\hat{d}_{\mathrm{d}} + G_{\mathrm{cLd-o}}\hat{d}_{\mathrm{d}} \tag{3.7}$$

$$\hat{y} = -G_{\mathrm{cLqd-o}}\frac{G_{\mathrm{cLdq-o}}G_{\mathrm{del}}\mathrm{G_{cc}}}{1 + G_{\mathrm{cLq-o}}G_{\mathrm{del}}G_{\mathrm{cc}}}\mathrm{G_{cc}}\hat{u} + G_{\mathrm{cLd-o}}G_{\mathrm{del}}\mathrm{G_{cc}}\hat{u} \tag{3.8}$$

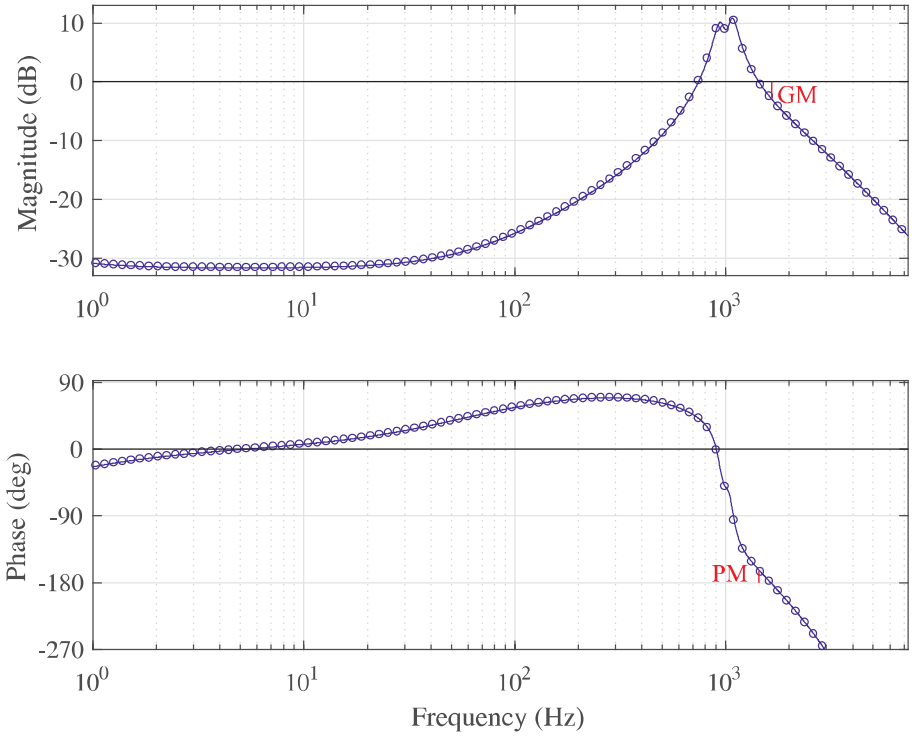


***Figure 3.4*** *Frequency response of the current loop $L_{\mathrm{outC-d}}$ of the grid-forming inverter with a current controller of the grid-feeding inverter. The cross coupling is excluded.*

$$L^{\mathrm{FO}}_{\mathrm{outC-d}} = \frac{\hat{y}}{\hat{u}} = G_{\mathrm{cLd-o}} G_{\mathrm{del}} \mathrm{G_{cc}} - \frac{G_{\mathrm{cLqd-o}} G_{\mathrm{cLdq-o}}}{1 + G_{\mathrm{cLq-o}} G_{\mathrm{del}} G_{\mathrm{cc}}} G_{\mathrm{del}} \mathrm{G_{cc}} G_{\mathrm{del}} \mathrm{G_{cc}} \tag{3.9}$$

Figure 3.5 shows the frequency response of $L^{\mathrm{FO}}_{\mathrm{outC-d}}$. It can be seen that the frequency response is affected by the cross coupling at the low frequencies. There is a peak in the frequency response at around 9 Hz and the phase approaches -180 ° at low frequencies. Also the resonant peaks at around 1 kHz are changed into one peak.

Closed loop transfer functions are calculated by using the matrix notation that was explained in Section 2.4.1. The open loop matrices are defined in Appendix A. At first the loop gain is expressed using the matrix notation. The cross coupling effect is not taken into account separately in the matrix loop gain. Thus, the analysis of the loop gain in (3.9) is required. However, in the closed loop system the cross coupling is taken into account, when calculating by the matrix notation. Equation (3.10) shows the current controller loop gain $\mathbf{L}_{\mathrm{outC}}$, where subscript C denotes current loop.

$$\mathbf{L}_{\mathrm{outC}} = \mathbf{G}_{\mathrm{cL-o}} \mathbf{G}_{\mathrm{del}} \mathbf{G}_{\mathrm{cc}} \mathbf{G}_{\mathrm{seC}} \tag{3.10}$$

The loop gain $\mathbf{L}_{\mathrm{outC}}$ is required to calculate the closed loop transfer functions from

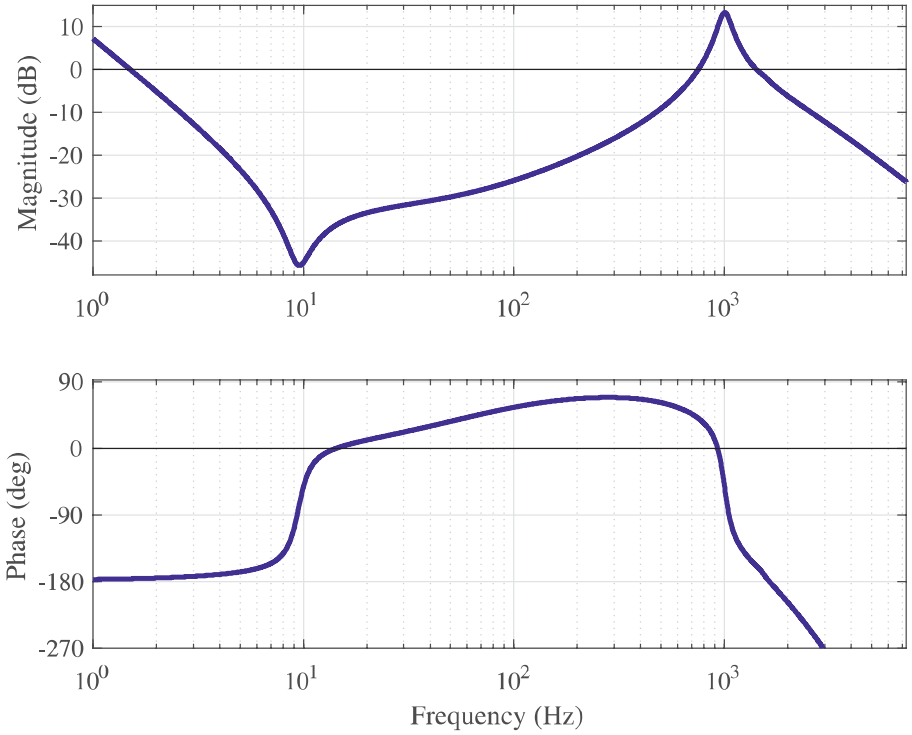


***Figure 3.5*** *Frequency response of the full-order current loop $L^{\mathrm{FO}}_{\mathrm{outC-d}}$ of the grid-forming inverter with a current controller of the grid-feeding inverter. The cross coupling is included.*

the input variables to the inductor current in (3.11)–(3.13). Superscript sec in the following transfer functions comes from the abbreviation for second and it denotes the secondary controller. The secondary controller of the cascaded control is the current controller. Subscript c denotes closed.

$$\mathbf{G}^{\mathrm{sec}}_{\mathrm{iL-c}} = (\mathbf{I} + \mathbf{L}_{\mathrm{outC}})^{-1}\mathbf{G}_{\mathrm{iL-o}} \tag{3.11}$$

$$\mathbf{G}^{\mathrm{sec}}_{\mathrm{oL-c}} = (\mathbf{I} + \mathbf{L}_{\mathrm{outC}})^{-1}\mathbf{G}_{\mathrm{oL-o}} \tag{3.12}$$

$$\mathbf{G}^{\mathrm{sec}}_{\mathrm{cL-c}} = (\mathbf{I} + \mathbf{L}_{\mathrm{outC}})^{-1}\mathbf{G}_{\mathrm{cL-o}}\mathbf{G}_{\mathrm{del}}\mathbf{G}_{\mathrm{cc}} \tag{3.13}$$

The above transfer function matrices are used to calculate the closed loop transfer functions to the input current and output voltages. They are shown in (3.14)–(3.19).

$$\mathbf{Y}^{\mathrm{sec}}_{\mathrm{in-c}} = \mathbf{Y}_{\mathrm{in-o}} - \mathbf{G}_{\mathrm{ci-o}}\mathbf{G}_{\mathrm{del}}\mathbf{G}_{\mathrm{cc}}\mathbf{G}_{\mathrm{seC}}\mathbf{G}^{\mathrm{sec}}_{\mathrm{iL-c}} \tag{3.14}$$

$$\mathbf{T}^{\mathrm{sec}}_{\mathrm{oi-c}} = \mathbf{T}_{\mathrm{oi-o}} - \mathbf{G}_{\mathrm{ci-o}}\mathbf{G}_{\mathrm{del}}\mathbf{G}_{\mathrm{cc}}\mathbf{G}_{\mathrm{seC}}\mathbf{G}^{\mathrm{sec}}_{\mathrm{oL-c}} \tag{3.15}$$

$$\mathbf{G}^{\mathrm{sec}}_{\mathrm{ci-c}} = \mathbf{G}_{\mathrm{ci-o}}\mathbf{G}_{\mathrm{del}}\mathbf{G}_{\mathrm{cc}} - \mathbf{G}_{\mathrm{ci-o}}\mathbf{G}_{\mathrm{del}}\mathbf{G}_{\mathrm{cc}}\mathbf{G}_{\mathrm{seC}}\mathbf{G}^{\mathrm{sec}}_{\mathrm{cL-c}} \tag{3.16}$$

$$\mathbf{G}^{\mathrm{sec}}_{\mathrm{io-c}} = \mathbf{G}_{\mathrm{io-o}} - \mathbf{G}_{\mathrm{co-o}}\mathbf{G}_{\mathrm{del}}\mathbf{G}_{\mathrm{cc}}\mathbf{G}_{\mathrm{seC}}\mathbf{G}^{\mathrm{sec}}_{\mathrm{iL-c}} \tag{3.17}$$

$$\mathbf{Z}^{\mathrm{sec}}_{\mathrm{o-c}} = \mathbf{Z}_{\mathrm{o-o}} + \mathbf{G}_{\mathrm{co-o}}\mathbf{G}_{\mathrm{del}}\mathbf{G}_{\mathrm{cc}}\mathbf{G}_{\mathrm{seC}}\mathbf{G}^{\mathrm{sec}}_{\mathrm{oL-c}} \tag{3.18}$$

$$\mathbf{G}^{\mathrm{sec}}_{\mathrm{co-c}} = \mathbf{G}_{\mathrm{co-o}}\mathbf{G}_{\mathrm{del}}\mathbf{G}_{\mathrm{cc}} - \mathbf{G}_{\mathrm{co-o}}\mathbf{G}_{\mathrm{del}}\mathbf{G}_{\mathrm{cc}}\mathbf{G}_{\mathrm{seC}}\mathbf{G}^{\mathrm{sec}}_{\mathrm{cL-c}} \tag{3.19}$$

In equation (3.18) a multiplication by minus one is done so that the definition of impedance holds still in the case of $\mathbf{Z}^{\mathrm{sec}}_{\mathrm{o-c}}$ .

### 3.1.2 Outer Loop Voltage Controller Tuning

The outer voltage controller is tuned according to the loop where the current control loop is closed. Figure 3.6 shows the voltage reference to output voltage small signal block diagram presentation of the cascaded controller. The transfer function from the current reference $\hat{\imath}^{\mathrm{ref}}_{\mathrm{Ld}}$ to output voltage $\hat{v}_{\mathrm{o-d}}$ can be solved from the control block diagram. However, it is already solved in (3.19). The transfer function $\mathbf{G}^{\mathrm{sec}}_{\mathrm{co-c}}$ contains the information and it is drawn by a dashed line as an alternative in Fig. 3.6. The first element of $\mathbf{G}^{\mathrm{sec}}_{\mathrm{co-c}}$ contains $G^{\mathrm{sec}}_{\mathrm{cod-c}}$ that includes the cross coupling effect that was separately calculated for the current loop in (3.9). The closed loop functions that are calculated by the matrix notation inherently include the cross coupling effect.

The frequency response of $G^{\mathrm{sec}}_{\mathrm{cod-c}}$ is used to tune the voltage controller and the frequency response is shown in Fig. 3.7. A PI-controller with two poles is tuned for the voltage loop. The voltage controller $G_{\mathrm{vc}}$ consists of an integrator, zero at 6 Hz, two poles at 100 Hz and 150 Hz and a gain of 17.4 dB.

The d-channel loop gains are defined in (3.20) and (3.21). The full-order loop gain is derived the same way as in the case of the current loop in (3.9). Figure 3.7 shows also the frequency response of the loop gains $L_{\mathrm{outV-d}}$, $L^{\mathrm{FO}}_{\mathrm{outV-d}}$ and a simulated frequency response of the voltage loop. The simulated frequency response is measured from a Matlab Simulink model of the grid-forming inverter. The Simulink

model corresponds to the grid-forming inverter that is shown in Fig. 2.4. Figure 3.7 indicates that derived transfer function $L^{\mathrm{FO}}_{\mathrm{outV-d}}$ is correct.

$$L_{\mathrm{outV-d}} = G^{\mathrm{sec}}_{\mathrm{cod-c}}\mathrm{G_{vc}} \tag{3.20}$$

$$L^{\mathrm{FO}}_{\mathrm{outV-d}} = G^{\mathrm{sec}}_{\mathrm{cod-c}}\mathrm{G_{vc}} - \frac{G^{\mathrm{sec}}_{\mathrm{codq-c}}G^{\mathrm{sec}}_{\mathrm{coqd-c}}}{1+G_{\mathrm{vc}}G^{\mathrm{sec}}_{\mathrm{coq-c}}}G_{\mathrm{vc}}G_{\mathrm{vc}} \tag{3.21}$$

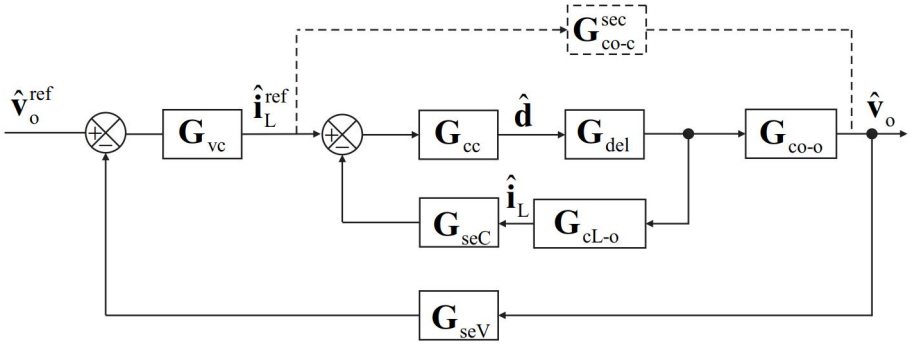


***Figure 3.6*** *Control block diagram of the cascaded controller.*

Equation (3.22) shows the output voltage loop gain $\mathbf{L}_{\mathrm{outV}}$, where $\mathbf{G}_{\mathrm{seV}}$ is the voltage sensing gain. The sensing gain is assumed to be unity so that is has no effect on

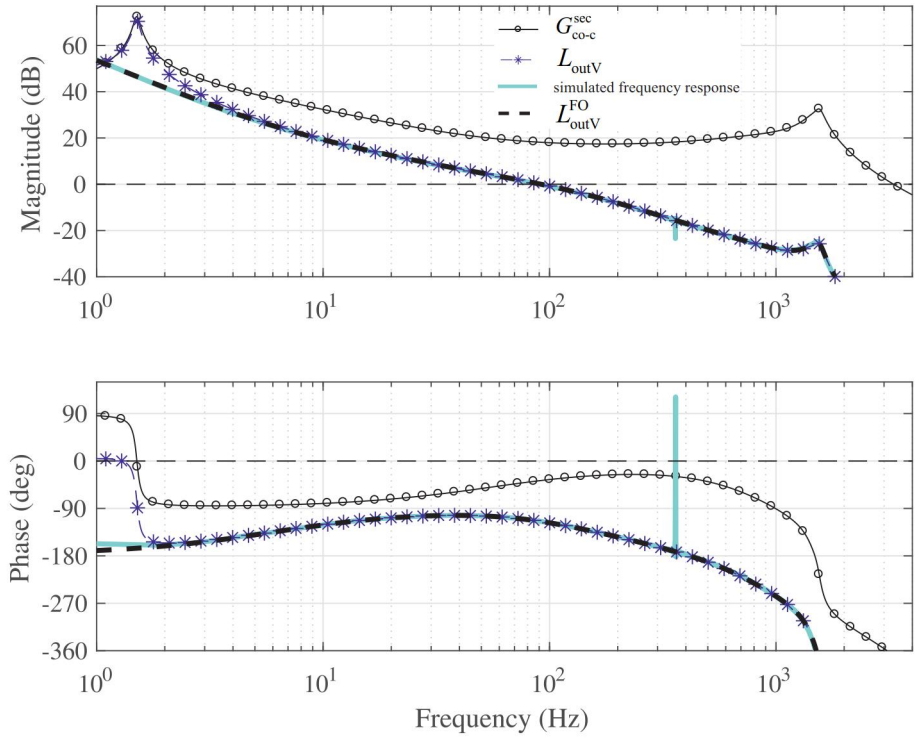


***Figure 3.7*** *Frequency responses of $G^{\mathrm{sec}}_{\mathrm{cod-c}}$, $L_{\mathrm{outV-d}}$ and $L^{\mathrm{FO}}_{\mathrm{outV-d}}$ and a simulated frequency response of the voltage loop gain.*

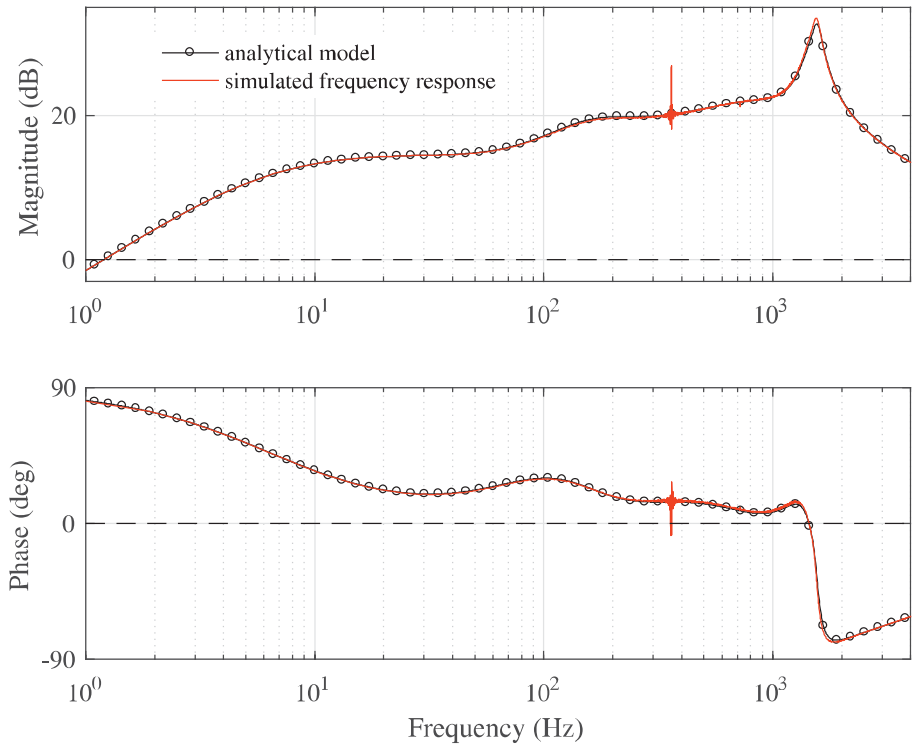


***Figure 3.8*** *Frequency response of $Z^{\text{tot}}_{\text{od-c}}$ and a simulated frequency response of the output impedance gain.*

the dynamics. The closed loop transfer functions where the output voltage loops are closed are shown in (3.23)–(3.31). Superscript tot denotes that both the current and voltage loop are closed.

$$\mathbf{L}_{\text{outV}} = \mathbf{G}^{\text{sec}}_{\text{co-c}}\mathbf{G}_{\text{vc}}\mathbf{G}_{\text{seV}} \tag{3.22}$$

$$\mathbf{G}^{\text{tot}}_{\text{io-c}} = (\mathbf{I} + \mathbf{L}_{\text{outV}})^{-1}\mathbf{G}^{\text{sec}}_{\text{io-c}} \tag{3.23}$$

$$\mathbf{Z}^{\text{tot}}_{\text{o-c}} = \left((\mathbf{I} + \mathbf{L}_{\text{outV}})^{-1}(\mathbf{Z}^{\text{sec}}_{\text{o-c}})\right) \tag{3.24}$$

$$\mathbf{G}^{\text{tot}}_{\text{co-c}} = (\mathbf{I} + \mathbf{L}_{\text{outV}})^{-1}\mathbf{G}^{\text{scc}}_{\text{co-c}}\mathbf{G}_{\text{vc}} \tag{3.25}$$

$$\mathbf{Y}^{\text{tot}}_{\text{in-c}} = \mathbf{Y}^{\text{sec}}_{\text{in-c}} - \mathbf{G}^{\text{sec}}_{\text{ci-c}}\mathbf{G}_{\text{vc}}\mathbf{G}_{\text{seV}}\mathbf{G}^{\text{tot}}_{\text{io-c}} \tag{3.26}$$

$$\mathbf{T}^{\text{tot}}_{\text{oi-c}} = \mathbf{T}^{\text{sec}}_{\text{oi-c}} - \mathbf{G}^{\text{sec}}_{\text{ci-c}}\mathbf{G}_{\text{vc}}\mathbf{G}_{\text{seV}}\mathbf{Z}^{\text{tot}}_{\text{o-c}} \tag{3.27}$$

$$\mathbf{G}^{\text{tot}}_{\text{ci}-\text{c}} = \mathbf{G}^{\text{sec}}_{\text{ci}-\text{c}}\mathbf{G}_{\text{vc}} - \mathbf{G}^{\text{sec}}_{\text{ci}-\text{c}}\mathbf{G}_{\text{vc}}\mathbf{G}_{\text{seV}}\mathbf{G}^{\text{tot}}_{\text{co}-\text{c}} \tag{3.28}$$

$$\mathbf{G}^{\text{tot}}_{\text{iL}-\text{c}} = \mathbf{G}^{\text{sec}}_{\text{iL}-\text{c}} - \mathbf{G}^{\text{sec}}_{\text{cL}-\text{c}}\mathbf{G}_{\text{vc}}\mathbf{G}_{\text{seV}}\mathbf{G}^{\text{tot}}_{\text{io}-\text{c}} \tag{3.29}$$

$$\mathbf{G}^{\text{tot}}_{\text{oL}-\text{c}} = \mathbf{G}^{\text{sec}}_{\text{oL}-\text{c}} + \mathbf{G}^{\text{sec}}_{\text{cL}-\text{c}}\mathbf{G}_{\text{vc}}\mathbf{G}_{\text{seV}}\mathbf{Z}^{\text{tot}}_{\text{o}-\text{c}} \tag{3.30}$$

$$\mathbf{G}^{\text{tot}}_{\text{cL}-\text{c}} = \mathbf{G}^{\text{sec}}_{\text{cL}-\text{c}}\mathbf{G}_{\text{vc}} - \mathbf{G}^{\text{sec}}_{\text{cL}-\text{c}}\mathbf{G}_{\text{vc}}\mathbf{G}_{\text{seV}}\mathbf{G}^{\text{tot}}_{\text{co}-\text{c}} \tag{3.31}$$

Figure 3.8 shows the frequency response of $Z^{\text{tot}}_{\text{od}-\text{c}}$ and the simulated frequency response of the output impedance. The correlation between the frequency responses indicates that the model is good.

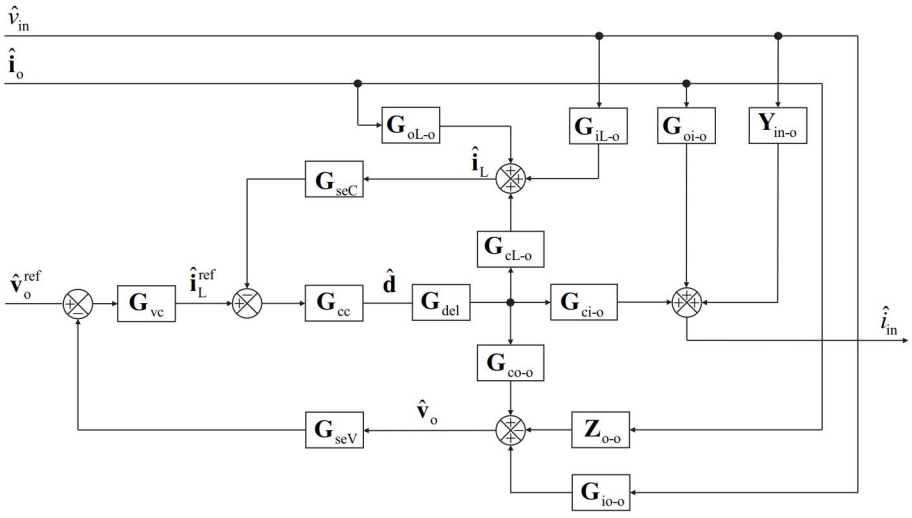


***Figure 3.9*** *Control block diagram of the dynamics of the grid-forming inverter.*

The block diagram of Fig. 3.6 forms the basis for the block diagram that includes the dynamics from disturbances to the outputs. Figure 3.9 shows a control block diagram of all input-to-output dynamics of the grid-forming inverter.

## 3.2 Control Performance of Cascade Control

Control performance of the cascaded controller in the time domain is tested by making step changes in the input voltage, output current d-component and output voltage reference d-component. In the previous sections 3.1.1 and 3.1.2 the loop gains and closed-loop transfer functions were derived. The current controller was tuned by using parameters that could be used to control the inductor current of a grid-feeding inverter. The outer voltage controller was tuned according to the model where the current loop is closed.

The output voltage response to step changes in input variables is shown in Fig. 3.10. The voltage d-component and q-component references are 169.7 V and 0 V, respectively. At $t = 0.5$ s the d-component reference is increased by a tenth of nominal value, at $t = 0.6$ s decreased by 0.3 times the nominal value and at $t = 0.65$ s increased back to nominal value. As it can be seen from Fig. 3.10 the output current $i_{\mathrm{od}}$ is decreased to 30 % of the nominal value at $t = 0.1$ s. At $t = 0.2$ s and $t = 0.3$ s the output current is increased to 90 % of the nominal value and back to the nominal value, respectively. The input voltage is increased by 10 % at $t = 0.75$ s and decreased back to nominal $t = 0.8$ s.

The voltage d-component response to output current step changes is not good. Due to the step change in the current, a high spike is caused to the voltage d-component. High output impedance that is shown in Fig. 3.8 implies that changes in the output current affect significantly the output voltage. It takes almost 0.1 s for the voltage to settle back to the reference value. The response to the voltage reference step changes is fast and there is no overshoot. At $t = 0.75$ s and 0.8 s the errors caused by the step changes in the input voltage are compensated fast by the controller.

The performance of the cascade controller is not good in the terms of output current disturbance rejection. Thus, the current controller is tuned especially for the grid-forming mode. However, the resonant peak is at disadvantageous frequency in $G_{\mathrm{cL-d}}\mathrm{G}_{\mathrm{del}}$ in Fig. 3.1. The whole current loop is damped by a gain of -62.5 Db. Hence, only a P-controller is used in the current loop. Figure 3.11 shows that there is no difference between frequency responses $L_{\mathrm{outV-d}}$ and $L^{\mathrm{FO}}_{\mathrm{outV-d}}$ with this controller tunning.

The closed loop functions are solved and $G^{\mathrm{sec}}_{\mathrm{cod-c}}$ is used to tune the voltage controller. Figure 3.12 shows the frequency response of $G^{\mathrm{sec}}_{\mathrm{cod-c}}$ and the loop gains $L_{\mathrm{outV-d}}$ and $L^{\mathrm{FO}}_{\mathrm{outV-d}}$. The simulated frequency response indicates that the full-order model of the voltage loop gain is correct. The controller $G_{\mathrm{vc}}$ consists of an integrator, zero at 150 Hz, two poles at 200 Hz, and gain of 66.4 dB. The phase margin is 65 °at 99.9 Hz

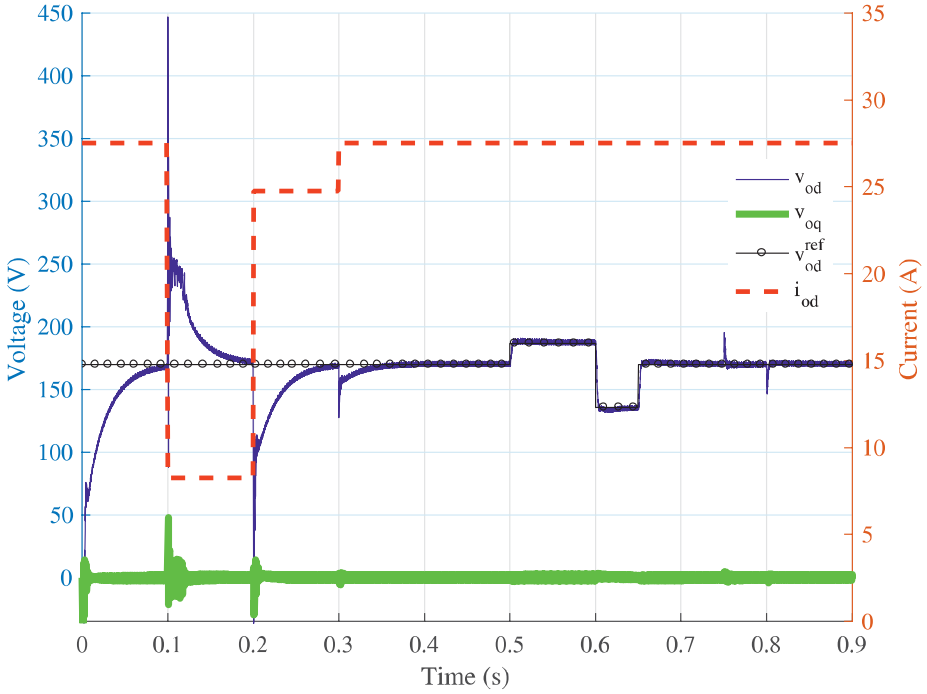


***Figure 3.10*** *Time domain response of output voltage d- and q-components to step changes in the input variables.*

and the gain margin is 17.3 dB at 482 Hz. The gain margin above the resonance at 937 Hz is 17.1 dB.

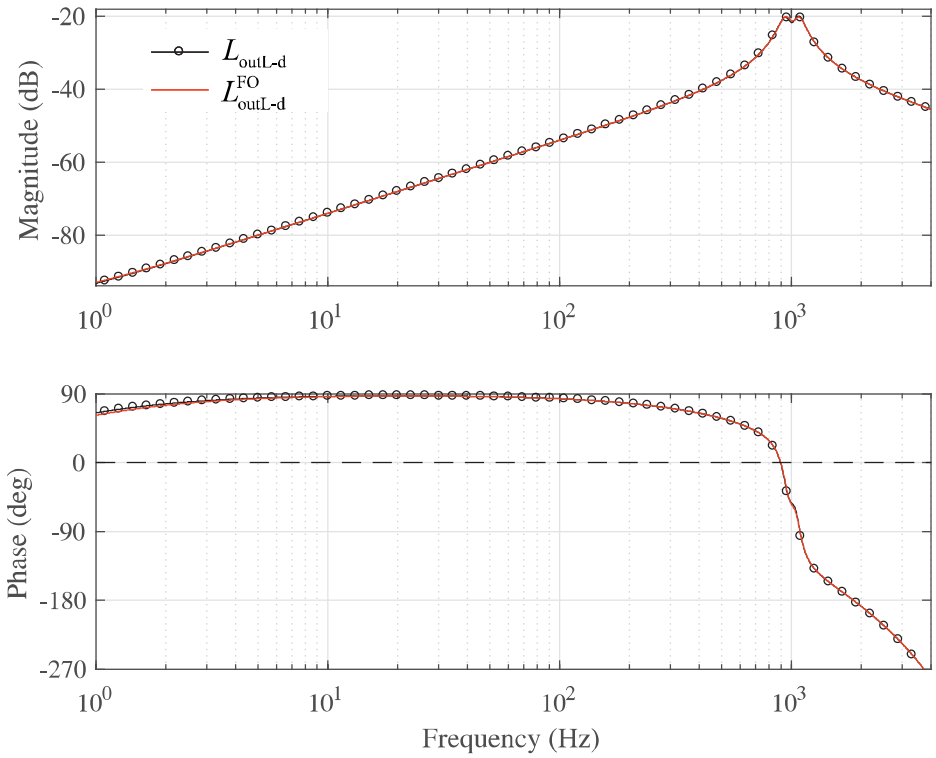


***Figure 3.11*** *Frequency responses of* $L_{\mathrm{outC-d}}$ *and* $L^{\mathrm{FO}}_{\mathrm{outC-d}}$

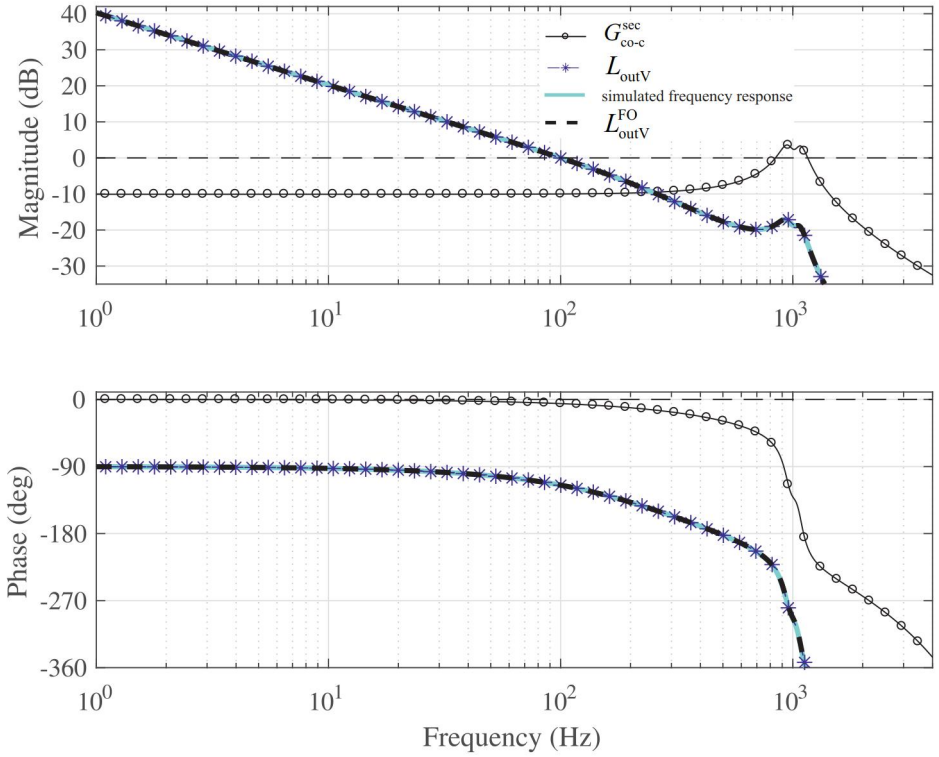


***Figure 3.12*** *Frequency responses of $G^{sec}_{cod-c}$, $L_{outV-d}$ and $L^{FO}_{outV-d}$ and a simulated frequency response of the voltage loop gain.*

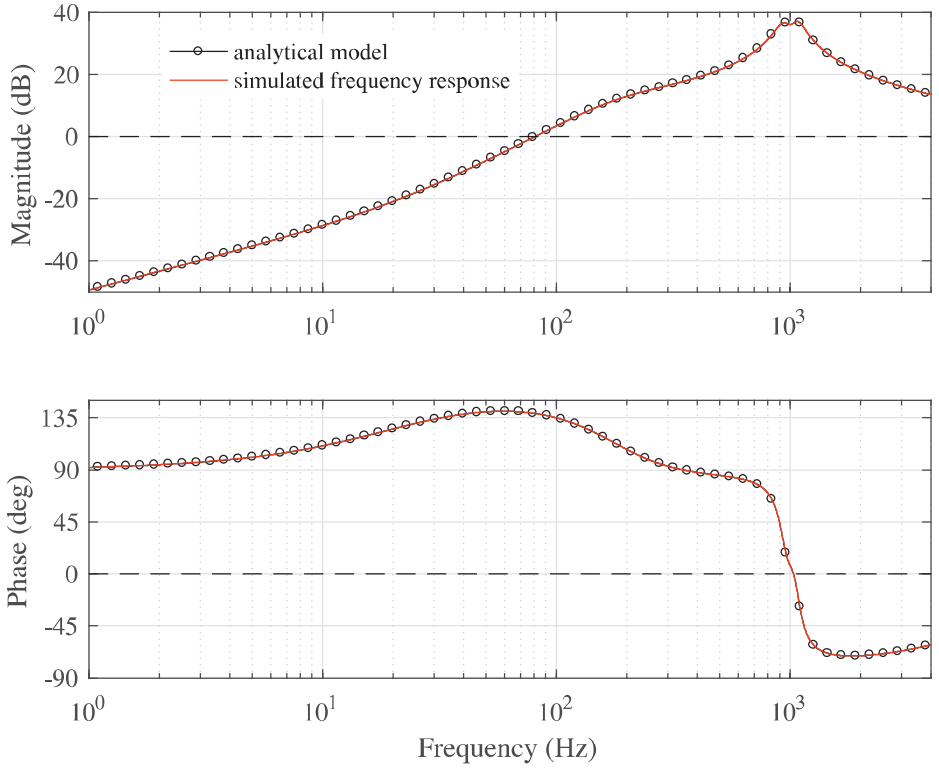


***Figure 3.13*** *Frequency response of $Z^{tot}_{od-c}$ and a simulated frequency response.*

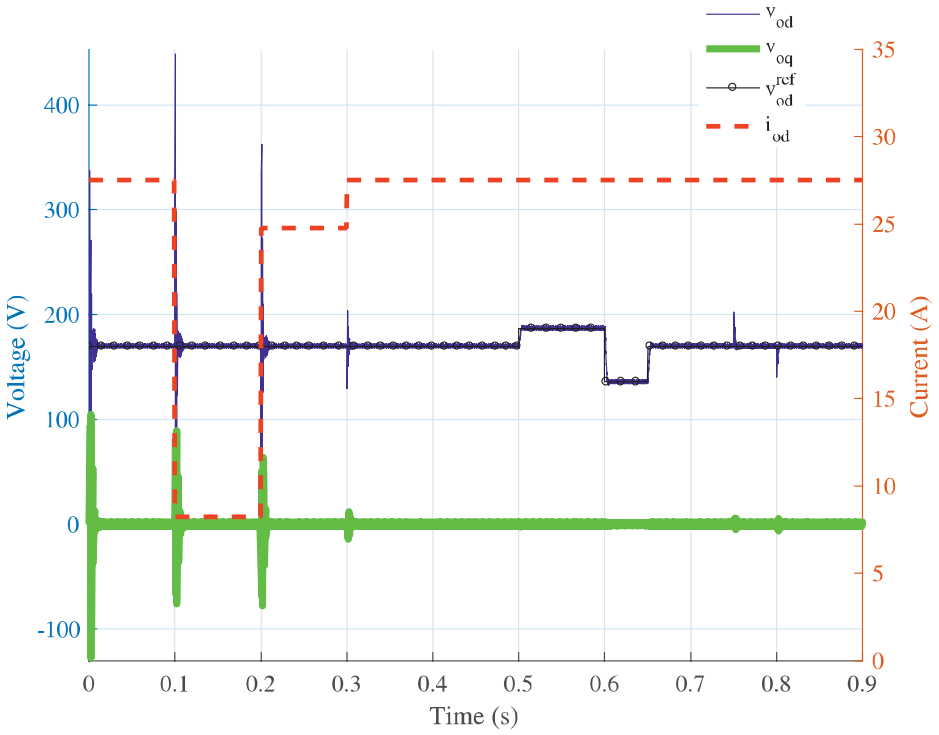


***Figure 3.14*** *Time domain response of output voltage d- and q-components to step changes in input variables.*

Figure 3.13 shows the frequency response of $Z^{\text{tot}}_{\text{od}-\text{c}}$. The output impedance is lower than with the previous controller. The voltage controller is essentially an I-controller since the poles cancel almost completely the zero and there is some oscillation in the time domain response. Figure 3.14 shows the time-domain response of the system. The voltage spikes are still high, but the voltage settles to the reference value significantly faster than with the previous cascaded controller in Fig. 3.10. The response to the voltage reference and input voltage step changes is similar to the response with the previous controllers.

### 3.2.1 The Effect of Larger Filter Capacitor

In section 2.4.3 it was discussed that increasing the filter capacitor size has beneficial effect on the grid-forming mode. As the capacitor size is increased the resonance in $G_{\text{cLd}-\text{o}}$ moves to lower frequencies and the open-loop output impedance $Z_{\text{od}-\text{o}}$ decreases. Now the filter capacitor $C_{\text{f}}$ is increased from its original value 10 $\mu$F in Table 2.1 to 100 $\mu$F. The inductor $L$ is increased to 3 mH.

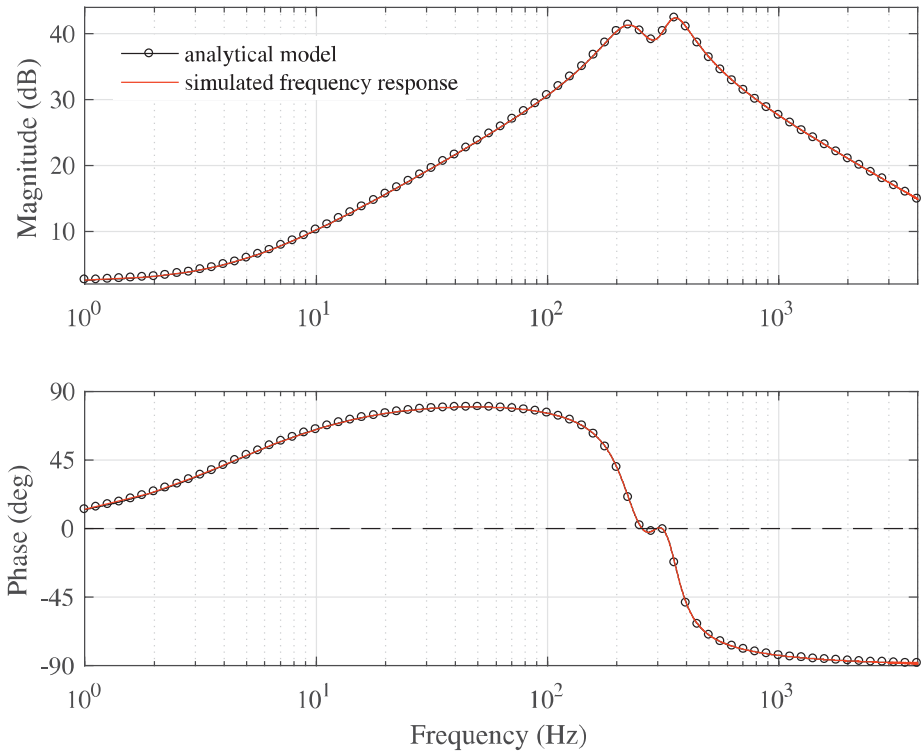


***Figure 3.15*** *Frequency response of $G_{\mathrm{cLd-o}}$ and a simulated frequency response of the transfer function.*

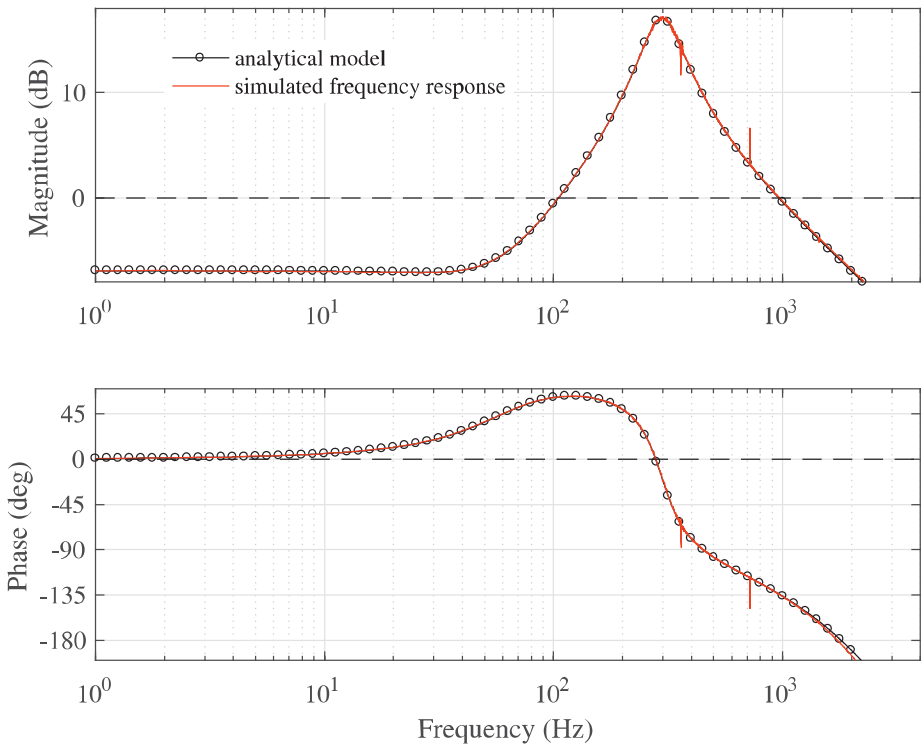


***Figure 3.16*** *Frequency response of $L^{\mathrm{FO}}_{\mathrm{outC-d}}$ and a simulated frequency response of the transfer function.*

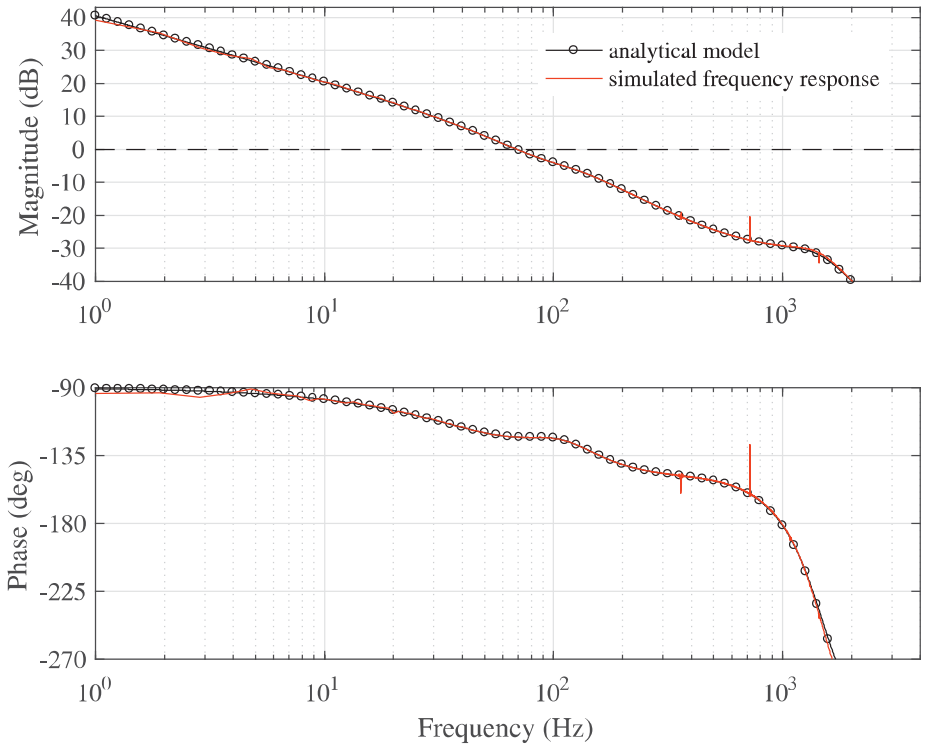


***Figure 3.17*** *Frequency response of $L^{\mathrm{FO}}_{\mathrm{outV-d}}$ with $C_{\mathrm{f}} = 100\ \mu F$ and a simulated frequency response of the voltage loop.*

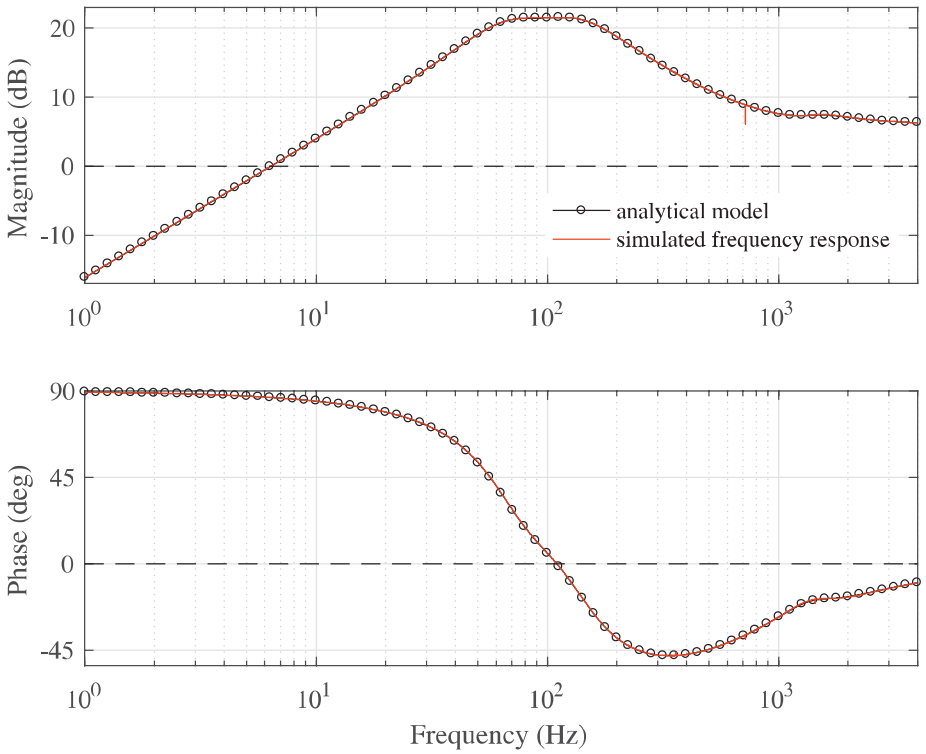


***Figure 3.18*** *Frequency response of $Z^{\mathrm{tot}}_{\mathrm{od-c}}$ and a simulated frequency response of the output impedance*

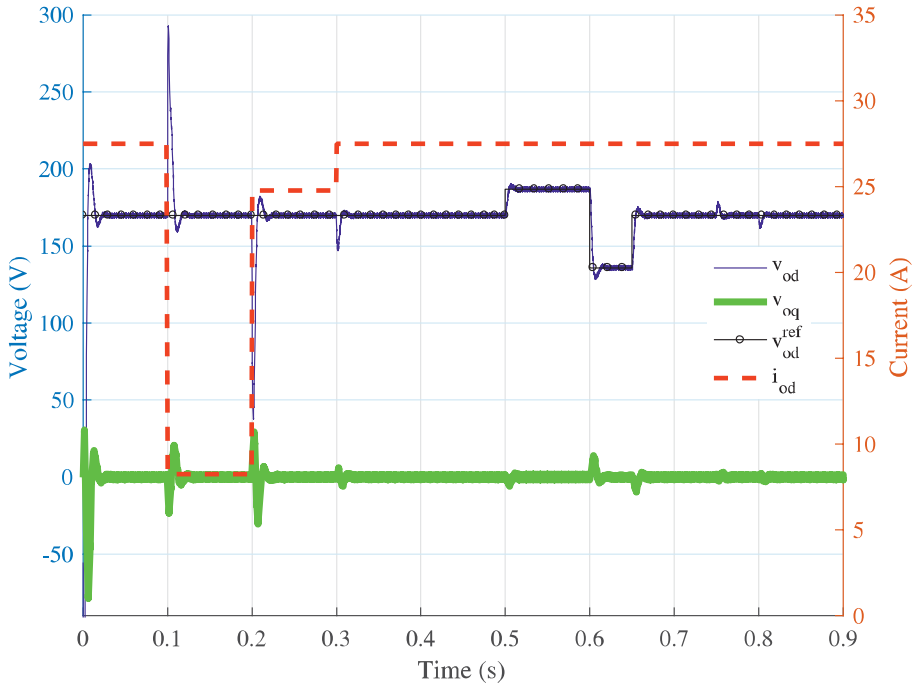


***Figure 3.19*** *Time domain response of output voltage d- and q-components to step changes in input variables.*

Figure 3.15 shows the bode diagram of $G_{\mathrm{cLd-o}}$. The model follows the exactly the simulated frequency response from a Simulink model. The highest peak of the parallel resonance is at 360 Hz. A P-controller is tuned for the system. A gain of -28 dB is chosen. The loop gain $L_{\mathrm{outC-d}}$ and the full-order one $L^{\mathrm{FO}}_{\mathrm{outC-d}}$ are shown in Fig. 3.16. The current loop bandwidth is from 105 Hz to 961 Hz. The gain margin is 6.01 dB at 1.8 kHz. The phase margin at 961 Hz is 46.3 °.

The voltage controller is tuned to control $G^{\mathrm{sec}}_{\mathrm{cod-c}}$. The controller consists of an integrator, zero at 500 Hz, pole at 1000 Hz and gain of 31.1 dB. Figure 3.17 shows the the frequency response of the full-oder voltage loop gain $L^{\mathrm{FO}}_{\mathrm{outV-d}}$ and the simulated frequency response. The bandwidth of the voltage loop is 68.9 Hz and the phase margin is 57.2 °. The gain margin is 29.3 dB.

The output impedance $Z^{\mathrm{tot}}_{\mathrm{od-c}}$ that is shown in Fig. 3.18 is lower than with the previous controllers. Naturally the open loop impedance $Z_{\mathrm{od-o}}$ that is affected by the large filter capacitor is the basis for the output impedance.

Figure 3.19 shows the time-domain response of the system. The disturbances injected to the system are described in Section 3.2. The first voltage spike is only 292.9 V now as it was up to 450 V in the case of Fig. 3.10. In addition the controller cancels out the error quicker than with the first controller tuning. However, there are small overshoots due to the output voltage reference d-component changes.

# 4. CURRENT CONTROLLER FEEDBACK VARIABLE ALTERNATIVES

Hitherto, the current feedback has been taken from the inductor current. However, there are still other alternatives. The capacitor current or the inductor current and the output current of which difference corresponds the capacitor current measurement can be measured. Obviously the latter is more expensive, but the overcurrent protection can be implemented in that case [44].

The reasoning for the use of capacitor current is that the changes in the output current have immediately effect on the capacitor current according to the circuit theory. The inductor current cannot change until the output voltage has decreased. In order to analyze the capacitor current feedback input-to-filter capacitor current transfer functions need to be solved. The filter capacitor current $i_{\mathrm{C_f}}$ is defined as the inductor current subtracted by the output current. Thus, it is simple to modify the coefficient matrix $\mathbf{D}$ of the state-space representation in (2.55) so that the intermediate output variable is the filter capacitor current instead of the inductor current. The coefficient matrices $\mathbf{A}$, $\mathbf{B}$, $\mathbf{C}$ and $\mathbf{D}$ are shown in Appendix C.

The transfer functions can be solved from the state-space representation the same way as in (2.57). The control to inductor current $G_{\mathrm{cLd-o}}$ and control to filter capacitor current $G_{\mathrm{cC_fd-o}}$ dynamics are identical. The similarity of the dynamics can be understood by keeping in mind that the output current is constant. Thus, the small signal deviations in the inductor current that come from the power stage have to occur also in the filter capacitor current since it is the only path available. Due to the identical dynamics no adjustments in the current controller tuning are needed when the feedback variable is changed from the inductor current to the filter capacitor current.

All the other transfer functions are identical between the both currents except the output-to-current transfer functions. The output current-to-capacitor current transfer function $G_{\mathrm{oC_fd-o}}$ differs greatly from $G_{\mathrm{oLd-o}}$. The differences in the dynamics can be understood by comparing frequency responses of the output-to-inductor current transfer function $G_{\mathrm{oLd-o}}$ and the output-to-capacitor current transfer function

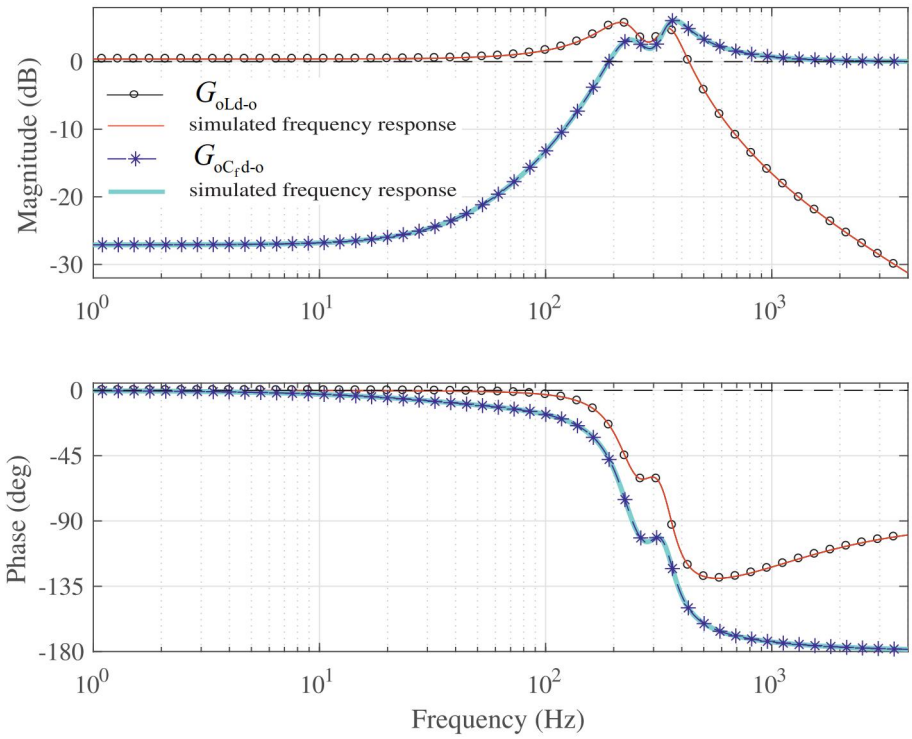


***Figure 4.1*** *Frequency responses of* $G_{\mathrm{oLd-o}}$ *and* $G_{\mathrm{oC_fd-o}}$ *along with the simulated frequency responses.*

$G_{\mathrm{oC_fd-o}}$ that are shown in Fig. 4.1. The simulated frequency responses that are also shown for both in the figure indicate that the models are correct.

It is important to analyze the gain behavior given the fact that current loop remains unchanged and the bandwidth is from 105 Hz to 961 Hz. The gain of $G_{\mathrm{oC_fd-o}}$ is positive in dB at frequencies above 200 Hz and approaches 0 dB at high frequencies This means that at high frequencies all the output current flows through capacitor as it is known by the circuit theory. At low frequencies the small signal output current has practically no effect on the capacitor current since the magnitude of the gain is very low. In the case of the inductor current it is the opposite. At low frequencies before the resonance the gain is high and decreases after the resonance. At around 100 Hz the phase in $G_{\mathrm{oLd-o}}$ begins to decrease. This means that the high frequency content of the output current disturbance is not seen instantly by the inductor current. Thus, output voltage is affected by disturbance before the current controller can react. The filter capacitor current has the same weakness that there is some phase shift in the current controller bandwidth. However, the phase approaches -180 ° that means multiplication by -1. With respect to output disturbance rejection this is beneficial. For example an increase in the load current causes a decrease in the capacitor current. Compensating the decreased capacitor current also compensates the error in the output voltage. The current controller

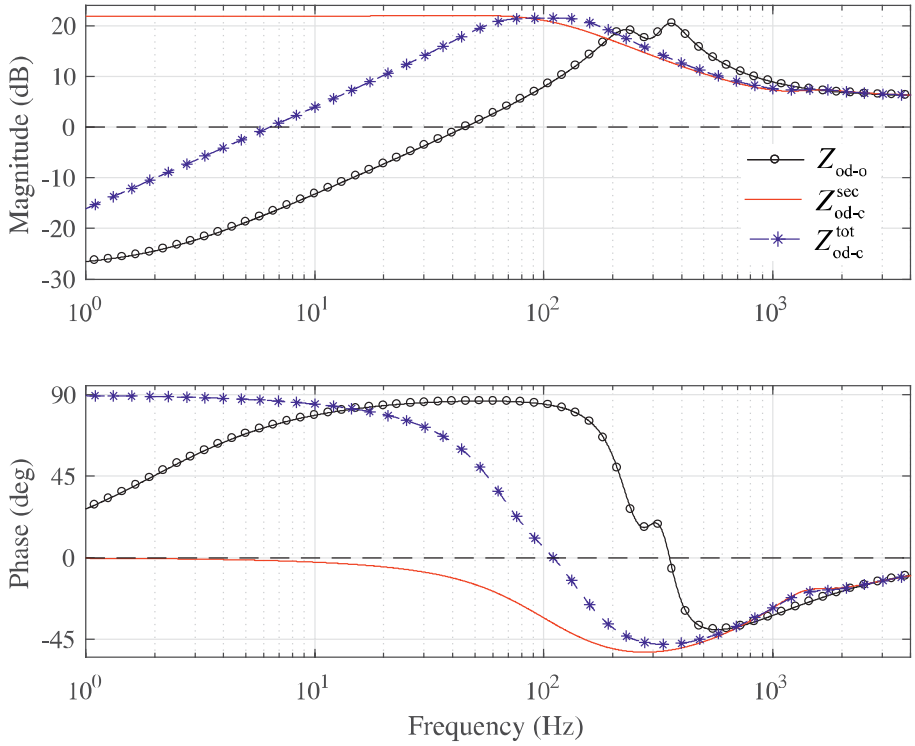


***Figure 4.2*** *Frequency response of the output impedance with the inductor current feedback.*

increases the duty-ratio so that the capacitor current increases and reduces the discharge of the filter capacitor.

In the case of inductor current feedback the effect of the increase in the output current on the output voltage is different. Due to the increased output current also the inductor current increases and the current controller decreases the duty-ratio. This means that less current is drawn from the input voltage source and more current is drawn from the capacitor. As a result the output voltage falls.

The comparison between the feedback alternatives can be made analyzing how the output-to-current transfer functions affect the closed-loop output impedance. In section 3.1.1 equations (3.12) and (3.18) show how the output-to-current open loop dynamics affect the closed loop current dynamics $\mathbf{G}^{sec}_{oL-c}$ output-to-current and output-to-output voltage $\mathbf{Z}^{sec}_{o-c}$. The total output impedance $\mathbf{Z}^{tot}_{o-c}$ is affected by $\mathbf{Z}^{sec}_{o-c}$ as shown in (3.24) in section 3.1.2. Figures 4.2 and 4.3 show the differences in $\mathbf{Z}^{sec}_{o-c}$ with the inductor current feedback and with the filter capacitor current feedback, respectively. It can be seen from Fig. 4.2 that the inductor current feedback increases the output impedance as it should be low in terms of the output current disturbance compensation. However, the LC-resonances at around 300 Hz are damped by the current loop. This is consistent with the research on the output impedance of a UPS inverter in [38]. Figure 4.2 shows that the output voltage feedback reduces the

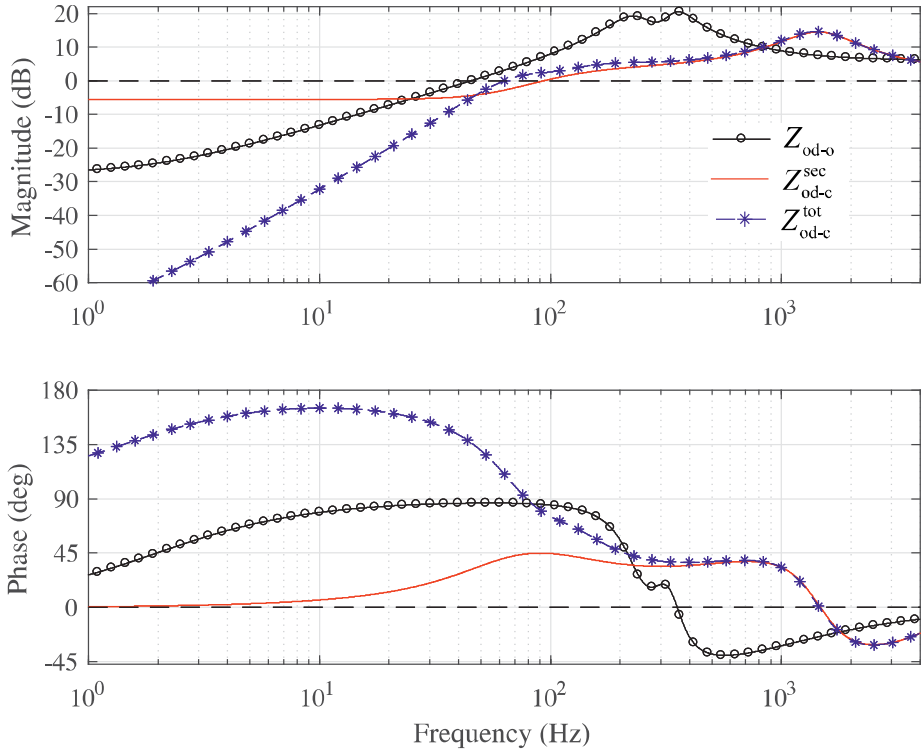


***Figure 4.3*** *Frequency response of the output impedance with the capacitor current feedback.*

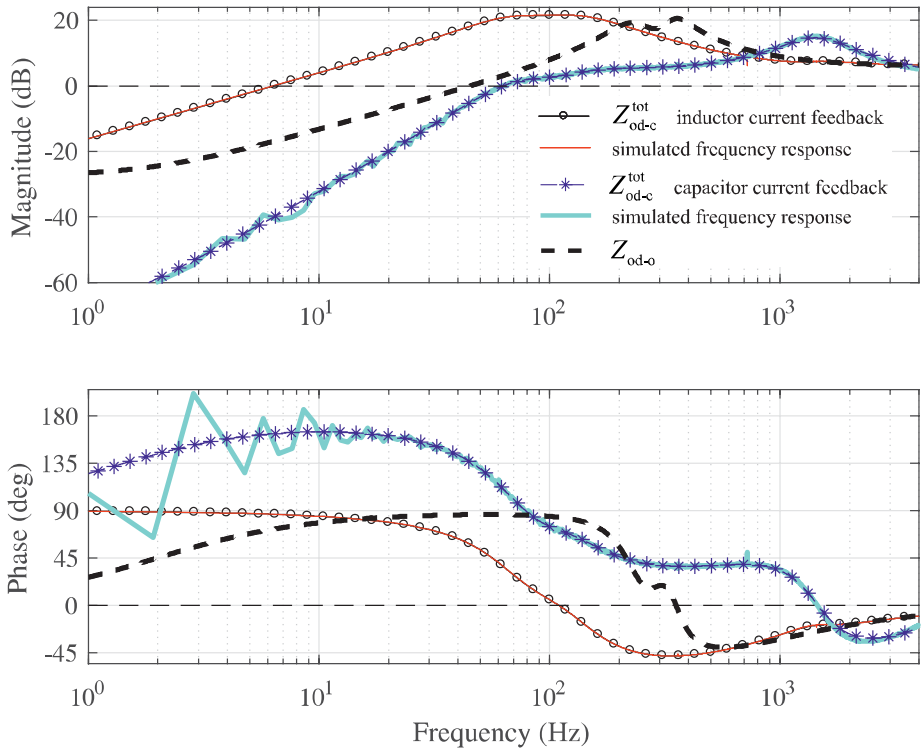


***Figure 4.4*** *Output impedance frequency response comparison.*

output impedance as it can be seen from the frequency response of $Z^{\text{tot}}_{\text{od}-\text{c}}$.

Figure 4.3 shows that in the case of the capacitor current feedback the output impedance is decreased by the current feedback. The output voltage control loop decreases the output impedance further. With respect to compensation of disturbances from the output current the capacitor current feedback seems to be superior. Figure 4.4 shows comparison of the frequency response of the output impedance with the inductor current feedback and with the filter capacitor current feedback, respectively. Simulate frequency responses indicate that the models are correct. In all probability the deviations is the simulated frequency response of $Z^{\text{tot}}_{\text{od}-\text{c}}$ in the case of capacitor current feedback are caused by the limited measurement accuracy. As the gain is under -30 dB the simulated frequency response measurement is no longer accurate. Appendix D shows the frequency responses of the cross coupling output impedances $Z^{\text{tot}}_{\text{odq}-\text{c}}$ and $Z^{\text{tot}}_{\text{oqd}-\text{c}}$ in the case of inductor current feedback.

The time-domain response comparison between the inductor and capacitor current feedbacks of the grid-forming inverter is shown in Fig. 4.5. The response to output current step changes that take place at $t = 0.1$ s, 0.2 s and 0.3 s is better with the capacitor current feedback. The voltage spike at $t = 0.1$ s is 292.9 V with the inductor current feedback, but decreases to 230.5 V with the capacitor current feedback. The input-to-current transfer functions like the control-to-current transfer functions are identical in the both cases. Thus, the voltage reference changes at

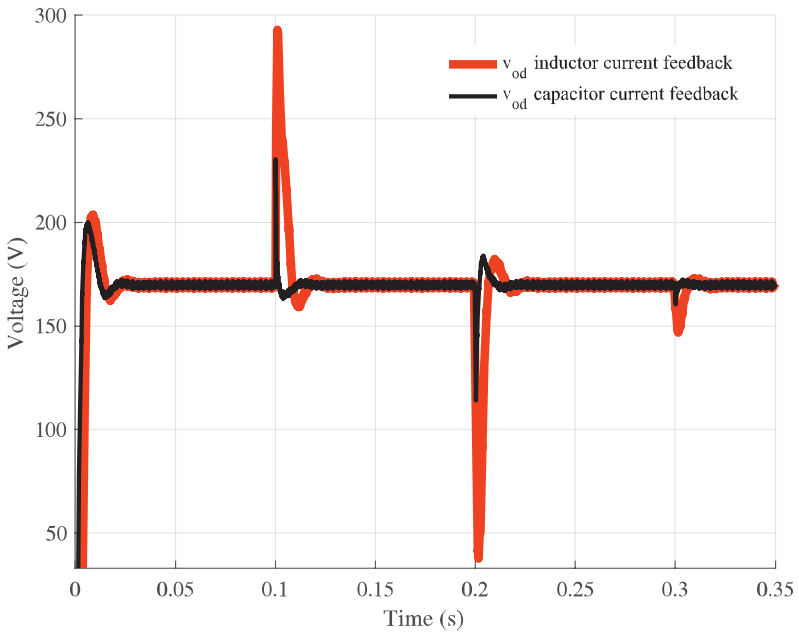


***Figure 4.5*** *Time domain response comparison.*

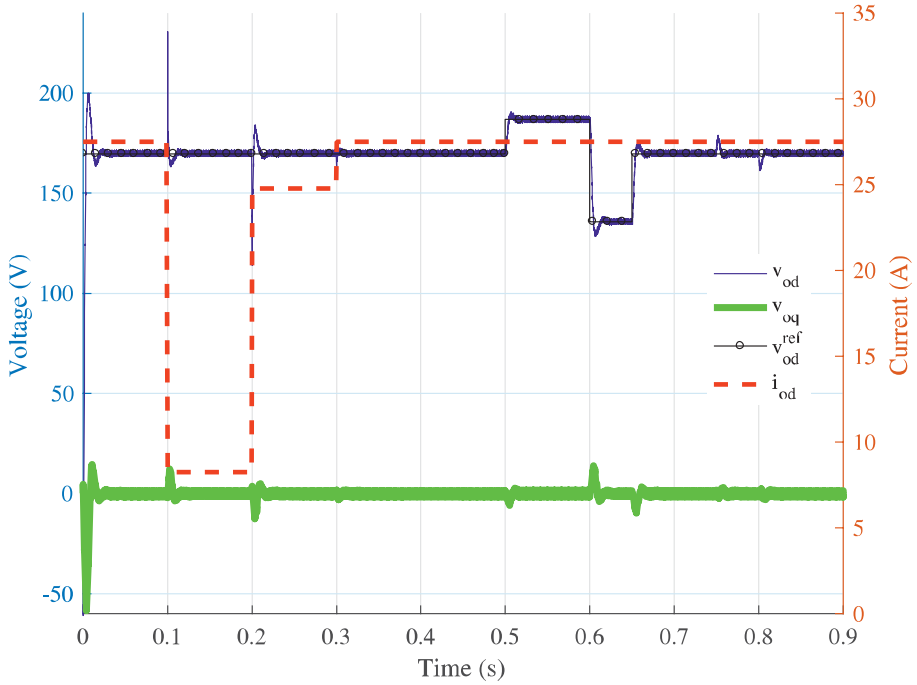


***Figure 4.6*** *Time domain response with capacitor current feedback.*

$t = 0.6$ s and 0.65 s and input voltage changes $t = 0.75$ s and 0.8 s cause identical responses as it is shown in Figures 4.6 and 3.19.

Although the capacitor voltage feedback provides significantly better output current disturbance rejection, there might be problems is real applications. The frequency response of $Z_{\mathrm{od-c}}^{\mathrm{tot}}$ with capacitor current feedback has its phase close to 180 °. It can cause stability problems with the load admittance. In this thesis the load admittance has been considered zero as the load has been modeled only by a current sink.

# 5. CONCLUSIONS

Energy storage systems make it possible to maintain the operation in an islanded micro-grid during a failure in the distribution grid. Inverters that normally feed the energy produced by the renewable energy sources to the distribution network have to form the grid during an islanded operation. In order to control the grid-forming inverter, the dynamics of the inverter must be known.

Few researchers have addressed the dynamics of grid-forming inverter with respect to controller tuning or output impedance analysis. For instance small-signal model of the three phase voltage source UPS inverter has been created in [37]. However, they use a series connection of a resistor and inductor as a load in each phase. The drawback of this load assumption in the dynamic analysis has been clearly recognized [27].

Output impedance transfer functions are derived in [38]. They show a small-signal circuit model of a UPS inverter. However, their explanation, how the transfer functions are derived from the circuit misses some steps and they solve only the output impedances. Solving transfer functions from a circuit is possible as it is shown in this thesis. However, it is laborious to solve transfer functions one by one from a linearized small signal circuit diagram if the cross coupling between d and q-component are taken into account. Thus, there is still need for a full order dynamic model of the grid-forming inverter that clearly represents the transfer functions from the input variables to the output variables of system.

In this thesis state-space average modeling is used. The linearized equations are presented in the state-space matrices and only few matrix operations are needed to solve the transfer functions. The transfer functions have been verified by simulated frequency responses from the Simulink model of the grid-forming inverter.

A cascaded controller is tuned for the grid-forming inverter by using frequency responses of the open-loop transfer functions. The control variable of the inner loop is the inductor current and the output voltage is controlled by the outer loop. Closed loop transfer functions are derived from the controller transfer functions and

the open-loop transfer functions. Simulated frequency responses from the Simulink model of the grid-forming inverter indicate that the models are correct.

The effect of current feedback variable on the ability to reject load voltage disturbances caused by the load current changes is inspected in [44], [35]. They come to the conclusion that the filter capacitor current feedback is superior to the inductor current feedback. The same result is achieved in this thesis. However, the analysis is facilitated by the derived transfer functions. Since the transfer functions were derived from all the input variables to all output and controllable variables, the output current-to-inductor current and output current-to-capacitor current transfer functions are easily available.

Based on the transfer functions it is easy to analyze how output current changes affect the possible feedback current in the open loop. Frequency responses of the closed-loop output impedances show, how the feedbacks affect the impedance. It is shown that the inductor current feedback mainly increases and the filter capacitor current feedback mainly decreases the output impedance of the grid-forming inverter. The effects of inductor current feedback on the output impedance is in line with the observations in [38]. The capacitor current feedback has been used in [45]. However, the open-loop dynamics of the inverter are not analyzed properly in [45].

It should noted that the model represented in this thesis has some limitations. The load of the grid-forming inverter is modeled as an ideal current sink that does not correspond to any real load. However, the unideal load can be included as a load effect in the dynamic model later. One next step to continue the research is to include the load effect and the load-side inductor of the LCL-filter in the model that could not be included in the model with the ideal load. Decoupling gains between d and q-components in the current and voltage controller have been widely used in the literature and they are still to be implemented to this model. Future work will also look into hardware-in-the-loop simulation that can be used to verify the model.

As stated in the introduction, the thesis was carried out in order to develop dynamic model of the grid-forming inverter. A full-order dynamic model that hasn't been represented before to this extent was made successfully and a cascaded control was tuned. The results achieved by analyzing the model correspond to findings in the literature. In addition the derived full order transfer functions facilitate the analysis of the grid-forming inverter and new more detailed findings than before can be found from the frequency responses of the system.

# REFERENCES

[1] M. Pacifici, P. Visconti, S. H. M. Butchart, J. E. M. Watson, F. M. Cassola, and C. Rondinini, 2017, "Species' traits influenced their response to recent climate change," *Nature Climate Change*, vol. 7, no. 3, pp. 205–208.

[2] K. Bilen, O. Ozyurt, K. Bakırcı, S. Karslı, S. Erdogan, M. Yılmaz, and O. Comaklı, 2008, "Energy production, consumption, and environmental pollution for sustainable development: A case study in Turkey," *Renewable and Sustainable Energy Reviews*, vol. 12, no. 6, pp. 1529–1561.

[3] J. Barnett and W. N. Adger, 2003, "Climate dangers and atoll countries," *Climatic Change*, vol. 61, no. 3, pp. 321–337.

[4] Ministry of Economic Affairs and Employment, Finland, 2017, "Government report on the National Energy and Climate Strategy for 2030."

[5] The European Parliament and the Council of the European Union, 2009, "Directive 2009/28/EC of the European Parliament and of the Council of 23 April 2009 on on the promotion of the use of energy from renewable sources and amending and subsequently repealing Directives 2001/77/EC and 2003/30/EC," *Official Journal of the European Union.*

[6] Bundesministerium der Justiz und für Verbraucherschutz, 2016, "Gesetz für den ausbau erneuerbarer energien (erneuerbare- energien-gesetz -eeg 2017)."

[7] Bundesministerium der Justiz und für Verbraucherschutz, 2013, "Gesetz füber die friedliche verwendung der kernenergie und den schutz gegen ihre gefahren (atomgesetz)."

[8] Eurostat, 2017, "Statistik der erneuerbaren energien," (accessed 03-04-2017). [Online]. Available: http://ec.europa.eu/eurostat/statistics-explained/index.php/Renewable_energy_statistics/de

[9] EurObserv'ER, "PHOTOVOLTAIC BAROMETER," 2016.

[10] H. Häberlin, *Photovoltaics System Design and Practice.* Hoboken, United States: John Wiley Sons, Incorporated, 2012.

[11] C. Liu, S. McArthur, and S. Lee, *Smart Grid Handbook, 3 Volume Set.* New York, United States: Wiley, 2016.

[12] A. Werth, N. Kitamura, I. Matsumoto, and K. Tanaka, "Evaluation of centralized and distributed microgrid topologies and comparison to Open Energy Systems (OES)," in *2015 IEEE 15th International Conference on Environment and Electrical Engineering (EEEIC)*. IEEE, 2015, pp. 492–497.

[13] L. Mackay, T. G. Hailu, G. C. Mouli, L. Ramirez-Elizondo, J. Ferreira, and P. Bauer, "From DC nano- and microgrids towards the universal DC distribution system - a plea to think further into the future," in *2015 IEEE Power & Energy Society General Meeting*. IEEE, 2015, pp. 1–5.

[14] R. Teodorescu, M. Liserre, and P. Rodriguez, *Grid Converters for Photovoltaic and Wind Power Systems*. Hoboken, United States: Wiley, 2011.

[15] Q. Zhong and T. Hornik, *Control of Power Inverters in Renewable Energy and Smart Grid Integration*. Hoboken, United States: Wiley, 2012.

[16] K. Lappalainen and S. Valkealahti, 2017, "Output power variation of different PV array configurations during irradiance transitions caused by moving clouds," *Applied Energy*, vol. 190, pp. 902–910.

[17] M. Bragard, N. Soltau, S. Thomas, and R. W. De Doncker, 2010, "The Balance of Renewable Sources and User Demands in Grids: Power Electronics for Modular Battery Energy Storage Systems," *IEEE Transactions on Power Electronics*, vol. 25, no. 12, pp. 3049–3056.

[18] X. Li, D. Hui, and X. Lai, 2013, "Battery Energy Storage Station (BESS)-Based Smoothing Control of Photovoltaic (PV) and Wind Power Generation Fluctuations," *IEEE Transactions on Sustainable Energy*, vol. 4, no. 2, pp. 464–473.

[19] European Comission, *European Technology Platform Smartgrids*, 2006.

[20] N. Pogaku, M. Prodanovic, and T. C. Green, 2007, "Modeling, Analysis and Testing of Autonomous Operation of an Inverter-Based Microgrid," *IEEE Transactions on Power Electronics*, vol. 22, no. 2, pp. 613–625.

[21] O. Palizban and K. Kauhaniemi, 2015, "Hierarchical control structure in microgrids with distributed generation: Island and grid-connected mode," *Renewable and Sustainable Energy Reviews*, vol. 44, pp. 797–813.

[22] J. Puukko, *Issues on Dynamic Modeling and Design of Grid-Connected Three-Phase VSIs in Photovoltaic Applications*. Tampere University of Technology, 2012.

[23] T. Messo, *Factors Affecting Stable Operation of Grid-Connected Three-Phase Photovoltaic Inverters.* Tampere University of Technology, 2014.

[24] A. Aapro, T. Messo, T. Roinila, and T. Suntio, 2017, "Effect of active damping on output impedance of three-phase grid-connected converter," *IEEE Transactions on Industrial Electronics*, vol. PP, no. 99, pp. 1–1.

[25] M. Liserre, F. Blaabjerg, and S. Hansen, 2005, "Design and Control of an LCL-Filter-Based Three-Phase Active Rectifier," *IEEE Transactions on Industry Applications*, vol. 41, no. 5, pp. 1281–1291.

[26] L. Nousiainen, J. Puukko, A. Mäki, T. Messo, J. Huusari, J. Jokipii, J. Viinamaäki, D. T. Lobera, S. Valkealahti, and T. Suntio, 2013, "Photovoltaic Generator as an Input Source for Power Electronic Converters," *IEEE Transactions on Power Electronics*, vol. 28, no. 6, pp. 3028–3038.

[27] T. Suntio, *Dynamic Profile of Switched-Mode Converter: Modeling, Analysis and Control.* Weinheim, Germany: Wiley, 2009.

[28] H. Abu-Rub, M. Malinowski, and K. Al-Haddad, *Power Electronics for Renewable Energy Systems, Transportation and Industrial Applications.* Wiley, 2014.

[29] I. J. Balaguer, Q. Lei, S. Yang, U. Supatti, and F. Z. Peng, 2011, "Control for Grid-Connected and Intentional Islanding Operations of Distributed Power Generation," *IEEE Transactions on Industrial Electronics*, vol. 58, no. 1, pp. 147–157.

[30] M. Monfared, S. Golestan, and J. M. Guerrero, 2014, "Analysis, Design, and Experimental Verification of a Synchronous Reference Frame Voltage Control for Single-Phase Inverters," *IEEE Transactions on Industrial Electronics*, vol. 61, no. 1, pp. 258–269.

[31] P. Das, S. Chattopadhyay, and M. Palmal, 2017, "A d-q Voltage Droop Control Method with Dynamically Phase Shifted Phase Locked Loop for Inverter Paralleling without Any Communication between Individual Inverters," *IEEE Transactions on Industrial Electronics*, vol. 64, no. 6, pp. 1–1.

[32] J. Wang, N. C. P. Chang, X. Feng, and A. Monti, 2015, "Design of a Generalized Control Algorithm for Parallel Inverters for Smooth Microgrid Transition Operation," *IEEE Transactions on Industrial Electronics*, vol. 62, no. 8, pp. 4900–4914.

[33] I. Mazhari, M. Chamana, B. H. Chowdhury, and B. Parkhideh, "Distributed PV-battery architectures with reconfigurable power conversion units," in *2014 IEEE Applied Power Electronics Conference and Exposition - APEC 2014*. IEEE, 2014, pp. 691–698.

[34] A. Merabet, K. Tawfique Ahmed, H. Ibrahim, R. Beguenane, and A. M. Y. M. Ghias, 2017, "Energy Management and Control System for Laboratory Scale Microgrid Based Wind-PV-Battery," *IEEE Transactions on Sustainable Energy*, vol. 8, no. 1, pp. 145–154.

[35] P. Loh and D. Holmes, 2005, "Analysis of Multiloop Control Strategies for LC/CL/LCL-Filtered Voltage-Source and Current-Source Inverters," *IEEE Transactions on Industry Applications*, vol. 41, no. 2, pp. 644–654.

[36] H. Deng, R. Oruganti, and D. Srinivasan, 2008, "A Simple Control Method for High-Performance UPS Inverters Through Output-Impedance Reduction," *IEEE Transactions on Industrial Electronics*, vol. 55, no. 2, pp. 888–898.

[37] N. Abdel-Rahim and J. Quaicoe, "Small-signal model and analysis of a multiple feedback control scheme for three-phase voltage-source UPS inverters," in *PESC Record. 27th Annual IEEE Power Electronics Specialists Conference*, vol. 1. IEEE, 1996, pp. 188–194.

[38] B. Wen, D. Boroyevich, R. Burgos, and P. Mattavelli, "Modeling the output impedance of three-phase uninterruptible power supply in D-Q frame," in *2014 IEEE Energy Conversion Congress and Exposition (ECCE)*. IEEE, 2014, pp. 163–169.

[39] R. Middlebrook and S. Cuk, "A general unified approach to modelling switching-converter power stages," in *1970 IEEE Power Electronics Specialists Conference*, vol. 21, no. 1. IEEE, 1976, pp. 18–34.

[40] A. Veltman, D. Pulle, and R. De Doncker, *Fundamentals of Electrical Drives*, ser. Power Systems. Cham, Switzerland: Springer International Publishing, 2016.

[41] G. Franklin, J. Powell, and A. Emami-Naeini, *Feedback control of dynamic systems*. Upper Saddle River, United States: Pearson, 2014.

[42] R. D. Middlebrook, 1988, "Small-signal modeling of pulse-width modulated switched-mode power converters," *Proceedings of the IEEE*, vol. 76, no. 4, pp. 343–354.

[43] J. He, Y. W. Li, D. Xu, X. Liang, B. Liang, and C. Wang, 2017, "Deadbeat weighted average current control with corrective feed-forward compensation for microgrid converters with nonstandard lcl filter," *IEEE Transactions on Power Electronics*, vol. 32, no. 4, pp. 2661–2674.

[44] Poh Chiang Loh, M. Newman, D. Zmood, and D. Holmes, 2003, "A comparative analysis of multiloop voltage regulation strategies for single and three-phase UPS systems," *IEEE Transactions on Power Electronics*, vol. 18, no. 5, pp. 1176–1185.

[45] L. Y. Wei, *Development of Power Conditioners and Controllers for Microgrids.* Nanyang Technological University, 2006.

# APPENDIX A. TRANSFER FUNCTION MATRICES

Equation (A1.1) shows the open-loop transfer function matrices.

$$
\begin{aligned}
\mathbf{Y}_{\mathrm{in-o}} &= \begin{bmatrix} Y_{\mathrm{in-o}} & 0 \\ 0 & 0 \end{bmatrix} & \mathbf{T}_{\mathrm{oi-o}} &= \begin{bmatrix} T_{\mathrm{oid-o}} & T_{\mathrm{oiq-o}} \\ 0 & 0 \end{bmatrix} \\
\mathbf{G}_{\mathrm{ci-o}} &= \begin{bmatrix} G_{\mathrm{cid-o}} & G_{\mathrm{ciq-o}} \\ 0 & 0 \end{bmatrix} & \mathbf{G}_{\mathrm{iL-o}} &= \begin{bmatrix} G_{\mathrm{iLd-o}} & 0 \\ G_{\mathrm{iLq-o}} & 0 \end{bmatrix} \\
\mathbf{G}_{\mathrm{oL-o}} &= \begin{bmatrix} G_{\mathrm{oLd-o}} & G_{\mathrm{oLqd-o}} \\ G_{\mathrm{oLdq-o}} & G_{\mathrm{oLq-o}} \end{bmatrix} & \mathbf{G}_{\mathrm{cL-o}} &= \begin{bmatrix} G_{\mathrm{cLd-o}} & G_{\mathrm{cLqd-o}} \\ G_{\mathrm{cLdq-o}} & G_{\mathrm{cLq-o}} \end{bmatrix} \\
\mathbf{G}_{\mathrm{io-o}} &= \begin{bmatrix} G_{\mathrm{iod-o}} & 0 \\ G_{\mathrm{ioq-o}} & 0 \end{bmatrix} & \mathbf{Z}_{\mathrm{o-o}} &= \begin{bmatrix} Z_{\mathrm{od-o}} & Z_{\mathrm{oqd-o}} \\ Z_{\mathrm{odq-o}} & Z_{\mathrm{oq-o}} \end{bmatrix} \\
\mathbf{G}_{\mathrm{co-o}} &= \begin{bmatrix} G_{\mathrm{cod-o}} & G_{\mathrm{coqd-o}} \\ G_{\mathrm{codq-o}} & G_{\mathrm{coq-o}} \end{bmatrix} & \mathbf{G}_{\mathrm{del}} &= \begin{bmatrix} G_{\mathrm{del}} & 0 \\ 0 & G_{\mathrm{del}} \end{bmatrix} \\
\mathbf{G}_{\mathrm{seC}} &= \begin{bmatrix} G_{\mathrm{seC}} & 0 \\ 0 & G_{\mathrm{seC}} \end{bmatrix} & \mathbf{G}_{\mathrm{seV}} &= \begin{bmatrix} G_{\mathrm{seV}} & 0 \\ 0 & G_{\mathrm{seV}} \end{bmatrix} \\
\mathbf{G}_{\mathrm{cc}} &= \begin{bmatrix} G_{\mathrm{cc}} & 0 \\ 0 & G_{\mathrm{cc}} \end{bmatrix} & \mathbf{G}_{\mathrm{vc}} &= \begin{bmatrix} G_{\mathrm{vc}} & 0 \\ 0 & G_{\mathrm{vc}} \end{bmatrix}
\end{aligned}
\tag{A1.1}
$$

# APPENDIX B. GRID-FEEDING INVERTER

The averaged and linearized equations describing the grid-feeding inverter that the grid-forming inverter is compared to are shown here. The averaged equations in the synchronous reference frame are shown in (B1.1)–(B1.10).

$$\frac{d\langle i_{\mathrm{L1d}}\rangle}{dt} = \frac{1}{L_1}\left[d_{\mathrm{d}}\langle v_{\mathrm{in}}\rangle - (r_{\mathrm{L}} + r_{\mathrm{sw}} + R_{\mathrm{d}})\langle i_{\mathrm{L1d}}\rangle + \omega_{\mathrm{s}} L \langle i_{\mathrm{L1q}}\rangle + R_{\mathrm{d}}\langle i_{\mathrm{L2d}}\rangle - \langle v_{\mathrm{Cfd}}\rangle\right] \tag{B1.1}$$

$$\frac{1}{L_1}\left[d_{\mathrm{q}}\langle v_{\mathrm{in}}\rangle - (r_{\mathrm{L}} + r_{\mathrm{sw}} + R_{\mathrm{d}})\langle i_{\mathrm{L1q}}\rangle - \omega_{\mathrm{s}} L \langle i_{\mathrm{L1d}}\rangle + R_{\mathrm{d}}\langle i_{\mathrm{L2q}}\rangle - \langle v_{\mathrm{Cfq}}\rangle\right] \tag{B1.2}$$

$$\frac{d\langle v_{\mathrm{Cfd}}\rangle}{dt} = \frac{1}{C_{\mathrm{f}}}\left[\langle i_{\mathrm{L1d}}\rangle - \langle i_{\mathrm{L2d}}\rangle + \omega_{\mathrm{s}} C_{\mathrm{f}}\langle v_{\mathrm{Cfq}}\rangle\right] \tag{B1.3}$$

$$\frac{d\langle v_{\mathrm{Cf}q}\rangle}{dt} = \frac{1}{C_{\mathrm{f}}}\left[\langle i_{\mathrm{L1q}}\rangle - \langle i_{\mathrm{L2q}}\rangle - \omega_{\mathrm{s}} C_{\mathrm{f}}\langle v_{\mathrm{Cfd}}\rangle\right] \tag{B1.4}$$

$$\frac{d\langle v_{\mathrm{C}}\rangle}{dt} = \frac{1}{C}\left[\frac{\langle v_{\mathrm{in}}\rangle}{r_{\mathrm{C}}} - \frac{\langle v_{\mathrm{C}}\rangle}{r_{\mathrm{C}}}\right] \tag{B1.5}$$

$$\langle i_{\mathrm{C}}\rangle = C\frac{d\langle v_{\mathrm{C}}\rangle}{dt} = \frac{\langle v_{\mathrm{in}}\rangle}{r_{\mathrm{C}}} - \frac{\langle v_{\mathrm{C}}\rangle}{r_{\mathrm{C}}} \tag{B1.6}$$

$$\langle i_{\mathrm{P}}\rangle = \frac{3}{2}\left(d_{\mathrm{d}}\langle i_{\mathrm{L1d}}\rangle + d_{\mathrm{q}}\langle i_{\mathrm{L1q}}\rangle\right) \tag{B1.7}$$

$$\langle i_{\mathrm{in}}\rangle = \langle i_{\mathrm{C}}\rangle + \langle i_{\mathrm{P}}\rangle = \frac{\langle v_{\mathrm{in}}\rangle}{r_{\mathrm{C}}} - \frac{\langle v_{\mathrm{C}}\rangle}{r_{\mathrm{C}}} + \frac{3}{2}\left(d_{\mathrm{d}}\langle i_{\mathrm{L1d}}\rangle + d_{\mathrm{q}}\langle i_{\mathrm{L1q}}\rangle\right) \tag{B1.8}$$

$$\frac{d\langle i_{\mathrm{L2d}}\rangle}{dt} = \frac{1}{L_2}\left[\langle v_{\mathrm{Cfd}}\rangle - (r_{\mathrm{L2}} + R_{\mathrm{d}})\langle i_{\mathrm{L2d}}\rangle + \omega_{\mathrm{s}} L_2 \langle i_{\mathrm{L2q}}\rangle + R_{\mathrm{d}}\langle i_{\mathrm{L1d}}\rangle - \langle v_{\mathrm{od}}\rangle\right] \tag{B1.9}$$

$$\frac{d\langle i_{\mathrm{L2q}}\rangle}{dt} = \frac{1}{L_2}\left[\langle v_{\mathrm{Cfq}}\rangle - (r_{\mathrm{L2}} + R_{\mathrm{d}})\langle i_{\mathrm{L2q}}\rangle - \omega_{\mathrm{s}} L_2 \langle i_{\mathrm{L2d}}\rangle + R_{\mathrm{d}}\langle i_{\mathrm{L1q}}\rangle - \langle v_{\mathrm{oq}}\rangle\right] \tag{B1.10}$$

The linearized equations are shown in (B1.11)–(B1.18).

$$\frac{d\widehat{i}_{\mathrm{L1d}}}{dt} = -\frac{(r_{\mathrm{L1}} + r_{\mathrm{sw}} + R_{\mathrm{d}})}{L_1}\widehat{i}_{\mathrm{L1d}} + \omega_{\mathrm{s}}\widehat{i}_{\mathrm{L1q}} - \frac{1}{L_1}\widehat{v}_{\mathrm{Cfd}} + \frac{D_{\mathrm{d}}}{L_1}\widehat{v}_{\mathrm{in}} + \frac{R_{\mathrm{d}}}{L_1}\widehat{i}_{\mathrm{L2d}} + \frac{V_{\mathrm{in}}}{L_1}\widehat{d}_{\mathrm{d}} \tag{B1.11}$$

$$\frac{d\widehat{i}_{\mathrm{L1q}}}{dt} = -\frac{(r_{\mathrm{L1}} + r_{\mathrm{sw}} + R_{\mathrm{d}})}{L_1}\widehat{i}_{\mathrm{L1q}} - \omega_{\mathrm{s}}\widehat{i}_{\mathrm{L1d}} - \frac{1}{L_1}\widehat{v}_{\mathrm{Cfq}} + \frac{D_{\mathrm{q}}}{L_1}\widehat{v}_{\mathrm{in}} + \frac{R_{\mathrm{d}}}{L_1}\widehat{i}_{\mathrm{L2q}} + \frac{V_{\mathrm{in}}}{L_1}\widehat{d}_{\mathrm{q}} \quad \text{(B1.12)}$$

$$\frac{d\widehat{i}_{\mathrm{L2d}}}{dt} = \frac{1}{L_2}\widehat{v}_{\mathrm{Cfd}} + \frac{R_d}{L_2}\widehat{i}_{\mathrm{L1d}} - \frac{(r_{L2} + R_d)}{L_2}\widehat{i}_{\mathrm{L2d}} + \omega_{\mathrm{s}}\widehat{i}_{\mathrm{L2q}} - \frac{1}{L_2}\widehat{v}_{\mathrm{od}} \quad \text{(B1.13)}$$

$$\frac{d\widehat{i}_{\mathrm{L2q}}}{dt} = \frac{1}{L_2}\widehat{v}_{\mathrm{Cfq}} + \frac{R_{\mathrm{d}}}{L_2}\widehat{i}_{\mathrm{L1q}} - \frac{(r_{\mathrm{L2}} + R_{\mathrm{d}})}{L_2}\widehat{i}_{\mathrm{L2q}} - \omega_{\mathrm{s}}\widehat{i}_{\mathrm{L2d}} - \frac{1}{L_2}\widehat{v}_{\mathrm{oq}} \quad \text{(B1.14)}$$

$$\frac{d\widehat{v}_{\mathrm{Cfd}}}{dt} = \frac{1}{C_{\mathrm{f}}}\widehat{i}_{\mathrm{L1d}} + \omega_{\mathrm{s}}\widehat{v}_{\mathrm{Cfq}} - \frac{1}{C_{\mathrm{f}}}\widehat{i}_{\mathrm{L2d}} \quad \text{(B1.15)}$$

$$\frac{d\widehat{v}_{\mathrm{Cfq}}}{dt} = \frac{1}{C_{\mathrm{f}}}\widehat{i}_{\mathrm{L1q}} - \omega_{\mathrm{s}}\widehat{v}_{\mathrm{Cfd}} - \frac{1}{C_{\mathrm{f}}}\widehat{i}_{\mathrm{L2q}} \quad \text{(B1.16)}$$

$$\frac{d\widehat{v}_{\mathrm{C}}}{dt} = -\frac{1}{r_{\mathrm{C}}C}\widehat{v}_{\mathrm{C}} + \frac{1}{r_{\mathrm{C}}C}\widehat{v}_{\mathrm{in}} \quad \text{(B1.17)}$$

$$\widehat{i}_{\mathrm{in}} = \widehat{i}_{\mathrm{C}} + \widehat{i}_{\mathrm{P}} = -\frac{1}{r_{\mathrm{C}}}\widehat{v}_{\mathrm{C}} + \frac{1}{r_{\mathrm{C}}}\widehat{v}_{\mathrm{in}} + \frac{3}{2}D_{\mathrm{d}}\widehat{i}_{\mathrm{L1d}} + \frac{3}{2}D_{\mathrm{q}}\widehat{i}_{\mathrm{L1q}} + \frac{3}{2}I_{\mathrm{L1d}}\widehat{d}_{\mathrm{d}} + \frac{3}{2}I_{\mathrm{L1q}}\widehat{d}_{\mathrm{q}} \quad \text{(B1.18)}$$

# APPENDIX C. FILTER CAPACITOR CURRENT FEEDBACK

The filter capacitor current is chosen as the intermediate output variable. Equation (C1.1) shows the small signal input, output and state variable vectors. The linearized state-space presentation in frequency domain is shown in (C1.2). Equation (C1.3) shows the state-space matrices.

$$\widehat{\mathbf{u}} = \begin{bmatrix} \hat{v}_{\mathrm{in}} \\ \hat{i}_{\mathrm{od}} \\ \hat{i}_{\mathrm{oq}} \\ \hat{d}_{\mathrm{d}} \\ \hat{d}_{\mathrm{q}} \end{bmatrix} \qquad \widehat{\mathbf{y}} = \begin{bmatrix} \hat{\hat{i}}_{\mathrm{in}} \\ \hat{\hat{i}}_{\mathrm{Cfd}} \\ \hat{\hat{i}}_{\mathrm{Cfq}} \\ \hat{v}_{\mathrm{od}} \\ \hat{v}_{\mathrm{oq}} \end{bmatrix} \qquad \widehat{\mathbf{x}} = \begin{bmatrix} \hat{\hat{i}}_{\mathrm{Ld}} \\ \hat{\hat{i}}_{\mathrm{Lq}} \\ \hat{v}_{\mathrm{Cfd}} \\ \hat{v}_{\mathrm{Cfq}} \\ \hat{v}_{\mathrm{C}} \end{bmatrix} \tag{C1.1}$$

$$\begin{aligned} s\mathbf{X}(s) &= \mathbf{A}\mathbf{X}(s) + \mathbf{B}\mathbf{U}(s) \\ \mathbf{Y}(s) &= \mathbf{C}\mathbf{X}(s) + \mathbf{D}\mathbf{U}(s) \end{aligned} \tag{C1.2}$$

$$\mathbf{A} = \begin{bmatrix} -\frac{(r_{\mathrm{L}}+r_{\mathrm{sw}}+R_{\mathrm{d}})}{L} & \omega_{\mathrm{s}} & -\frac{1}{L} & 0 & 0 \\ -\omega_{\mathrm{s}} & -\frac{(r_{\mathrm{L}}+r_{\mathrm{sw}}+R_{\mathrm{d}})}{L} & 0 & -\frac{1}{L} & 0 \\ \frac{1}{C_{\mathrm{f}}} & 0 & 0 & \omega_{\mathrm{s}} & 0 \\ 0 & \frac{1}{C_{\mathrm{f}}} & -\omega_{\mathrm{s}} & 0 & 0 \\ 0 & 0 & 0 & 0 & -\frac{1}{r_{\mathrm{C}}C} \end{bmatrix}$$

$$\mathbf{B} = \begin{bmatrix} \frac{D_{\mathrm{d}}}{L} & \frac{R_{\mathrm{d}}}{L} & 0 & \frac{V_{\mathrm{in}}}{L} & 0 \\ \frac{D_{\mathrm{q}}}{L} & 0 & R_{\mathrm{d}} & 0 & \frac{V_{\mathrm{in}}}{L} \\ 0 & -\frac{1}{C_{\mathrm{f}}} & 0 & 0 & 0 \\ 0 & 0 & -\frac{1}{C_{\mathrm{f}}} & 0 & 0 \\ \frac{1}{r_{\mathrm{C}}C} & 0 & 0 & 0 & 0 \end{bmatrix} \quad \mathbf{C} = \begin{bmatrix} \frac{3D_{\mathrm{d}}}{2} & \frac{3D_{\mathrm{q}}}{2} & 0 & 0 & \frac{-1}{r_{\mathrm{C}}} \\ 1 & 0 & 0 & 0 & 0 \\ 0 & 1 & 0 & 0 & 0 \\ R_{\mathrm{d}} & 0 & 1 & 0 & 0 \\ 0 & R_{\mathrm{d}} & 0 & 1 & 0 \end{bmatrix}$$

$$\mathbf{D} = \begin{bmatrix} \frac{1}{r_{\mathrm{C}}} & 0 & 0 & \frac{3I_{\mathrm{Ld}}}{2} & \frac{3I_{\mathrm{Lq}}}{2} \\ 0 & -1 & 0 & 0 & 0 \\ 0 & 0 & -1 & 0 & 0 \\ 0 & -R_{\mathrm{d}} & 0 & 0 & 0 \\ 0 & 0 & -R_{\mathrm{d}} & 0 & 0 \end{bmatrix} \tag{C1.3}$$

# APPENDIX D. OUTPUT IMPEDANCE AFFECTED BY INDUCTOR CURRENT FEEDBACK

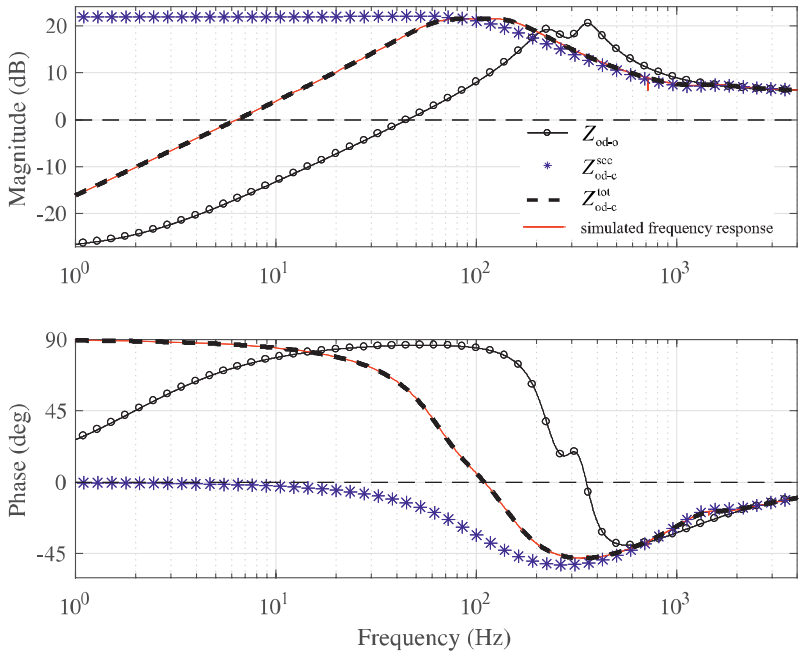


***Figure D.1*** *Frequency responses of* $Z_{\mathrm{od}}$ *in open loop and closed loop.*

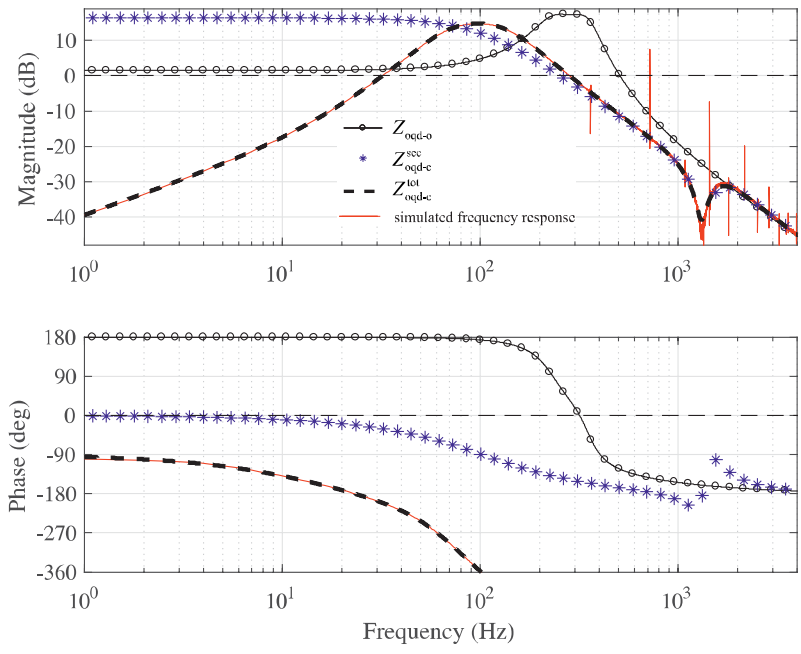


***Figure D.2*** *Frequency responses of* $Z_{\mathrm{oqd}}$ *in open loop and closed loop.*

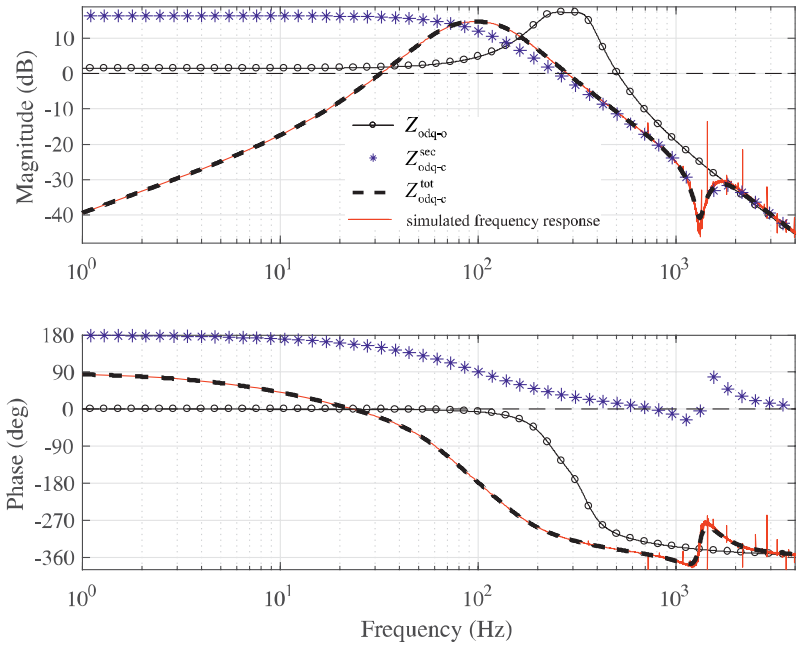


***Figure D.3*** *Frequency responses of* $Z_{\mathrm{odq}}$ *in open loop and closed loop.*

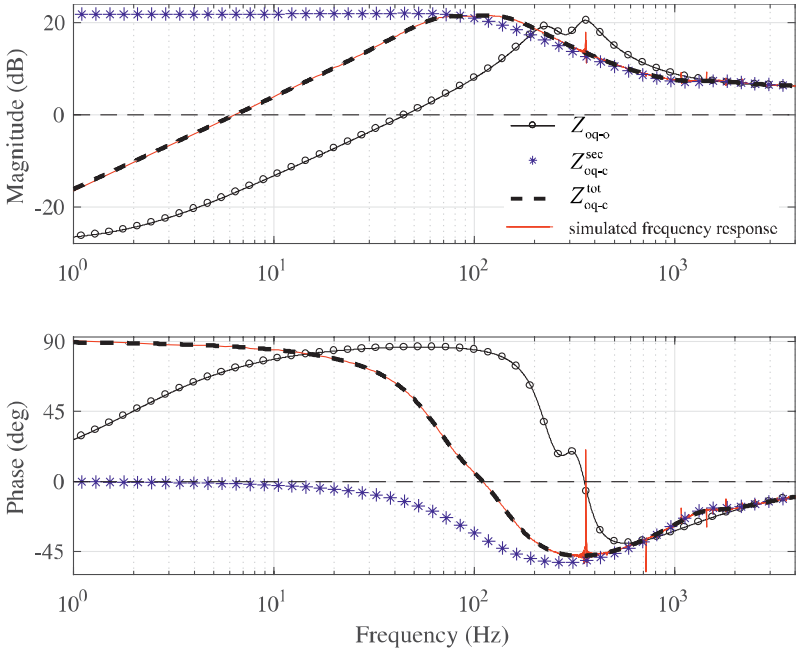


***Figure D.4*** *Frequency responses of* $Z_{\mathrm{oq}}$ *in open loop and closed loop.*